NATIONAL ADVISORY COMMITTEE FOR AERONAUTICS

TECHNICAL NOTE 3421

AERODYNAMICS OF A RECTANGULAR WING OF INFINITE ASPECT RATIO AT HIGH ANGLES OF ATTACK AND SUPERSONIC SPEEDS

By John C. Martin and Frank S. Malvestuto, Jr.

Langley Aeronautical Laboratory
Langley Field, Va.

Washington
July 1955

NATIONAL ADVISORY COMMITTEE FOR AERONAUTICS

TECHNICAL NOTE 3421

AERODYNAMICS OF A RECTANGULAR WING OF INFINITE ASPECT RATIO AT HIGH ANGLES OF ATTACK AND SUPERSONIC SPEEDS

By John C. Martin and Frank S. Malvestuto, Jr.

SUMMARY

Perturbation of the flow over a two-dimensional flat plate at finite angles of attack is used to obtain a first-order evaluation of the damping in roll, the lift and moment due to an increment in angle of attack, and the lift and moment due to a steady pitching velocity for a rectangular wing of infinite aspect ratio at supersonic speeds. Approximate expressions are derived for the lift and moment due to a constant vertical acceleration.

The results are valid for the ranges of Mach number and angle of attack for which the flow behind the shock is supersonic. The analysis is based on the equations for rotational flow, so that the change of entropy is taken into account.

Design charts are presented which permit rapid estimations to be made of the aerodynamic derivatives for a given Mach number and a given angle of attack.

The results for the infinite-aspect-ratio wing are used to make estimates of a number of the aerodynamic derivatives for rectangular wings at finite angles of attack.

INTRODUCTION

The development of the linearized theory of supersonic flow has permitted a first-order evaluation of a number of aerodynamic stability derivatives for a variety of plan forms at an angle of attack of 0°. Second-order theories similar to the one introduced by Busemann (ref. 1) and extended by Van Dyke (refs. 2 and 3) have been used to obtain second-order evaluations of a number of the aerodynamic derivatives for a few simple airfoils (refs. 4 to 6) at supersonic speeds. The second-order theories predict no variation in the aerodynamic derivatives with angle of attack. There is a need, however, for values of aerodynamic derivatives

at angles of attack beyond the validity of the second-order theories developed in references 4 to 6. At the present time, little published information can be found on the aerodynamic derivatives at finite angles of attack and supersonic speeds.

The only published papers associated with these aerodynamic derivatives that have come to the authors' attention are the analyses of Ivey (ref. 7), Carrier (refs. 8 and 9), and Chu (ref. 10). The analyses by Carrier and Chu make use of the linear perturbation theory for rotational flow (refs. 11 to 13) which allows first-order estimates to be made of the flow variables behind a strong shock attached to the leading edge of a two-dimensional wedge or within the region bounded by the lower surface of an airfoil at finite angles of attack and the strong shock from the leading edge of the airfoil.

The present paper contains a first-order evaluation of a number of aerodynamic derivatives for a rectangular wing of infinite aspect ratio at finite angles of attack, based upon the linear perturbation theory for rotational flow. This analysis, including the development of the linearized rotational-flow equations, was performed independently of previous analyses, an attempt being made to present a completely unified treatment leading directly to the evaluation of aerodynamic stability derivatives. Wherever possible, similarity of results from the present and previous analyses are noted.

The results are valid for the ranges of Mach number and angle of attack for which the flow behind the shock from the leading edge is supersonic. A first-order evaluation of the following aerodynamic derivatives is made: the lift-curve slope C_{L_α}, the rate of change of pitching moment with angle of attack C_{m_α}, the damping in roll $C_{l_{p'}}$, the lift due to constant pitching C_{L_q}, and the moment produced by a constant rate of pitch C_{m_q}.

Simple approximate relations for C_{L_α}, C_{m_α}, $C_{l_{p'}}$, C_{L_q}, and C_{m_q} are derived. These approximate relations yield results which are in good agreement with the exact first-order values, except at angles of attack near the angle where the flow behind the shock is sonic. In addition, approximate expressions are determined for $C_{L_{\dot{\alpha}}}$ and $C_{m_{\dot{\alpha}}}$, the lift and pitching moment due to a constant vertical acceleration. It should be noted that, although the shock-expansion theory can be used to calculate C_{L_α} and C_{m_α} (see ref. 7) with relatively little effort, the use of this theory to evaluate the remaining derivatives becomes difficult, if not impossible. The methods used herein yield the first-order evaluation of the aerodynamic derivatives for the airfoil considered with relatively little effort.

A series of design charts presented herein permits rapid estimations of the aerodynamic derivatives to be made for a given Mach number and a given angle of attack.

The results for the wing of infinite aspect ratio are used to make estimates of a number of the aerodynamic derivatives for rectangular wings at finite angles of attack.

SYMBOLS

A	aspect ratio
$a = 1 + \frac{K_{II}}{M_1^2\gamma(\gamma - 1)}$	
$B = \sqrt{M^2 - 1}$	
$B_o = \sqrt{M_o^2 - 1}$	
$B_1 = \sqrt{M_1^2 - 1}$	
$B_2 = \sqrt{M_2^2 - 1}$	
b	wing span
b_1, b_2, b_3, b_4	constants
c	chord
c_1	velocity of sound behind shock
c_2	velocity of sound in flow over upper surface of airfoil
c_v	specific heat at constant volume
$G(x,y,z) = 0$	equation of perturbed shock surface
g	acceleration due to gravity
g_1, g_2	arbitrary functions of $(x - B_1 z)$ and $(x + B_1 z)$, respectively

h_o	enthalpy in free stream
h_1	enthalpy in flow behind shock from leading edge
i,j,k	unit vectors in x-, y-, and z-direction, respectively
J	mechanical equivalent of heat
K	constant
K_I	parameter defined by equation (47)
K_{II}	parameter defined by equation (52)
K_{III}	parameter defined by equation (92)
M	Mach number
M_o	free-stream Mach number
M_1	Mach number behind shock
M_2	Mach number of flow over upper surface
m	slope of shock (see fig. 5)
P	pressure coefficient
$P^{p'}$	pressure coefficient due to a constant rate of roll
P^q	pressure coefficient due to a constant rate of pitch
P^α	pressure coefficient due to an increment in angle of attack
$P^{\dot{\alpha}}$	pressure coefficient due to a constant vertical acceleration
p	pressure
p'	rate of roll
p_o	free-stream pressure
p_1	pressure behind shock in unperturbed flow

p_2 pressure in unperturbed flow over upper surface of airfoil

δp_1 first-order perturbation in pressure of flow behind shock

q rate of pitch

S entropy

δS_1 first-order perturbation in entropy

s distance along shock from leading edge of airfoil in xz-plane

T temperature

t time

u,v,w perturbation velocity components in x-, y-, and z-direction, respectively

$\bar{q} = iu + jv + kw$

V_o free-stream velocity

V_{o_n} component of free-stream velocity that is normal to the shock

V_{o_t} component of free-stream velocity that is tangential to the shock

V_1 velocity of unperturbed flow behind shock

V_2 velocity of unperturbed flow over upper surface of airfoil

V_1' velocity vector of perturbed flow behind shock

V_{1_n}' normal component of velocity in perturbed flow behind shock

V_{1_t}' tangential component of velocity in perturbed flow behind shock

$\left(V_{o_t}\right)_{xy}$ component of V_{o_t} in xy-plane

$\left(V_{1_t}'\right)_{xy}$ component of V_{1_t}' in xy-plane

W_{max} maximum value of W

$\bar{W} = (V_1 + u)i + vj + wk$

w_a vertical velocity of airfoil associated with $\Delta\alpha$

x_{cg} distance from leading edge of airfoil to center-of-gravity location

x,y,z rectangular coordinates

α angle of attack

α_o fixed value of α

$\dot{\alpha} = \frac{\partial\alpha}{\partial t}$ motion of the wing corresponding to a constant vertical acceleration; sometimes referred to as a plunging motion

γ ratio of specific heat at constant pressure to specific heat at constant volume (1.400 for all calculations)

θ angle between free-stream direction and unperturbed shock profile (see fig. 5)

$\lambda = \frac{\partial G}{\partial y}$

ρ density

ρ_o free-stream density

ρ_1 density in unperturbed flow behind shock

ρ_2 density in unperturbed flow over upper surface of airfoil

$\delta\rho_1$ first-order perturbation in density behind shock

Φ scalar potential function defined by equation (97)

ϕ scalar potential function

$\phi^{p'}$ scalar potential function associated with rolling

ϕ^q scalar potential function associated with a steady pitching velocity

ϕ^α scalar potential function associated with perturbation in α

$\phi^{\dot{\alpha}}$ scalar potential function associated with a constant vertical acceleration

$$\nabla = i\frac{\partial}{\partial x} + j\frac{\partial}{\partial y} + k\frac{\partial}{\partial z}$$

$$\nabla_h = iB_1^2\frac{\partial}{\partial x} + j\frac{\partial}{\partial y} + k\frac{\partial}{\partial z}$$

C_N normal-force coefficient, $\dfrac{\text{Force}}{\frac{1}{2}\rho_o V_o^2 \times \text{Plan-form area}}$

C_m pitching-moment coefficient, $\dfrac{\text{Pitching moment}}{\frac{1}{2}\rho_o V_o^2 c \times \text{Plan-form area}}$

C_l rolling-moment coefficient about stability axis, $\dfrac{\text{Rolling moment}}{\frac{1}{2}\rho_o V_o^2 c \times \text{Plan-form area}}$

$$C_{L_\alpha} = \left[\left(\frac{\partial C_N}{\partial \alpha}\right)_{\alpha=\alpha_o} \cos \alpha_o\right]$$

$$C_{L_{\dot{\alpha}}} = \left[\left(\frac{\partial C_N}{\frac{\partial \dot{\alpha} c}{2V_o}}\right)_{\alpha=\alpha_o} \cos \alpha_o\right]$$

$$C_{L_q} = \left[\left(\frac{\partial C_N}{\partial \frac{qc}{2V_o}}\right)_{\alpha=\alpha_o} \cos \alpha_o\right]$$

Note that C_{L_α}, $C_{L_{\dot{\alpha}}}$, and C_{L_q} as defined herein are the component derivatives normal to the free stream.

$$C_{m_\alpha} = \left(\frac{\partial C_m}{\partial \alpha}\right)_{\alpha=\alpha_o}$$

$$C_{m_q} = \left(\frac{\partial C_m}{\partial \frac{qc}{2V_o}}\right)_{\alpha=\alpha_o}$$

$$C_{m_{\dot{\alpha}}} = \left(\frac{\partial C_m}{\partial \frac{\dot{\alpha}c}{2V_o}}\right)_{\alpha=\alpha_o}$$

$$C_{l_{p'}} = \left(\frac{\partial C_l}{\partial \frac{p'b}{2V_o}}\right)_{\alpha=\alpha_o}$$

Wherever the variables x, y, z, and t are used as subscripts, a differentiation process with respect to these variables is indicated.

PRELIMINARY REMARKS

The airfoil considered in this paper is a rectangular wing of infinite aspect ratio at finite angles of attack (fig. 1). The airfoil is taken to be thin so that the thickness effects can be neglected in the first-order evaluation of the aerodynamic derivatives formulated herein. The aerodynamic derivatives are obtained by finding the first-order perturbation in the flow over a two-dimensional flat plate at a finite angle of attack (fig. 1(a)). The reader is assumed to be familiar with the shock-expansion theory of two-dimensional supersonic flows. The stability axes used in the analysis are shown in figure 1(b).

The C_{L_α} and C_{m_α} derivatives are determined by considering the effect of an infinitesimal increment in α. The C_{l_p} derivative is determined by analyzing the effect of an infinitesimal constant rate of roll about the x stability axis.

The C_{L_q} and C_{m_q} derivatives are determined by considering a constant infinitesimal rate of pitch about the y stability axis. Since the type of motion analyzed in finding C_{L_q} and C_{m_q} is often misunderstood, this motion is discussed in detail. A constant rate of pitch is associated with a constant rate of rotation about the axis of pitch while the angle of attack with respect to the free stream remains constant. Viewed from a point fixed with reference to the undisturbed air, the wing is flying in a circle of radius V_o/q with a constant angular velocity q and with a constant angle of attack (fig. 2). Note that the flow associated with this motion is steady. Since the rates of pitch considered are very small, the radius of the circle is very large and the basic flow for the airfoil considered herein can be taken to be the steady flow over a two-dimensional flat plate.

The approximate expressions for the $C_{L_{\dot{\alpha}}}$ and $C_{m_{\dot{\alpha}}}$ derivatives are determined by assuming a constant infinitesimal acceleration in the z-direction of the stability axes.

In general, the boundary conditions on the airfoil surface are complicated by the presence of the shock and expansion fan from the leading edge of the wing. As an example, take the case of a small increment in the angle of attack, which can be considered as the result of a small constant vertical velocity w_a superimposed on the original flow. In the stability-axes system (which is fixed relative to the airfoil), the free-stream direction has changed by the angle $\Delta\alpha$ (fig. 3). Since the shock and the expansion fan at the leading edge change the direction of the flow so that it becomes parallel to the airfoil surface, the normal component of the perturbation velocity on the surface must be directly proportional to $\Delta\alpha$ times the unperturbed flow parallel to the surface. The normal component of the perturbation velocities is related to the angle of attack only through the unperturbed flow parallel to the surface. The boundary conditions on the surface due to other types of motions can be determined in a similar manner.

PERTURBED FLOW OVER UPPER SURFACE

The basic unperturbed flow over the upper surface is uniform and irrotational. The flow begins with the termination of the expansion fan

around the leading edge of the airfoil. Inasmuch as the flow is irrotational and the small disturbances produced on the upper surface will not interact with shock waves upstream of the trailing edge of the wing, these disturbances can be calculated by the use of a potential function.

The coordinate axes used in the analysis of the flow over the upper surface are indicated in figure 4. The potential function must satisfy the following partial differential equations:

For steady flows,

$$-B_2^2\phi_{xx} + \phi_{yy} + \phi_{zz} = 0 \tag{1a}$$

For unsteady flows,

$$-B_2^2\phi_{xx} + \phi_{yy} + \phi_{zz} - \frac{2V_2}{c_2^2}\phi_{xt} - \frac{1}{c_2^2}\phi_{tt} = 0 \tag{1b}$$

The subscript 2 refers to the conditions on the upper surface of the airfoil.

The boundary conditions associated with the various motions are:

Upstream of the end of the expansion fan from the leading edge of the airfoil,

$$\phi \equiv 0$$

For an increment in α,

$$\left(\phi_z^{\alpha}\right)_{z=0} = -\Delta\alpha\, V_2$$

For a constant rate of pitch,

$$\left(\phi_z^{q}\right)_{z=0} = -q\left(x - x_{cg}\right)$$

For a constant rate of roll,

$$\left(\phi_z^{p'}\right)_{z=0} = -p'y$$

For a constant vertical acceleration,

$$\left(\phi_z^{\dot{\alpha}}\right)_{z=0} = -\dot{\alpha}V_2 t$$

The potential functions associated with the various motions are:

For an increment in α,

$$\phi^{\alpha} = \frac{\Delta\alpha\, V_2(x - B_2 z)}{B_2}$$

For a constant rate of pitch,

$$\phi^{q} = \frac{q(x - B_2 z)^2}{2B_2} - \frac{q x_{cg}(x - B_2 z)}{B_2}$$

where the axis of pitch is located a distance x_{cg} from the leading edge of the wing.

For a constant rate of roll,

$$\phi^{p'} = \frac{p'y(x - B_2 z)}{B_2}$$

For a constant vertical acceleration,

$$\phi^{\dot{\alpha}} = \frac{\dot{\alpha}}{B_2}\left[-\frac{M_2^2 x^2}{2B_2^2} + \frac{M_2^2}{2} z^2 + V_2 t(x - B_2 z)\right]$$

The pressure coefficient based on the free-stream conditions is given by

$$P = -\frac{2M_2^2 p_2}{M_o^2 p_o}\left(\frac{\phi_x}{V_2} + \frac{\phi_t}{V_2^2}\right) \qquad (2a)$$

or

$$P = -\frac{2M_2}{M_o}\sqrt{\frac{p_2\rho_2}{p_o\rho_o}}\left(\frac{\phi_x}{V_o} + \frac{\phi_t}{V_2V_o}\right) \tag{2b}$$

It follows that the perturbation pressure on the upper surface of the airfoil resulting from the various motions is:

For an increment in α,

$$p^{\alpha} = -\frac{\Delta\alpha\ 2M_2^2p_2}{B_2M_o^2p_o} \tag{3a}$$

For a constant rate of pitch,

$$p^{q} = -\frac{qc}{2V_o}\frac{4M_2}{B_2M_o}\sqrt{\frac{p_2\rho_2}{p_o\rho_o}}\frac{x - x_{cg}}{c} \tag{3b}$$

For a constant rate of roll,

$$p^{p'} = -\frac{p'y}{2V_o}\frac{4M_2}{B_2M_o}\sqrt{\frac{p_2\rho_2}{p_o\rho_o}} \tag{3c}$$

For a constant vertical acceleration,

$$p^{\dot{\alpha}} = \frac{\dot{\alpha}c}{2V_o}\frac{4M_2}{B_2^3M_o}\sqrt{\frac{p_2\rho_2}{p_o\rho_o}}\left(\frac{x}{c} - \frac{V_2B_2^2t}{c}\right) \tag{3d}$$

STEADY TWO-DIMENSIONAL PERTURBED FLOW BEHIND AN INCLINED SHOCK

The perturbed flow over the lower surface of the airfoil due to steady pitching and a small increment in α is a special case of the first-order, steady, two-dimensional perturbation of the flow behind a two-dimensional inclined shock. This flow may not be irrotational; therefore, the analysis is based on the equations for rotational flow. As stated in the introduction, expressions for the evaluation of first-order perturbations of flow variables behind a strong shock have been derived in a number of papers. The development and application herein of the linearized equations of rotational flow are an effort to present a complete unified treatment appropriate for the evaluation of aerodynamic derivatives. The coordinate axes and some other data used in the analysis are indicated in figure 5.

The equations for rotational flow are (p. 202 of ref. 14):

The Euler equations of motion,

$$\nabla \frac{W^2}{2} + (\nabla \times W) \times W = - \frac{1}{\rho} \nabla p \tag{4}$$

The equation of continuity,

$$\nabla . \rho W = 0 \tag{5}$$

The entropy equation,

$$\frac{p}{\rho^\gamma} = e^{S/c_v} \tag{6}$$

The equation for conservation of enthalpy,

$$\frac{\gamma}{\gamma - 1} \frac{p}{\rho} + \frac{W^2}{2} = \frac{W_{max}^2}{2} \tag{7}$$

The preceding equations are presented in their three-dimensional forms because these are needed in the analysis of the rolling motion. Equations (4) to (7) represent six equations for five variables (p, ρ, and

the three components of W) since the entropy S is determined from the boundary conditions. It follows that there are only five independent relations contained in these equations. The six equations are retained, however, because the sixth equation is used to shorten the analysis.

The flow behind the shock can be expressed as:

$$W = i(V_1 + u) + jv + kw \tag{8a}$$

$$\rho = \rho_1 + \delta\rho_1 \tag{8b}$$

$$p = p_1 + \delta p_1 \tag{8c}$$

$$S = S_1 + \delta S_1 \tag{8d}$$

where u, v, and w are perturbations in the velocity and $\delta\rho_1$, δp_1, and δS_1 are the first-order perturbations in density, in pressure, and in entropy, respectively. The subscript 1 refers to conditions on the lower surface of the airfoil.

Substituting equations (8) into equations (4) to (7) and retaining only the first-order terms yields (these operations are given in the appendix):

$$\nabla u + j\left(\frac{\partial v}{\partial x} - \frac{\partial u}{\partial y}\right) + k\left(\frac{\partial w}{\partial x} - \frac{\partial u}{\partial z}\right) = -\frac{1}{V_1\rho_1}\nabla\delta p_1 \tag{9}$$

$$\frac{\partial u}{\partial x} + \frac{\partial v}{\partial y} + \frac{\partial w}{\partial z} = -\frac{V_1}{\rho_1}\frac{\partial\delta\rho_1}{\partial x} \tag{10}$$

$$\frac{\delta p_1}{p_1} - \gamma\frac{\delta\rho_1}{\rho_1} = \frac{\delta S_1}{c_v} \tag{11}$$

$$\frac{\delta p_1}{p_1} - \frac{\delta \rho_1}{\rho_1} = - \frac{\gamma - 1}{\gamma} \frac{V_1 \rho_1}{p_1} u = \frac{\delta T_1}{T_1} \tag{12}$$

Inasmuch as the entropy is constant along streamlines, the change of entropy δS_1 is a function of z only. The initial values of δS_1 at the shock are part of the boundary conditions on the shock.

When the perturbation flow is two-dimensional, v and all quantities operated on by $\frac{\partial}{\partial y}$ are zero, and equations (9) and (10) reduce to

$$\nabla u + k\left(\frac{\partial w}{\partial x} - \frac{\partial u}{\partial z}\right) = - \frac{\nabla \delta p_1}{V_1 \rho_1} \tag{13}$$

$$\frac{\partial u}{\partial x} + \frac{\partial w}{\partial z} = - \frac{V_1}{\rho_1} \frac{\partial \delta \rho_1}{\partial x} \tag{14}$$

The partial differential equations for u and w can be obtained as follows: Since δS_1 is not a function of x, the partial derivatives of equations (11) and (12) with respect to x are

$$\frac{1}{p_1} \frac{\partial \delta p_1}{\partial x} - \frac{\gamma}{\rho_1} \frac{\partial \delta \rho_1}{\partial x} = 0 \tag{15}$$

and

$$\frac{1}{p_1} \frac{\partial \delta p_1}{\partial x} - \frac{1}{\rho_1} \frac{\partial \delta \rho_1}{\partial x} + \frac{\gamma - 1}{\gamma} \frac{V_1 \rho_1}{p_1} \frac{\partial u}{\partial x} = 0 \tag{16}$$

By eliminating $\partial\delta p_1/\partial x$ and $\partial\delta\rho_1/\partial x$ from equations (14) to (16) and by using the relation

$$c_1^2 = \frac{\gamma p_1}{\rho_1}$$

the following equation can be obtained:

$$B_1^2 \frac{\partial u}{\partial x} = \frac{\partial w}{\partial z} \tag{17}$$

Equation (17) is one relation between u and w. A second relation can be obtained as follows: The perturbation pressure can be eliminated from the z-component of equations (11) and (13) to yield

$$\frac{\partial w}{\partial x} = -\frac{\gamma p_1}{V_1 \rho_1^2}\frac{\partial \delta\rho_1}{\partial z} - \frac{p_1}{V_1 \rho_1 c_v}\frac{\partial \delta s_1}{\partial z} \tag{18}$$

The perturbation pressure can also be eliminated from equations (11) and (12) to give

$$\frac{\delta\rho_1}{\rho_1} = -\frac{V_1 \rho_1}{\gamma p_1} u - \frac{\delta s_1}{(\gamma - 1)c_v} \tag{19}$$

Equations (18) and (19) can be combined to yield

$$\frac{\partial w}{\partial x} = \frac{\partial u}{\partial z} + \frac{p_1}{V_1 \rho_1 c_v(\gamma - 1)}\frac{\partial \delta s_1}{\partial z} \tag{20}$$

Equation (20) is the second relation between u and w.

The following partial differential equations for u and w can be obtained from equations (17) and (20):

$$B_1^2 \frac{\partial^2 u}{\partial x^2} - \frac{\partial^2 u}{\partial z^2} = \frac{p_1}{V_1 \rho_1 c_v (\gamma - 1)} \frac{\partial^2 \delta S_1}{\partial z^2} \tag{21}$$

$$B_1^2 \frac{\partial^2 w}{\partial x^2} - \frac{\partial^2 w}{\partial z^2} = 0 \tag{22}$$

The general solutions of equations (21) and (22) can be written as

$$u = - \frac{g_1(x - B_1 z)}{B_1} + \frac{g_2(x + B_1 z)}{B_1} - \frac{p_1 \, \delta S_1(z)}{V_1 \rho_1 (\gamma - 1) c_v} \tag{23}$$

$$w = g_1(x - B_1 z) + g_2(x + B_1 z) \tag{24}$$

From equations (11) and (12), the perturbation pressure is related to u by

$$\delta p_1 = - V_1 \rho_1 u - \frac{p_1 \, \delta S_1}{(\gamma - 1) c_v} \tag{25}$$

Also from equations (11) and (12), the perturbation density is related to u by

$$\delta \rho_1 = - \frac{M_1^2 \rho_1 u}{V_1} - \frac{\rho_1 \, \delta S_1}{(\gamma - 1) c_v} \tag{26}$$

Equations (23) to (26) are the solutions of equations (11) to (14). The functions g_1, g_2, and δS_1 must be determined from the boundary conditions on the surface of the body and on the shock.

The boundary condition on the surface is given by

$$(w)_{z=0} = V_1 f(x) \tag{27}$$

where $f(x)$ is a known function of x determined by the type of disturbance being investigated.

It should be noted that although the shock surface is free to move and deform, the boundary conditions are not satisfied on the actual surface but along the shock profile of the unperturbed flow. This approximation is valid within the bounds of the linearization process used herein.

The boundary conditions on the shock must be determined from the basic shock equations. These equations are (from pp. 97 and 98 of ref. 14):

$$\rho_o V_{o_n} = \rho_1 V_{1_n}' \tag{28}$$

$$\rho_o V_{o_n}^2 + p_o = \rho_1 \left(V_{1_n}'\right)^2 + p_1 \tag{29}$$

$$\rho_o V_{o_n} V_{o_t} = \rho_1 V_{1_n}' V_{1_t}' \tag{30}$$

$$Jh_o + \frac{1}{2g} V_{o_n}^2 = Jh_1 + \frac{1}{2g}\left(V_{1_n}'\right)^2 \tag{31}$$

From equations (28) and (30) it follows that

$$V_{o_t} = V_{1_t}' \tag{32}$$

Since (from p. 99 of ref. 14)

$$Jh_o = \frac{\gamma}{\gamma - 1} \frac{p_o}{g\rho_o}$$

and

$$Jh_1 = \frac{\gamma}{\gamma - 1}\frac{p_1}{g\rho_1}$$

equation (31) can be expressed as

$$\frac{\gamma}{\gamma - 1}\frac{p_o}{\rho_o} + \frac{1}{2}V_{o_n}^2 = \frac{\gamma}{\gamma - 1}\frac{p_1}{\rho_1} + \frac{1}{2}\left(V_{1_n}'\right)^2 \tag{33}$$

The normal and tangential velocity components can be written as (see fig. 6):

$$V_{o_n} = V_o \sin\theta \qquad V_{1_n}' = V_1'\sin(\theta - \alpha)$$

$$V_{o_t} = V_o \cos\theta \qquad V_{1_t}' = V_1'\cos(\theta - \alpha)$$

Substituting these four relations into equations (28), (29), (32), and (33) yields

$$\rho_o V_o \sin\theta = \rho_1 V_1'\sin(\theta - \alpha) \tag{34}$$

$$\rho_o V_o^2\sin^2\theta + p_o = \rho_1\left(V_1'\right)^2\sin^2(\theta - \alpha) + p_1 \tag{35}$$

$$V_o \cos\theta = V_1'\cos(\theta - \alpha) \tag{36}$$

$$\frac{\gamma}{\gamma - 1}\frac{p_o}{\rho_o} + \frac{V_o^2\sin^2\theta}{2} = \frac{\gamma}{\gamma - 1}\frac{p_1}{\rho_1} + \frac{\left(V_1'\right)^2\sin^2(\theta - \alpha)}{2} \tag{37}$$

The first-order variations across the shock wave can be determined by taking the total derivative of the preceding equations while considering

p_o, ρ_o, and V_o as constants. The differentials dp_1, $d\rho_1$, $d\theta$, $d\alpha$, and dV_1' can be considered as first-order variations of the variables. Thus, from the four preceding equations, the differentials are related by the following equations:

$$\rho_o V_o \cos\theta\, d\theta - V_1'\sin(\theta - \alpha)\, d\rho_1 - \rho_1 \sin(\theta - \alpha)\, dV_1' -$$

$$\rho_1 V_1'\cos(\theta - \alpha)(d\theta - d\alpha) = 0 \tag{38}$$

$$2\rho_o V_o^2 \sin\theta \cos\theta\, d\theta - \left(V_1'\right)^2 \sin^2(\theta - \alpha)\, d\rho_1 - 2\rho_1 V_1' \sin^2(\theta - \alpha)\, dV_1' -$$

$$2\rho_1\left(V_1'\right)^2 \sin(\theta - \alpha)\cos(\theta - \alpha)(d\theta - d\alpha) - dp_1 = 0 \tag{39}$$

$$-V_o \sin\theta\, d\theta - \cos(\theta - \alpha)\, dV_1' + V_1'\sin(\theta - \alpha)(d\theta - d\alpha) = 0 \tag{40}$$

$$V_o^2 \sin\theta \cos\theta\, d\theta - \frac{\gamma}{\gamma - 1}\frac{dp_1}{\rho_1} + \frac{\gamma}{\gamma - 1}\frac{p_1}{\rho_1}\frac{d\rho_1}{\rho_1} - V_1'\sin^2(\theta - \alpha)\, dV_1' -$$

$$\left(V_1'\right)^2 \sin(\theta - \alpha)\cos(\theta - \alpha)(d\theta - d\alpha) = 0 \tag{41}$$

From figure 6 it can be seen that

$$dV_1' = u$$

and

$$d\alpha = \frac{w}{V_1}$$

By making use of these relations and equations (34) to (37), equations (38) to (41) can be expressed as

$$\left(\rho_o - \rho_1\right)V_o \cos\theta\, d\theta - \frac{\rho_o V_o}{V_1} u \sin\theta + \frac{\rho_1 V_o}{V_1} w \cos\theta - \frac{V_o \rho_o}{\rho_1} \sin\theta\, d\rho_1 = 0 \tag{42}$$

$$\frac{2\rho_o{}^2 V_o{}^2}{\rho_1 V_1} u \sin^2\theta - \frac{2V_o{}^2}{V_1} \rho_o w \sin\theta \cos\theta + \left(\frac{\rho_o}{\rho_1}\right)^2 V_o{}^2 \sin^2\theta\, d\rho_1 + dp_1 = 0 \tag{43}$$

$$\frac{\rho_1 - \rho_o}{\rho_1} V_o \sin\theta\, d\theta + \frac{V_o}{V_1} u \cos\theta + \frac{\rho_o}{\rho_1}\frac{V_o}{V_1} w \sin\theta = 0 \tag{44}$$

$$\left(1 - \frac{\rho_o}{\rho_1}\right)V_o{}^2 \sin\theta \cos\theta\, d\theta - \left(\frac{\rho_o}{\rho_1}\right)^2 \frac{V_o{}^2}{V_1} u \sin^2\theta + \frac{\rho_o V_o{}^2}{\rho_1 V_1} w \sin\theta \cos\theta - \frac{\gamma}{\gamma - 1}\frac{dp_1}{\rho_1} + \frac{\gamma}{\gamma - 1}\frac{p_1 d\rho_1}{\left(\rho_1\right)^2} = 0 \tag{45}$$

Equations (42) to (45) are linear with respect to the differentials and, since there are five differentials and four equations, linear relationships can be obtained between any two of the differentials. For the boundary conditions on the shock, a relation between u and w will be used. This relation is

$$(u)_{z=mx} = (K_I)_{z=mx} \tag{46}$$

where

$$K_I = - \frac{\left[1 + \frac{\rho_1}{\rho_o} + \gamma M_o^2 \frac{p_o}{p_1}\left(\frac{\rho_o}{\rho_1} - 1\right)\sin^2\theta\right]\cot\theta}{\frac{\gamma M_o^2 p_o \rho_1}{p_1 \rho_o}\left(\frac{\rho_o}{\rho_1} - 1 + \frac{1}{\gamma}\right)\cos^2\theta - \left(1 - \frac{\rho_1}{\rho_o}\cot^2\theta\right) + \frac{M_o^2 \rho_o p_o}{\rho_1 p_1}\sin^2\theta} \tag{47}$$

Note that for zero angle of attack

$$\left(K_I\right)_{\alpha_o=0} = - \frac{1}{B_o}$$

Values of K_I are given in table I for various angles of attack and Mach numbers.

Equation (47) is one of the boundary conditions on the shock. It remains to determine the values of δS_1 in the flow behind the shock. Since δS_1 is constant along streamlines (and hence is a function of z only) the values of δS_1 are determined by the conditions on the downstream side of the shock surface.

The expression for S_1/c_v is (from p. 202 of ref. 14)

$$\frac{S_1}{c_v} = \log_e p_1 - \gamma \log_e \rho_1 \tag{48}$$

Taking the total differential of equation (48) yields

$$\frac{dS_1}{c_v} = \frac{\delta S_1}{c_v} = \frac{\delta p_1}{p_1} - \gamma \frac{\delta \rho_1}{\rho_1} \tag{49}$$

This equation is true for points located directly behind the shock; thus for points on the downstream side of the shock, equation (49) becomes

$$\frac{\delta S_1}{c_v} = \frac{dp_1}{p_1} - \gamma \frac{d\rho_1}{\rho_1} \tag{50}$$

Expressing dp_1 and $d\rho_1$ in terms of u by the use of equations (42) to (45) gives for equation (50):

$$\frac{\delta S_1}{c_v} = \left(K_{II} \frac{u}{V_1}\right)_{z=mx} \tag{51}$$

where

$$K_{II} = -\frac{M_o^2 \frac{p_o}{p_1}\left(\frac{\rho_1}{\rho_o}\right)^2 (\gamma - 1)\left(1 - \frac{\rho_1}{\rho_o}\right)\left(M_o^2 \frac{p_o}{p_1} \frac{\rho_o}{\rho_1} \sin^2\theta - 1\right)\left[\cos^2\theta + \left(\frac{\rho_o}{\rho_1}\right)^2 \sin^2\theta\right]}{M_o^2 \frac{p_o}{p_1}\left(1 - \frac{\rho_1}{\rho_o}\right)\sin^2\theta + \frac{\rho_1}{\gamma p_o}\left(1 + \frac{\rho_1}{\rho_o}\right)} \tag{52}$$

Values of K_I are presented in table I for various angles of attack and Mach numbers. Equation (51) concludes the expressions for the boundary conditions. The other expressions for the boundary conditions are equations (27) and (46).

The boundary condition on the lower surface of an airfoil due to a small increment in the angle of attack is (in the coordinates shown in fig. 7)

$$(w)_{z=0} = \Delta\alpha \, V_1 = g_1(x) + g_2(x) \tag{53}$$

It follows from equation (53) that

$$w = \Delta\alpha \, V_1$$

and from equation (46) that

$$u = K_I \Delta\alpha V_1 \tag{54}$$

The perturbation pressure is (from eqs. (26) and (54))

$$\delta p_1 = -\rho_1 V_1 \left[K_I \Delta\alpha V_1 + \frac{p_1 \delta S_1(z)}{V_1 \rho_1 (\gamma - 1) c_v} \right] \tag{55}$$

Since (from eqs. (51) and (54))

$$\frac{\delta S_1}{c_v} = K_{II} K_I \Delta\alpha$$

equation (55) can be written as

$$\delta p_1 = -\rho_1 V_1^2 K_I \Delta\alpha \left[1 + \frac{K_{II}}{M_1^2 \gamma (\gamma - 1)} \right] \tag{56}$$

This expression for the pressure has previously been derived by Chu (ref. 10). The quantity $K_I \left[1 + \frac{K_{II}}{M_1^2 \gamma (\gamma - 1)} \right]$ equals $-\tan \lambda$ in equation (43) of Chu's paper. The increment in the pressure coefficient based on the free-stream conditions is

$$\frac{P}{\Delta\alpha} = -\frac{2M_1^2}{M_o^2} K_I \frac{p_1}{p_o} \left[1 + \frac{K_{II}}{M_1^2 \gamma (\gamma - 1)} \right] \tag{57}$$

Figure 8 presents the variation of $\Delta P/\Delta\alpha$ with angle of attack for various

Mach numbers. The values of M_1, $\frac{p_1}{p_o}$, $\frac{\rho_1}{\rho_o}$, and θ were taken from reference 15 and from unpublished calculations.

The effect of the change in entropy in the perturbed flow can be evaluated by setting K_{II} equal to zero in equation (57). The change in entropy is retained in the boundary condition on the shock which relates the velocity components u and w. Figure 9 presents a comparison of values of $\Delta P/\Delta\alpha$ with and without the change in entropy included in the perturbed flow.

An approximation to the pressure due to an increment in α can be obtained by assuming that the presence of the shock in the perturbed flow can be neglected and by assuming that the perturbed-flow velocity components can be expressed by derivatives of a potential function. This potential function is similar to the function associated with the flow over the upper surface and is based on the velocity V_1. Under these assumptions, the velocity component u can be expressed as

$$u \approx -\frac{\Delta\alpha\, V_1}{B_1} \tag{58}$$

The pressure coefficient associated with equation (58) and based on the free-stream conditions is

$$\frac{P}{\Delta\alpha} \approx \frac{2M_1^2 p_1}{B_1 M_o^2 p_o} \tag{59}$$

Figure 10 presents a comparison between exact and approximate values of the increment in the pressure coefficient on the lower surface of an airfoil for an increment in α at various Mach numbers. In view of the assumptions involved in the approximation, figure 10 indicates that equation (59) is a very good approximation to the pressure coefficient except in a very small angle-of-attack range near the angle of attack for which $M_1 = 1$.

PERTURBED FLOW OVER LOWER SURFACE DUE TO STEADY PITCHING

The boundary condition on the lower surface of a pitching airfoil is (in the coordinate system shown in fig. 7)

$$(w)_{z=0} = q(x - x_{cg}) = g_1(x) + g_2(x) \tag{60}$$

If $g_1(x-B_1z)$ and $g_2(x+B_1z)$ for $z \neq 0$ are assumed to be of the form

$$g_1(x-B_1z) = qb_1(x - B_1z) + b_2$$

$$g_2(x+B_1z) = qb_3(x + B_1z) + b_4$$

where b_1, b_2, b_3, and b_4 are constants, then u and w are given by (from eqs. (23), (24), and (51))

$$w = q(b_1 + b_3)x - q(b_1 - b_3)B_1z + b_2 + b_4 \tag{61}$$

$$u = -\frac{q(b_1 - b_3)}{B_1}x + q(b_1 + b_3)z - \frac{b_2 - b_4}{B_1} - \left[\frac{K_{II}}{M_1^2\gamma(\gamma - 1)}u\right]_{z=mx} \tag{62}$$

From equation (60),

$$q\left(x - x_{cg}\right) = q(b_1 + b_3)x + b_2 + b_4$$

Equating powers of x yields

$$b_2 + b_4 = -qx_{cg} \tag{63}$$

$$b_1 + b_3 = 1 \tag{64}$$

On the shock (from eqs. (46), (61), and (62)),

$$-\frac{q(b_1 - b_3)mz}{B_1a} + \frac{q(b_1 + b_3)z}{a} - \frac{b_2 - b_4}{B_1a} =$$

$$\left[q(b_1 + b_3)mz - q(b_1 - b_3)B_1z + b_2 + b_4\right]K_I \tag{65}$$

where

$$a = 1 + \frac{K_{II}}{M_1^2\gamma(\gamma - 1)}$$

Equating powers of z in equation (65) yields

$$-\frac{1 + K_I B_1 a}{B_1 a} b_2 + \frac{1 - K_I B_1 a}{B_1 a} b_4 = 0 \tag{66}$$

$$\frac{1 + K_I B_1 a}{B_1 a}(m - B_1) b_1 - \frac{1 - K_I B_1 a}{B_1 a}(m + B_1) b_3 = 0 \tag{67}$$

Equations (63), (64), (66), and (67) are four equations containing the four unknown constants b_1, b_2, b_3, and b_4. Solving for the unknown constants yields

$$b_1 = \frac{(m + B_1)(1 - K_I B_1 a)}{2(m - K_I B_1^2 a)}$$

$$b_2 = -\frac{q x_{cg}}{2}(1 - K_I B_1 a)$$

$$b_3 = \frac{(m - B_1)(1 + K_I B_1 a)}{2(m - K_I B_1^2 a)}$$

$$b_4 = -\frac{q x_{cg}}{2}(1 + K_I B_1 a)$$

The velocity components w and u are

$$w = \frac{q}{m - K_I B_1^2 a}\left[\left(m - K_I B_1^2 a\right)x - \left(1 - K_I ma\right)B_1^2 z\right] - qx_{cg} \tag{68}$$

$$u = -\frac{q}{m - K_I B_1^2 a}\left[\left(1 - K_I ma\right)x - \left(m - K_I B_1^2 a\right)z\right] - qx_{cg}K_I a + \frac{qK_{II}K_I}{M_1^2\gamma(\gamma - 1)}\left(x_{cg} - \frac{m^2 - B_1^2}{m - K_I B_1^2 a}z\right) \tag{69}$$

The pressure on the surface is (from eqs. (25) and (69))

$$\delta p_1 = \rho_1 V_1 q \frac{m - K_I a}{1 - K_I B_1^2 ma}x + x_{cg}K_I a \tag{70}$$

This expression for the pressure can also be readily extracted from Chu's analysis (ref. 10) by substituting in equation (72) of that paper qx/V_1 for $f'(x)$, the condition requiring the flow to be tangential to the airfoil surface.

The pressure coefficient on the lower surface of the airfoil is

$$P = \frac{qc}{2V_o}\frac{4M_1}{M_o}\sqrt{\frac{p_1\rho_1}{p_o\rho_o}}\frac{m - K_I a}{1 - K_I B_1^2 ma}\frac{x}{c} + K_I a\frac{x_{cg}}{c} \tag{71}$$

Figure 11 presents the chordwise pressure distribution on the lower surface of an airfoil for various angles of attack at $M_o = 2.00$ where the axis of pitch is located at the midchord point.

The effect of neglecting the change in entropy in the perturbed flow can be obtained from equation (71) by replacing a by unity. The change in entropy is retained in the boundary condition on the shock which relates the velocity components u and w. Thus, the pressure coefficient on the lower surface of a pitching airfoil with the change in entropy neglected is

$$P = \frac{qc}{2V_o} \frac{4M_1}{M_o} \sqrt{\frac{p_1\rho_1}{p_o\rho_o}} \left(\frac{1 - K_I m}{m - K_I B_1^2} \frac{x}{c} + K_I \frac{x_{cg}}{c} \right) \tag{72}$$

Figure 12 presents the chordwise variations of the pressure coefficient including and neglecting the change in entropy for $M_o = 2.00$, for two angles of attack with the axis of pitch located at the midchord point. This figure indicates that the change in entropy has a strong effect on the pressure for the higher angles of attack.

An approximation to the pressure due to pitching can be obtained by making the same assumptions as were made for the approximation to the pressure due to an increment in α. This procedure will lead to the following relation for u:

$$u \approx - \frac{q\left(x - x_{cg}\right)}{B_1} \tag{73}$$

The pressure coefficient associated with equation (73) and based on the free-stream conditions is

$$P \approx \frac{qc}{2V_o} \frac{4M_1}{B_1 M_o} \sqrt{\frac{p_1\rho_1}{p_o\rho_o}} \left(\frac{x}{c} - \frac{x_{cg}}{c} \right) \tag{74}$$

Note that equation (74) can also be obtained by replacing K_I by $-1/B_1$ in equation (72). Figure 13 presents exact (from eq. (71)) and approximate (from eq. (74)) values of the chordwise pressure on the lower surface of a pitching airfoil for two angles of attack at $M_o = 2.00$ with the axis of pitch located at the midchord point. This figure indicates that equation (74) is a good approximation to the pressure distribution for $\alpha_o = 9.7^\circ$ and 20.7°.

PERTURBED FLOW OVER LOWER SURFACE DUE TO ROLLING

The perturbed flow over the lower surface of an airfoil due to rolling can be determined from equations (9) to (12). The coordinate axes used are shown in figure 7 where the y-axis is directed into the plane of the page.

The boundary condition on the surface is

$$(w)_{z=0} = p'y \tag{75}$$

The boundary conditions on the shock are determined from the equations expressing the conservation of mass, momentum, and energy. The continuity of mass flow requires that (eq. (28))

$$\rho_o V_{o_n} = \rho_1 V_{1_n}' \tag{76}$$

It can be seen in figure 14 that

$$V_{o_n} = V_o \sin\theta \cos(d\lambda)$$

$$V_{1_n}' = V_1' \sin(\theta - \alpha) \cos(d\lambda)$$

To the first order in $d\lambda$ the preceding equations become

$$V_{o_n} = V_o \sin\theta \tag{77a}$$

$$V_{1_n}' = V_1' \sin(\theta - \alpha) \tag{77b}$$

Thus, to the first order in $d\lambda$ equation (76) becomes

$$\rho_o V_o \sin\theta = \rho_1 V_1' \sin(\theta - \alpha) \tag{78}$$

This equation is the same as the corresponding relation for the two-dimensional case.

The conservation of momentum in the direction normal to the shock requires that (eq. (29))

$$\rho_o V_{o_n}^2 + p_o = \rho_1 \left(V_{1_n}'\right)^2 + p_1 \tag{79}$$

From equations (77), the preceding equation can be written (to the first order in $d\lambda$) as

$$\rho_o V_o^2 \sin^2\theta + p_o = \rho_1 (V_1')^2 \sin^2(\theta - \alpha) + p_1 \tag{80}$$

This is the same as the corresponding relation for the two-dimensional case.

The conservation of the tangential momentum requires that (eq. (30))

$$\rho_o V_{o_n} V_{o_t} = \rho_1 V_{1_n}' V_{1_t}' \tag{81}$$

It follows from equation (76) that

$$V_{o_t} = V_{1_t}' \tag{82}$$

Figure 14(a) shows that the tangential components in the xz-plane are

$$(V_{o_t})_{xz} = V_o \cos\theta \tag{83a}$$

$$(V_{1_t}')_{xz} = V_1' \cos(\theta - \alpha) \tag{83b}$$

Thus (eq. (36)),

$$V_o \cos\theta = V_1' \cos(\theta - \alpha) \tag{84}$$

This is the same as the corresponding relation for the two-dimensional case.

From the preceding results, the energy law can be expressed as (eq. (37))

$$\frac{\gamma}{\gamma - 1}\frac{p_o}{\rho_o} + \frac{V_o^2 \sin^2\theta}{2} = \frac{\gamma}{\gamma - 1}\frac{p_1}{\rho_1} + \frac{(V_1')^2 \sin^2(\theta - \alpha)}{2} \tag{85}$$

This is the same as the corresponding relation for two-dimensional flows.

The equation for the conservation of mass flow, the equation for the conservation of momentum in the direction normal to the shock, the energy equation, and the equation of the tangential velocity components in the xz-plane are the same as the corresponding equations for the two-dimensional case. It follows from the analysis of these relations given for the two-dimensional case that two of the boundary conditions on the shock are given by equations (46) and (51).

Figure 14(b) shows that the tangential velocity components in the y-direction are (to the first order in $d\lambda$)

$$\left(V_{o_t}\right)_y = V_o \sin\theta \, d\lambda \tag{86a}$$

$$\left(V_{1_t}'\right)_y = V_1 \sin(\theta - \alpha) \, d\lambda - v \tag{86b}$$

Thus, from equation (82),

$$V_o \sin\theta \, d\lambda = V_1 \sin(\theta - \alpha) \, d\lambda - v$$

or

$$v = -\left[V_o \sin\theta - V_1 \sin(\theta - \alpha)\right] d\lambda \tag{87}$$

The slope of the shock surface in the y-direction $d\lambda$ is given by

$$d\lambda = \frac{\partial G}{\partial y} \tag{88}$$

where $G(x,y,z) = 0$ is the equation of the perturbed shock surface. This surface G can be expressed as

$$G = \int_0^s d\theta \, ds \tag{89}$$

where s is the distance along the shock surface in the xz-plane measured from the leading edge of the airfoil. From equations (87), (88), and (89), the velocity component v can be expressed as

$$v = -\left[V_o \sin\theta - V_1 \sin(\theta - \alpha)\right] \frac{\partial}{\partial y} \int_0^s d\theta \, ds \tag{90}$$

From equations (42) to (45), the velocity component u and $d\theta$ are related by

$$d\theta = \left(K_{III} \frac{u}{V_1}\right)_{z=mx} \tag{91}$$

where

$$K_{III} = \frac{\left(1 - M_o^2 \frac{p_o}{p_1} \frac{\rho_o}{\rho_1} \sin^2\theta\right)\left[1 + \left(\frac{\rho_1}{\rho_o}\right)^2 \cot^2\theta\right]}{\left(1 - \frac{\rho_1}{\rho_o}\right) \cot\theta \left[1 + \frac{\rho_1}{\rho_o} - M_o^2 \frac{p_o \gamma}{p_1} \sin^2\theta \left(1 - \frac{\rho_o}{\rho_1}\right)\right]} \tag{92}$$

Values of K_{III} are given in table I for various angles of attack and Mach numbers. Substituting equation (91) into equation (90) yields

$$v = -\left[V_o \sin\theta - V_1 \sin(\theta - \alpha)\right] \frac{K_{III}}{V_1} \left[\int_0^s \left(\frac{\partial u}{\partial y}\right)_{z=mx} ds\right] \tag{93}$$

Equations (46), (51), and (93) are the boundary conditions on the shock surface.

The following relation can be obtained in a manner similar to that used in deriving equation (21):

$$-B_1^2 \frac{\partial u}{\partial x} + \frac{\partial v}{\partial y} + \frac{\partial w}{\partial z} = 0 \tag{94}$$

The components of equation (9) are

$$\frac{\partial u}{\partial x} = -\frac{1}{V_1 \rho_1}\frac{\partial \delta p_1}{\partial x} \tag{95a}$$

$$\frac{\partial v}{\partial x} = -\frac{1}{V_1 \rho_1}\frac{\partial \delta p_1}{\partial y} \tag{95b}$$

$$\frac{\partial w}{\partial x} = -\frac{1}{V_1 \rho_1}\frac{\partial \delta p_1}{\partial z} \tag{95c}$$

Eliminating δp_1 from equations (95) yields

$$\frac{\partial^2 u}{\partial x\, \partial y} = \frac{\partial^2 v}{\partial x^2}$$

$$\frac{\partial^2 u}{\partial x\, \partial z} = \frac{\partial^2 w}{\partial x^2}$$

$$\frac{\partial^2 v}{\partial x\, \partial z} = \frac{\partial^2 w}{\partial x\, \partial y}$$

These equations can be expressed by the vector equation

$$\nabla \times \frac{\partial \bar{q}}{\partial x} = 0 \tag{96}$$

Since the vector $\partial\bar{q}/\partial x$ is irrotational, it can be described in terms of a scalar potential function where

$$\nabla\Phi = \frac{\partial\bar{q}}{\partial x} \tag{97}$$

From equation (94), it follows that

$$\nabla_h \cdot \frac{\partial\bar{q}}{\partial x} = 0 \tag{98}$$

Substituting equation (97) into equation (98) yields the following partial differential equation for Φ:

$$-B_1{}^2\Phi_{xx} + \Phi_{yy} + \Phi_{zz} = 0 \tag{99}$$

Thus, the scalar potential function Φ must satisfy the three-dimensional wave equation.

The boundary condition on the surface for Φ is (from eq. (75))

$$(\Phi_z)_{z=0} = 0 \tag{100}$$

The boundary conditions on the shock surface are expressed in terms of u, v, and w and are not easily expressed as conditions on Φ.

A solution of equation (99) which satisfies the condition given by equation (100) is

$$\Phi = Ky$$

where K is a constant. If the conditions on the shock can be satisfied, the partial derivatives of the velocity components with respect to x are given by

$$\frac{\partial\Phi}{\partial x} = \frac{\partial u}{\partial x} = 0$$

$$\frac{\partial \Phi}{\partial y} = \frac{\partial v}{\partial x} = K$$

$$\frac{\partial \Phi}{\partial z} = \frac{\partial w}{\partial x} = 0$$

Thus, the velocity components u and w are independent of x and can be written as

$$u(x,y,z) = u(mz,y,z) \tag{101a}$$

$$w(x,y,z) = w(mz,y,z) \tag{101b}$$

The boundary condition on the surface requires that

$$(w)_{z=0} = p'y$$

Thus, the velocity component w must be of the form

$$w = p'y + \Omega(z) \tag{102}$$

where $\Omega(z)$ is an unknown function of z which is zero when z is zero. The velocity component u is given (from eqs. (46), (101a), and (102)) by

$$u = K_I\left[p'y + \Omega(z)\right] \tag{103}$$

Since

$$\frac{\partial v}{\partial x} = K$$

then by integration

$$v = (v)_{x=mz} + K(x - mz)$$

From equations (93), (101b), and (103),

$$(v)_{x=mz} = \left[V_o \sin\theta - V_1 \sin(\theta - \alpha)\right] K_{III}K_I\sqrt{m^2 + 1}\, p'z$$

Thus,

$$v = \left[V_o \sin\theta - V_1 \sin(\theta - \alpha)\right] \frac{K_{III}K_I}{V_1}\sqrt{m^2 + 1}\, p'z + K(x - mz) \tag{104}$$

Substituting equations (102), (103), and (104) into equation (94) yields the relation

$$\frac{\partial w}{\partial z} = \frac{d\Omega(z)}{dz} = 0$$

Thus,

$$\Omega(z) = 0$$

because $\Omega(0) = 0$.

The velocity components u and w are

$$u = K_I p'y \tag{105}$$

$$w = p'y \tag{106}$$

The change in entropy is given (from eqs. (51) and (105)) by

$$\frac{\delta S_1}{c_v} = \frac{K_{II}K_I p'y}{V_1} \tag{107}$$

The pressure is (from eqs. (25), (105), and (107))

$$\delta p_1 = -V_1 \rho_1 K_I p'y - \frac{p_1 K_{II} K_I p'y}{(\gamma - 1)V_1} \tag{108}$$

From equations (95b), (104), and (108) and the relation

$$\frac{\partial v}{\partial x} = K$$

the constant K is found to be given by

$$K = K_I a p'$$

Thus, equation (104) becomes

$$v = \left[V_o \sin \theta - V_1 \sin(\theta - \alpha)\right] \frac{K_I K_{III}}{V_1} \sqrt{m^2 + 1}\, p'z + K_I a p'(x - mz) \tag{109}$$

The pressure coefficient based on the free-stream conditions is given by

$$\frac{P}{\frac{p'y}{2V_o}} = -\frac{4K_I M_1}{M_o} \sqrt{\frac{p_1 \rho_1}{p_o \rho_o}} \left[1 + \frac{K_{II}}{M_1^2 \gamma(\gamma - 1)}\right] \tag{110}$$

Figure 15 presents the variation of $\frac{P}{p'y/2V_o}$ with angle of attack for various Mach numbers.

The effect of the change in entropy in the perturbed flow can be evaluated by setting K_{II} equal to zero in equation (110). The change in entropy is retained in the boundary condition on the shock which relates the velocity components u and w. An examination of equations (57) and (110) indicates that the percentage changes in the pressure coefficients which result from neglecting the change in entropy are the same for a small increment in α and for a small rate of roll.

Thus, the effect on $\frac{P}{p'y/2V_o}$ of neglecting the change in entropy can be obtained from the values of $\Delta P/\Delta\alpha$ given in figure 9.

An approximation to the pressure due to rolling can be obtained by neglecting the presence of the shock and assuming that the perturbed-flow velocity components can be expressed by derivatives of a potential function. This potential function is based on the velocity V_1 and is similar to the potential function associated with the flow over the upper surface. Under these assumptions, the velocity component u can be expressed as

$$u \approx -\frac{p'y}{B_1} \tag{111}$$

The pressure coefficient associated with equation (111) and based on the free-stream conditions is

$$\frac{P}{\frac{p'y}{2V_o}} \approx \frac{8M_1}{B_1M_o}\sqrt{\frac{p_1\rho_1}{p_o\rho_o}} \tag{112}$$

Figure 16 presents a comparison between exact and approximate values of the pressure coefficient on the lower surface of a rolling airfoil for various Mach numbers. This figure indicates that equation (112) is a good approximation to the pressure coefficient, except in a very small angle-of-attack range near the angle of attack where $M_1 = 1$.

AERODYNAMIC DERIVATIVES FOR RECTANGULAR WING OF INFINITE ASPECT RATIO

The expressions for the pressure coefficients on the upper and lower surfaces of an airfoil due to the various motions considered permit the calculation of the aerodynamic derivatives associated with these motions.

The derivative C_{L_α} for an airfoil at an arbitrary angle of attack α_o will be defined as

$$C_{L_\alpha} = \left[\left(\frac{\partial C_N}{\partial \alpha}\right)_{\alpha=\alpha_o} \cos \alpha_o\right]$$

It follows from equations (3a) and (57) that C_{L_α} is given by

$$C_{L_\alpha} = -\frac{2}{M_o^2}\left\{M_1^2 K_I \frac{p_1}{p_o}\left[1 + \frac{K_{II}}{M_1^2\gamma(\gamma - 1)}\right] - \frac{M_2^2}{B_2}\frac{p_2}{p_o}\right\}\cos \alpha_o \qquad (113)$$

Note that the center of pressure remains at the midchord point. Figure 17 presents the variation of C_{L_α} with angle of attack for various Mach numbers.

The derivatives C_{L_q} and C_{m_q} for an airfoil are (from eqs. (3b) and (71))

$$C_{L_q} = \frac{2}{M_o}\left[M_1\sqrt{\frac{p_1\rho_1}{p_o\rho_o}}\left(\frac{m - K_I a}{1 - K_I a B_1^2 m}\right) + \frac{2K_I a x_{cg}}{c} + \frac{2M_2}{B_2}\sqrt{\frac{p_2\rho_2}{p_o\rho_o}}\left(\frac{1}{2} - \frac{x_{cg}}{c}\right)\right]\cos \alpha_o \qquad (114)$$

$$C_{m_q} = -\frac{4M_1}{M_o}\sqrt{\frac{p_1\rho_1}{p_o\rho_o}}\left[\frac{m - K_I a}{1 - K_I a B_1^2 m}\left(\frac{1}{3} - \frac{x_{cg}}{2c}\right) + \frac{K_I a x_{cg}}{c}\left(\frac{1}{2} - \frac{x_{cg}}{c}\right)\right] -$$

$$\frac{4M_2}{3M_o B_2}\sqrt{\frac{p_2\rho_2}{p_o\rho_o}}\left[1 - 3\frac{x_{cg}}{c} + 3\left(\frac{x_{cg}}{c}\right)^2\right] \qquad (115)$$

Figures 18 and 19 present the variations of C_{L_q} and C_{m_q}, respectively, with angle of attack for various Mach numbers when the axis of pitch is located at the midchord point.

The derivative $C_{l_{p'}}$ of an airfoil is (from eqs. (3c) and (110))

$$C_{l_{p'}} = \frac{1}{\beta M_o}\left\{M_1 K_I \sqrt{\frac{p_1\rho_1}{p_o\rho_o}}\left[1 + \frac{K_{II}}{M_1^2\gamma(\gamma - 1)}\right] - \frac{M_2}{B_2}\sqrt{\frac{p_2\rho_2}{p_o\rho_o}}\right\}\cos\alpha \quad (116)$$

Figure 20 presents the variation of $C_{l_{p'}}$ with angle of attack for various Mach numbers.

APPROXIMATIONS TO AERODYNAMIC DERIVATIVES FOR WING OF INFINITE ASPECT RATIO

The approximate expressions for the pressure coefficients on the lower surface of an airfoil permit the derivation of simple approximate expressions for the aerodynamic coefficients associated with the motions considered previously.

An approximate expression for C_{L_α} is (from eqs. (3a) and (59))

$$C_{L_\alpha} \approx \frac{2}{M_o^2}\left(\frac{M_1^2}{B_1}\frac{p_1}{p_o} + \frac{M_2^2}{B_2}\frac{p_2}{p_o}\right)\cos\alpha_o \quad (117)$$

Figure 21 presents a comparison between exact and approximate values of C_{L_α} for various Mach numbers. This figure indicates that equation (117) yields a good approximation to the exact linearized value of C_{L_α} given by equation (113), except in a very small angle-of-attack range near the angle of attack for which $M_1 = 1$.

Approximate expressions for C_{L_q} and C_{m_q} are (from eqs. (3b) and (74))

$$C_{L_q} \approx \frac{4}{M_o}\left(\frac{M_1}{B_1}\sqrt{\frac{p_1\rho_1}{p_o\rho_o}} + \frac{M_2}{B_2}\sqrt{\frac{p_2\rho_2}{p_o\rho_o}}\right)\left(\frac{1}{2} - \frac{x_{cg}}{c}\right)\cos \alpha_o \qquad (118)$$

$$C_{m_q} \approx -\frac{4}{3M_o}\left(\frac{M_1}{B_1}\sqrt{\frac{p_1\rho_1}{p_o\rho_o}} + \frac{M_2}{B_2}\sqrt{\frac{p_2\rho_2}{p_o\rho_o}}\right)\left[1 - 3\,\frac{x_{cg}}{c} + 3\left(\frac{x_{cg}}{c}\right)^2\right] \qquad (119)$$

Note that the approximation for C_{L_q} (eq. (118)) yields a value of zero when the axis of pitch is located at the midchord point.

Figure 22 presents a comparison between exact and approximate values of C_{m_q} over a range of angles of attack for an axis of pitch located at the midchord point. This figure indicates that equation (119) is a good approximation to equation (115), except near the angle of attack for which $M_1 = 1$, when the axis of pitch is located at the midchord point.

An approximate expression for $C_{l_p'}$ is (from eqs. (3c) and (112))

$$C_{l_p'} \approx -\frac{1}{3M_o}\left(\frac{M_1}{B_1}\sqrt{\frac{p_1\rho_1}{p_o\rho_o}} + \frac{M_2}{B_2}\sqrt{\frac{p_2\rho_2}{p_o\rho_o}}\right)\cos \alpha_o \qquad (120)$$

Figure 23 presents a comparison between exact and approximate values of $C_{l_p'}$ for angles of attack up to the point where $M_1 = 1$, for various Mach numbers. This figure indicates that equation (120) is a good approximation to equation (116), except near the angle of attack where $M_1 = 1$.

The results of the approximate expressions for the pressures and aerodynamic coefficients indicate that these expressions are in good agreement with the exact values except for angles of attack in a small range near the angle of attack where $M_1 = 1$. An approximate expression for the pressure on the lower surface of an airfoil which has a constant vertical acceleration can be obtained by neglecting the presence of the

shock and by using a potential function based on the velocity V_1. This potential function is given by

$$\phi = \frac{\dot{\alpha}}{B_1}\left[-\frac{M_1^2x^2}{2B_1^2} + \frac{M_1^2}{2}z^2 + V_1t\left(x - B_1z\right)\right] \tag{121}$$

The approximate pressure coefficient based on the free-stream conditions is, for $t = 0$,

$$\frac{P}{\frac{\dot{\alpha}c}{2V_o}} \approx -\frac{4}{B_1^3}\frac{M_1}{M_o}\sqrt{\frac{p_1\rho_1}{p_o\rho_o}}\frac{x}{c} \tag{122}$$

Approximate expressions for $C_{L_{\dot{\alpha}}}$ and $C_{m_{\dot{\alpha}}}$ are (from eqs. (3d) and (122))

$$C_{L_{\dot{\alpha}}} \approx -\frac{2}{M_o}\left(\frac{M_1}{B_1^3}\sqrt{\frac{p_1\rho_1}{p_o\rho_o}} + \frac{M_2}{B_2^3}\sqrt{\frac{p_2\rho_2}{p_o\rho_o}}\right)\cos\alpha_o \tag{123}$$

$$C_{m_{\dot{\alpha}}} \approx \frac{4}{M_o}\left(\frac{M_1}{B_1^3}\sqrt{\frac{p_1\rho_1}{p_o\rho_o}} + \frac{M_2}{B_2^3}\sqrt{\frac{p_2\rho_2}{p_o\rho_o}}\right)\left(\frac{1}{3} - \frac{x_{cg}}{2c}\right) \tag{124}$$

Figure 24 presents the variation of the approximate values of $\frac{2C_{L_{\dot{\alpha}}}}{\cos\alpha_o}$ or $\frac{C_{m_{\dot{\alpha}}}}{\frac{1}{3} - \frac{x_{cg}}{2c}}$ with angle of attack for various Mach numbers.

The sum of the aerodynamic coefficients C_{m_q} and $C_{m_{\dot{\alpha}}}$ partly determines the damping of longitudinal oscillations of aircraft and is directly proportional to the aerodynamic damping of slowly oscillating airfoils (see appendix B of ref. 6); for these reasons the sum $C_{m_q} + C_{m_{\dot{\alpha}}}$

is considered separately. Figures 25 to 28 present the variation of $C_{m_q} + C_{m_{\dot{\alpha}}}$ (calculated from the approximate relations, eqs. (119) and (124)) with angle of attack for various Mach numbers and center-of-gravity locations. These figures indicate that, for an axis of rotation located between zero and the midchord point, $C_{m_q} + C_{m_{\dot{\alpha}}}$ is positive (destabilizing) for some part, or all, of the angle-of-attack range for which the results apply. Figure 28 indicates that, for an axis of rotation located at the three-quarter-chord point, $C_{m_q} + C_{m_{\dot{\alpha}}}$ is negative (stabilizing) for all angles of attack for which the results apply.

ESTIMATES OF AERODYNAMIC DERIVATIVES FOR RECTANGULAR WINGS OF FINITE ASPECT RATIO

The development of exact and approximate expressions for the aerodynamic derivatives of the wing with infinite aspect ratio permits estimations of the aerodynamic derivatives for rectangular wings. These estimations can be based on either the exact or the approximate expressions for the infinite-aspect-ratio wing. The approximate expressions will be used because they are much simpler and they yield results which are within a few percent of the exact values for most of the angle-of-attack range for which the expressions will be used.

The pressure within the tip regions can be approximated by assuming that the chordwise and spanwise variation of the pressure in this region is the same as the pressure variation determined by linear theory for small angles of surface deviation. The Mach number associated with the values from the linear theory is taken to be the Mach number of the flow over the surface in the region which is unaffected by the tips. Thus, the Mach number associated with the linear-theory values for the flow over the upper surface is M_2, and the Mach number associated with the flow over the lower surface is M_1. With these assumptions, the following approximate expressions for the aerodynamic derivatives based on the approximate expressions for the wing of infinite aspect ratio and the exact linear-theory expressions (from ref. 16) can be written as

$$C_{L_\alpha} \approx 2\left[\left(\frac{M_1}{M_o}\right)^2 \frac{p_1}{p_o}\left(\frac{1}{B_1} - \frac{1}{2AB_1^2}\right) + \left(\frac{M_2}{M_o}\right)^2 \frac{p_2}{p_o}\left(\frac{1}{B_2} - \frac{1}{2AB_2^2}\right)\right] \cos \alpha_o \qquad (125)$$

$$C_{m_\alpha} \approx \left\{ \left(\frac{M_1}{M_o}\right)^2 \frac{p_1}{p_o} \frac{1}{B_1}\left[\frac{2}{3AB_1} - 1 + 2\frac{x_{cg}}{c}\left(1 - \frac{1}{2AB_1}\right)\right] + \left(\frac{M_2}{M_o}\right)^2 \frac{p_2}{p_o} \frac{1}{B_2}\left[\frac{2}{3AB_2} - 1 + 2\frac{x_{cg}}{c}\left(1 - \frac{1}{2AB_2}\right)\right]\right\} \tag{126}$$

$$C_{L_q} \approx \left\{ \frac{M_1}{M_o}\sqrt{\frac{p_1\rho_1}{p_o\rho_o}} \frac{1}{B_1}\left[\frac{6AB_1 - 2}{3AB_1} - 4\frac{x_{cg}}{c}\left(1 - \frac{1}{2AB_1}\right)\right] + \frac{M_2}{M_o}\sqrt{\frac{p_2\rho_2}{p_o\rho_o}} \frac{1}{B_2}\left[\frac{6AB_2 - 2}{3AB_2} - 4\frac{x_{cg}}{c}\left(1 - \frac{1}{2AB_2}\right)\right]\right\} \cos \alpha_o \tag{127}$$

$$C_{m_q} \approx \frac{M_1}{M_o}\sqrt{\frac{p_1\rho_1}{p_o\rho_o}} \frac{1}{2B_1}\left[\frac{3 - 8AB_1}{3AB_1} + \frac{x_{cg}}{c}\left(8 - \frac{4}{AB_1}\right) - \left(\frac{x_{cg}}{c}\right)^2\left(8 - \frac{4}{AB_1}\right)\right] + \frac{M_2}{M_o}\sqrt{\frac{p_2\rho_2}{p_o\rho_o}} \frac{1}{2B_2}\left[\frac{3 - 8AB_2}{3AB_2} + \frac{x_{cg}}{c}\left(8 - \frac{4}{AB_2}\right) - \left(\frac{x_{cg}}{c}\right)^2\left(8 - \frac{4}{AB_2}\right)\right] \tag{128}$$

$$C_{l_{p'}} \approx -\left[\frac{M_1}{2B_1M_o}\sqrt{\frac{p_1\rho_1}{p_o\rho_o}}\left(\frac{2}{3} - \frac{1}{AB_1} + \frac{1}{3A^2B_1^2} + \frac{1}{12A^3B_1^3}\right) + \frac{M_2}{2B_2M_o}\sqrt{\frac{p_2\rho_2}{p_o\rho_o}}\left(\frac{2}{3} - \frac{1}{AB_2} + \frac{1}{3A^2B_2^2} + \frac{1}{12A^3B_2^3}\right)\right] \cos \alpha_o \tag{129}$$

$$C_{L_{\dot{\alpha}}} \approx \left[\frac{M_1}{M_o} \sqrt{\frac{p_1 \rho_1}{p_o \rho_o}} \frac{1}{B_1^3} \left(-2 + \frac{4 + 2B_1^2}{3AB_1} \right) + \frac{M_2}{M_o} \sqrt{\frac{p_2 \rho_2}{p_o \rho_o}} \frac{1}{B_2^3} \left(-2 + \frac{4 + 2B_2^2}{3AB_2} \right) \right] \cos \alpha_o \tag{130}$$

$$C_{m_{\dot{\alpha}}} \approx \frac{M_1}{M_o} \sqrt{\frac{p_1 \rho_1}{p_o \rho_o}} \frac{1}{B_1^3} \left(\frac{4}{3} - \frac{2x_{cg}}{c} - \frac{2 + B_1^2}{2AB_1} + \frac{x_{cg}}{c} \frac{4 + 2B_1^2}{3AB_1} \right) +$$

$$\frac{M_2}{M_o} \sqrt{\frac{p_2 \rho_2}{p_o \rho_o}} \frac{1}{B_2^3} \left(\frac{4}{3} - 2 \frac{x_{cg}}{c} - \frac{2 + B_2^2}{2AB_2} + \frac{x_{cg}}{c} \frac{4 + 2B_2^2}{3AB_2} \right) \tag{131}$$

The expressions for the aerodynamic derivatives based on the linearized theory which were used in equations (125) to (131) are limited to cases where the parameter AB is equal to or greater than 1. Thus, equations (125) to (131) are limited to angles of attack and Mach numbers where AB_1 is equal to or greater than 1. For angles of attack and Mach numbers that cause AB_1 to lie between 1 and 2, the tips affect over one-half the wing area on the lower surface; thus the values calculated from equations (125) to (131) may differ considerably from the true values. Figures 29 to 39 present the variations of the estimated aerodynamic coefficients of rectangular wings with angle of attack for aspect ratios of 2 and 4. In these figures the dashed portions of the curves indicate the region where the parameter AB_1 lies between 1 and 2.

DISCUSSION OF RESULTS

If the change in entropy in the perturbed flow is neglected and the change in entropy in the boundary conditions on the perturbation velocity components on the shock surface is retained, a large error results for Mach numbers of 3 and 4. The results also indicate that the aerodynamic derivatives for the wing of infinite aspect ratio can be approximated very well by simple expressions over most of the angle-of-attack range for which the theory is valid.

The results for the aerodynamic derivatives seem to indicate that there is a rough analogy between increasing the angle of attack at a given Mach number and decreasing the Mach number at zero angle of attack. For example, the approximate expression for C_{L_α} given by equation (117) can be written as

$$\left(C_{L_\alpha}\right)_{\alpha=\alpha_o} \approx \left[\left(\frac{M_1}{M_o}\right)^2 \frac{p_1}{p_o} \frac{C_{L_\alpha}}{2}\right]_{\substack{B=B_1 \\ \alpha=0}} + \left[\left(\frac{M_2}{M_o}\right)^2 \frac{p_2}{p_o} \frac{C_{L_\alpha}}{2}\right]_{\substack{B=B_2 \\ \alpha=0}}$$

As the angle of attack increases, the first term on the right-hand side of the preceding equation increases, and the second term on the right-hand side decreases. Inasmuch as $\left(C_{L_\alpha}\right)_{\alpha=0}$ approaches infinity as the Mach number approaches 1, this type of variation will dominate the variation of equation (117) as the angle of attack approaches the angle for which $M_1 = 1$. An examination of the other approximate expressions for the aerodynamic derivatives shows similar analogies between increasing the angle of attack at a given Mach number and decreasing the Mach number at zero angle of attack.

The calculated values of the aerodynamic derivatives show very rapid changes with angle of attack near the angle of attack where $M_1 = 1$. It is expected that, provided the lower surface of the airfoil is not flat, the thickness of the airfoil may tend to modify the rapid changes with angle of attack because the thickness of the airfoil would change the local flow over the lower surface.

The variations of the estimated aerodynamic coefficients of rectangular wings with angle of attack presented in figures 29 to 39 indicate that the effect of aspect ratio on the variation of these coefficients with angle of attack is quite strong. These variations can be explained on the basis of the results from the wing of infinite aspect ratio at finite angles of attack and the results from rectangular wings at zero angle of attack (linearized theory). For example, consider the variations of the estimated C_{L_α} with angle of attack for $M_o = 4.0$ as shown in figure 29. At the higher angles of attack, the changes in the pressures, the densities, and the local Mach numbers in the basic flow cause the contribution to the estimated C_{L_α} of the lower surface to outweigh greatly the contribution to the estimated C_{L_α} of the upper surface. The region influenced by the tips on the lower surface increases as the angle of attack increases; thus, the tips tend to decrease the estimated C_{L_α} at

the higher angles of attack. This effect causes the curves of the estimated C_{L_α} at the higher angles of attack and the higher Mach numbers to have slopes considerably lower than those of the curves for the wing of infinite aspect ratio.

CONCLUDING REMARKS

Perturbation of the flow over a two-dimensional flat plate at finite angles of attack is used to obtain a first-order evaluation of the damping in roll, the lift and pitching moment due to an increment in the angle of attack, and the lift and pitching moment due to a steady pitching velocity for a rectangular wing of infinite aspect ratio at supersonic speeds. Approximations based on the results of the linearized theory and on the flow over a two-dimensional flat plate at finite angles of attack are derived and are shown to yield results which are in good agreement with the exact first-order theory. Approximate expressions are also derived for the lift and pitching moment due to a constant vertical acceleration. Estimations of the aerodynamic derivatives for rectangular wings of finite aspect ratio are derived by the combined use of the approximate relations for the infinite-aspect-ratio wing at finite angles of attack and the results of the linearized theory for vanishingly small angles of attack.

The same type of analysis used herein can be applied to the swept-back wing of infinite aspect ratio with supersonic leading edges. The results for the aerodynamic derivatives of this wing could also be used to make estimations of the aerodynamic derivatives for a number of finite-aspect-ratio wings in certain Mach number ranges in a manner similar to the method used in the present paper for the rectangular wing.

Langley Aeronautical Laboratory,
National Advisory Committee for Aeronautics,
Langley Field, Va., January 25, 1955.

APPENDIX

DETERMINATION OF FIRST-ORDER-PERTURBATION EQUATIONS FOR FLOW BEHIND A TWO-DIMENSIONAL SHOCK

Consider first the vector form of the Euler equations of motion (eq. (4)):

$$\nabla \frac{W^2}{2} + (\nabla \times W) \times W = -\frac{1}{\rho} \nabla p \tag{A1}$$

The first term of the preceding equation can be written, by the use of equation (8a), as

$$\nabla \frac{W^2}{2} = \nabla\left(\frac{V_1^2 + 2V_1 u + u^2}{2} + \frac{v^2}{2} + \frac{w^2}{2}\right)$$

$$= i\left(V_1 \frac{\partial u}{\partial x} + u \frac{\partial u}{\partial x} + v \frac{\partial v}{\partial x} + w \frac{\partial w}{\partial x}\right) +$$

$$j\left(V_1 \frac{\partial u}{\partial y} + u \frac{\partial u}{\partial y} + v \frac{\partial v}{\partial y} + w \frac{\partial w}{\partial y}\right) +$$

$$k\left(V_1 \frac{\partial u}{\partial z} + u \frac{\partial u}{\partial z} + v \frac{\partial v}{\partial z} + w \frac{\partial w}{\partial z}\right)$$

When only the first-order terms are retained, this expression becomes

$$\nabla \frac{W^2}{2} = V_1 \nabla u \tag{A2}$$

The second term of equation (A1) can be expressed, by the use of equation (8a), as

$$(\nabla \times W) \times W = i\left(w\frac{\partial u}{\partial z} - w\frac{\partial w}{\partial x} - v\frac{\partial v}{\partial x} + v\frac{\partial u}{\partial y}\right) +$$

$$j\left[\left(V_1 + u\right)\frac{\partial v}{\partial x} - \left(V_1 + u\right)\frac{\partial u}{\partial y} - w\frac{\partial w}{\partial y} + w\frac{\partial v}{\partial z}\right] +$$

$$k\left[v\frac{\partial w}{\partial y} - v\frac{\partial v}{\partial z} - \left(V_1 + u\right)\frac{\partial u}{\partial z} + \left(V_1 + u\right)\frac{\partial w}{\partial x}\right]$$

When only the first-order terms are retained, this expression becomes

$$(\nabla \times W) \times W = i(0) + jV_1\left(\frac{\partial v}{\partial x} - \frac{\partial u}{\partial y}\right) + kV_1\left(\frac{\partial w}{\partial x} - \frac{\partial u}{\partial z}\right) \tag{A3}$$

The last term of equation (A1) can be expressed as

$$-\frac{1}{\rho}\Delta p = -\frac{1}{\rho_1 + \delta\rho_1}\nabla\left(p_1 + \delta p_1\right)$$

$$= -\frac{1}{\rho_1}\left(1 - \frac{\delta\rho_1}{\rho_1} + \cdots\right)\nabla\delta p_1$$

When only the first-order terms are retained, this expression becomes

$$-\frac{1}{\rho}\nabla p = -\frac{1}{\rho_1}\nabla\delta p_1 \tag{A4}$$

To the first order, equation (A1) can now be expressed, from equations (A2), (A3), and (A4), as

$$\nabla u + j\left(\frac{\partial v}{\partial x} - \frac{\partial u}{\partial y}\right) + k\left(\frac{\partial w}{\partial x} - \frac{\partial u}{\partial z}\right) = - \frac{1}{V_1 \rho_1} \nabla \delta p_1 \tag{A5}$$

This is equation (9) in the body of the paper.

Consider now the equation of continuity (eq. (5)). This equation can be expressed as

$$\nabla \cdot \rho W = \nabla \cdot \left(\rho_1 + \delta\rho_1\right)\left[i\left(V_1 + u\right) + jv + kw\right] = 0 \tag{A6}$$

When only the first-order terms are retained, the preceding equation can be expressed as (eq. (10))

$$\frac{\partial u}{\partial x} + \frac{\partial v}{\partial y} + \frac{\partial w}{\partial z} = -\frac{V_1}{\rho_1} \frac{\partial \delta\rho_1}{\partial x} \tag{A7}$$

The entropy equation can be expressed as

$$p_1 + \delta p_1 = \left(\rho_1 + \delta\rho_1\right)^{\gamma} e^{\frac{S_1 + \delta S_1}{c_v}}$$

or

$$p_1 + \delta p_1 = {\rho_1}^{\gamma} e^{S_1/c_v} + \gamma\, \delta\rho_1\, {\rho_1}^{\gamma-1} e^{S_1/c_v} + \frac{\delta S_1}{c_v} {\rho_1}^{\gamma} e^{S_1/c_v} + \cdots \tag{A8}$$

since (from eq. (6))

$$p_1 = {\rho_1}^{\gamma} e^{S_1/c_v}$$

Thus, to the first order in pressure, density, and entropy, equation (A8) becomes equation (11):

$$\frac{\delta p_1}{p_1} - \gamma \frac{\delta \rho_1}{\rho_1} = \frac{\delta S_1}{c_v} \tag{A9}$$

Now equation (A1) can be written, by the use of equations (8), as

$$\frac{\gamma}{\gamma - 1} \frac{p_1 + \delta p_1}{\rho_1 + \delta \rho_1} + \frac{V_1^2 + 2V_1 u + u^2}{2} + \frac{v^2}{2} + \frac{w^2}{2} = \frac{W_{max}^2}{2}$$

or as

$$\frac{\gamma}{\gamma - 1}\left(p_1 + \delta p_1\right)\frac{1}{\rho_1}\left(1 - \frac{\delta \rho_1}{\rho_1} + \cdots\right) + \frac{V_1^2 + 2V_1 u + u^2}{2} + \frac{v^2}{2} + \frac{w^2}{2} = \frac{W_{max}^2}{2} \tag{A10}$$

When only the terms up to and including the first-order are retained, equation (A10) becomes

$$\frac{\gamma}{\gamma - 1} \frac{p_1}{\rho_1} + \frac{\gamma}{\gamma - 1} \frac{\delta p_1}{\rho_1} - \frac{\gamma}{\gamma - 1} \frac{p_1}{\rho_1} \frac{\delta \rho_1}{\rho_1} + \frac{V_1^2}{2} + V_1 u = \frac{W_{max}^2}{2} \tag{A11}$$

Since

$$\frac{\gamma}{\gamma - 1} \frac{p_1}{\rho_1} + \frac{V_1^2}{2} = \frac{W_{max}^2}{2}$$

equation (A11) can be reduced to equation (12):

$$\frac{\delta p_1}{p_1} - \frac{\delta \rho_1}{\rho_1} = -\frac{\gamma - 1}{\gamma} \frac{V_1 \rho_1}{p_1} u = \frac{\delta T_1}{T_1}$$

REFERENCES

1. Busemann, A.: Aerodynamic Lift at Supersonic Speeds. Rep. No. Ae. Techl. 1201 (Rep. No. 2844, British A.R.C.), Feb. 3, 1937. (From Luftfahrtforschung, Bd. 12, Nr. 6, Oct. 3, 1935, pp. 210-220.)

2. Van Dyke, Milton D.: A Study of Second-Order Supersonic Flow Theory. NACA Rep. 1081, 1952. (Supersedes NACA TN 2200.)

3. Van Dyke, Milton D.: First- and Second-Order Theory of Supersonic Flow Past Bodies of Revolution. Jour. Aero. Sci., vol. 18, no. 3, Mar. 1951, pp. 161-178.

4. Martin, John C., and Gerber, Nathan: On the Effect of Thickness on the Damping in Roll of Airfoils at Supersonic Speeds. Rep. No. 843, Ballistic Res. Labs., Aberdeen Proving Ground, Jan. 1953.

5. Martin, John C., and Gerber, Nathan: The Effect of Thickness on Pitching Airfoils at Supersonic Speeds. Rep. No. 859, Ballistic Res. Labs., Aberdeen Proving Ground, Apr. 1953.

6. Martin, John C., and Gerber, Nathan: The Effect of Thickness on Airfoils With Constant Vertical Acceleration at Supersonic Speeds. Rep. No. 866, Ballistic Res. Labs., Aberdeen Proving Ground, May 1953.

7. Ivey, H. Reese: Notes on the Theoretical Characteristics of Two-Dimensional Supersonic Airfoils. NACA TN 1179, 1947.

8. Carrier, G. F.: The Oscillating Wedge in a Supersonic Stream. Jour. Aero. Sci., vol. 16, no. 3, Mar. 1949, pp. 150-152.

9. Carrier, G. F.: On the Stability of the Supersonic Flows Past a Wedge. Quarterly Appl. Math., vol. VI, no. 4, Jan. 1949, pp. 367-378.

10. Chu, Boa-Teh: On Weak Interaction of Strong Shock and Mach Waves Generated Downstream of the Shock. Jour. Aero. Sci., vol. 19, no. 7, July 1952, pp. 433-446.

11. Carrier, G. F., and Carlson, F. D.: On the Propagation of Small Disturbances in a Moving Compressible Fluid. Quarterly Appl. Math., vol. IV, no. 1, Apr. 1946, pp. 1-12.

12. Schaefer, M.: The Relation Between Wall Curvature and Shock Front Curvature in Two-Dimensional Gas Flow. Tech. Rep. No. F-TS-1202-IA, Air Materiel Command, U. S. Air Force, Jan. 1949.

13. Sears, W. R.: The Linear-Perturbation Theory for Rotational Flow. Jour. Math. and Phys., vol. XXVIII, no. 4, Jan. 1950, pp. 268-271.

14. Sauer, Robert: Introduction to Theoretical Gas Dynamics. J. W. Edwards (Ann Arbor, Mich.), 1947.

15. Ames Research Staff: Equations, Tables, and Charts for Compressible Flow. NACA Rep. 1135, 1953. (Supersedes NACA TN 1428.)

16. Harmon, Sidney M.: Stability Derivatives at Supersonic Speeds of Thin Rectangular Wings With Diagonals Ahead of Tip Mach Lines. NACA Rep. 925, 1949. (Supersedes NACA TN 1706.)

TABLE I

FUNCTIONS ASSOCIATED WITH THE PERTURBED FLOW OVER LOWER SURFACE

α, deg	θ, deg	K_I	K_{II}	K_{III}
$M_o = 1.25$				
0	53.1	-1.33	0	-1.04
2.07	57.0	-1.67	-.002	-1.27
3.34	60.0	-2.09	-.005	-1.29
4.30	63.0	-2.84	-.008	-1.33
4.76	65.0	-3.77	-.010	-1.36
5.31	66.4	-5.12	-.011	-1.40
$M_o = 1.5$				
0	41.8	-0.89	0	-1.01
.18	42.0	-.90	0	-1.18
1.95	44.0	-.97	-.003	-1.20
2.78	45.0	-1.02	-.004	-1.20
3.58	46.0	-1.07	-.010	-1.19
5.08	48.0	-1.18	-.019	-1.18
7.08	51.0	-1.41	-.031	-1.16
8.77	54.0	-1.73	-.043	-1.13
10.13	57.0	-2.25	-.052	-1.11
11.16	60.0	-3.22	-.058	-1.10
11.64	62.0	-4.55	-.061	-1.09
11.69	62.25	-4.80	-.061	-1.09
$M_o = 1.75$				
0	34.85	-0.70	0	-1.07
1.27	36.0	-.72	-.002	-1.28
3.35	38.0	-.78	-.013	-1.27
5.30	40.0	-.85	-.030	-1.25
7.11	42.0	-.93	-.048	-1.23
11.8	48.0	-1.29	-.095	-1.14
13.8	51.0	-1.57	-.109	-1.09
15.3	54.0	-2.00	-.117	-1.04
16.6	57.0	-2.72	-.120	-1.00
17.5	60.0	-4.26	-.119	-.96
17.7	61.0	-5.26	-.118	-.95
17.8	61.3	-5.66	-.117	-.95
$M_o = 2.0$				
0	30.0	-0.58	0	-1.15
3.56	33.0	-.64	-.023	-1.39
6.07	35.0	-.69	-.053	-1.37
7.79	37.0	-.76	-.085	-1.34
9.71	39.0	-.83	-.115	-1.30
14.7	45.0	-1.14	-.180	-1.17
16.9	48.0	-1.37	-.195	-1.10
19.3	52.0	-1.83	-.200	-1.02
20.7	55.0	-2.40	-.195	-.96
22.4	60.0	-4.91	-.177	-.88
22.7	61.5	-7.13	-.170	-.86
$M_o = 2.25$				
0	26.4	-0.50	0	-1.26
2.09	28.0	-.52	-.013	-1.52
4.53	30.0	-.56	-.050	-1.51
7.90	33.0	-.64	-.13	-1.47
9.96	35.0	-.72	-.17	-1.42
15.5	41.0	-.95	-.28	-1.26
20.0	47.0	-1.34	-.31	-1.10
21.9	50.0	-1.64	-.30	-1.03
23.6	53.0	-2.09	-.28	-.96
25.0	56.0	-2.81	-.27	-.89
26.0	59.0	-4.28	-.24	-.84
26.4	61.0	-6.56	-.22	-.80
26.6	62.0	-9.05	-.21	-.79

α, deg	θ, deg	K_I	K_{II}	K_{III}
$M_o = 2.5$				
0	23.6	-0.44	0	-1.36
1.94	25.0	-.46	-.016	-1.67
4.49	27.0	-.49	-.075	-1.65
6.86	29.0	-.54	-.15	-1.62
7.99	30.0	-.56	-.19	-1.60
16.8	39.0	-.87	-.41	-1.33
21.6	45.0	-1.22	-.42	-1.14
25.4	51.0	-1.82	-.38	-.98
28.3	57.0	-3.24	-.31	-.84
29.2	60.0	-5.21	-.28	-.78
29.6	62.0	-8.85	-.25	-.75
29.7	62.6	-11.4	-.25	-.74
$M_o = 2.75$				
0	21.3	-0.39	0	-1.48
2.34	23.0	-.41	-.032	-1.80
4.93	25.0	-.45	-.12	-1.80
7.34	27.0	-.49	-.16	-1.76
11.7	31.0	-.59	-.42	-1.63
20.0	40.0	-.94	-.57	-1.29
26.3	49.0	-1.61	-.50	-1.01
29.7	55.0	-2.61	-.40	-.86
31.7	61.0	-6.39	-.31	-.73
31.9	62.0	-8.45	-.29	-.72
32.1	63.2	-14.16	-.27	-.70
$M_o = 3.0$				
0	19.5	-0.35	0	-1.59
2.18	21.0	-.37	-.039	-1.95
4.83	23.0	-.40	-.16	-1.95
7.28	25.0	-.44	-.31	-1.90
8.45	26.0	-.47	-.38	-1.87
20.1	38.0	-.87	-.74	-1.37
27.0	47.0	-1.44	-.62	-1.05
30.5	53.0	-2.20	-.50	-.89
31.9	56.0	-2.91	-.44	-.82
33.0	59.0	-4.26	-.38	-.75
33.8	62.0	-8.04	-.32	-.69
34.0	63.8	-17.30	-.29	-.66
$M_o = 3.5$				
0	16.6	-0.30	0	-1.83
2.06	18.0	-.31	-.063	-2.25
4.77	20.0	-.34	-.28	-2.25
7.25	22.0	-.38	-.53	-2.19
8.43	23.0	-.40	-.67	-2.15
12.8	27.0	-.50	-.98	-1.93
17.7	32.0	-.66	-1.13	-1.65
25.2	41.0	-1.05	-.99	-1.25
29.5	47.0	-1.47	-.81	-1.04
33.1	53.0	-2.21	-.62	-.87
35.7	59.0	-4.14	-.45	-.73
36.5	62.0	-7.36	-.38	-.67
36.7	63.0	-10.0	-.36	-.65
36.8	64.0	-15.7	-.34	-.63
36.8	64.6	-23.5	-.32	-.62
$M_o = 4.0$				
0	14.5	-0.26	0	-2.07
2.27	16.0	-.27	-.12	-2.56
4.97	18.0	-.31	-.49	-2.57
7.44	20.0	-.34	-.87	-2.46
9.74	22.0	-.38	-1.18	-2.34
14.0	26.0	-.49	-1.53	-2.05
17.8	30.0	-.61	-1.60	-1.79
22.2	35.0	-.79	-1.49	-1.50
29.1	44.0	-1.26	-1.09	-1.12
33.1	50.0	-1.79	-.83	-.94
34.8	53.0	-2.39	-.71	-.85
36.2	56.0	-2.87	-.61	-.78
37.4	59.0	-4.04	-.51	-.71
38.3	62.0	-6.88	-.42	-.65
38.6	64.0	-13.3	-.37	-.61
38.7	65.0	-25.5	-.35	-.59
38.8	65.25	-33.3	-.34	-.59

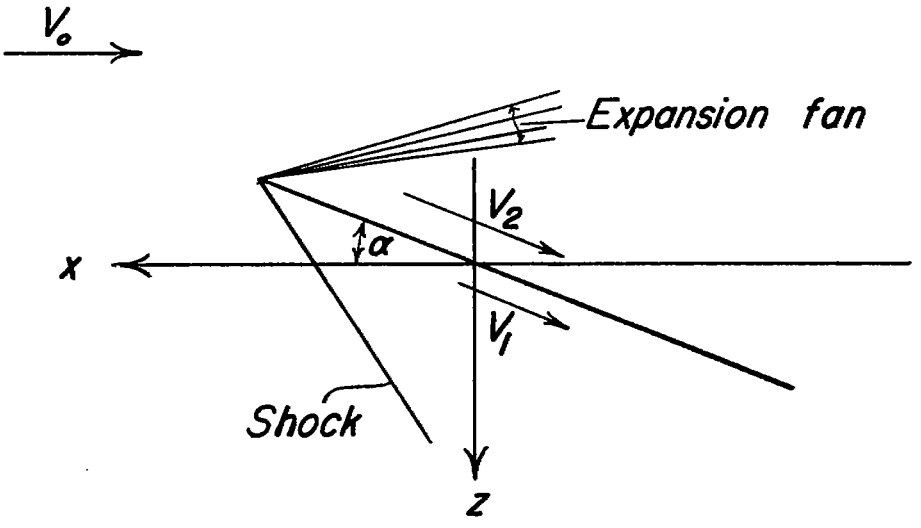

(a) Basic flow.

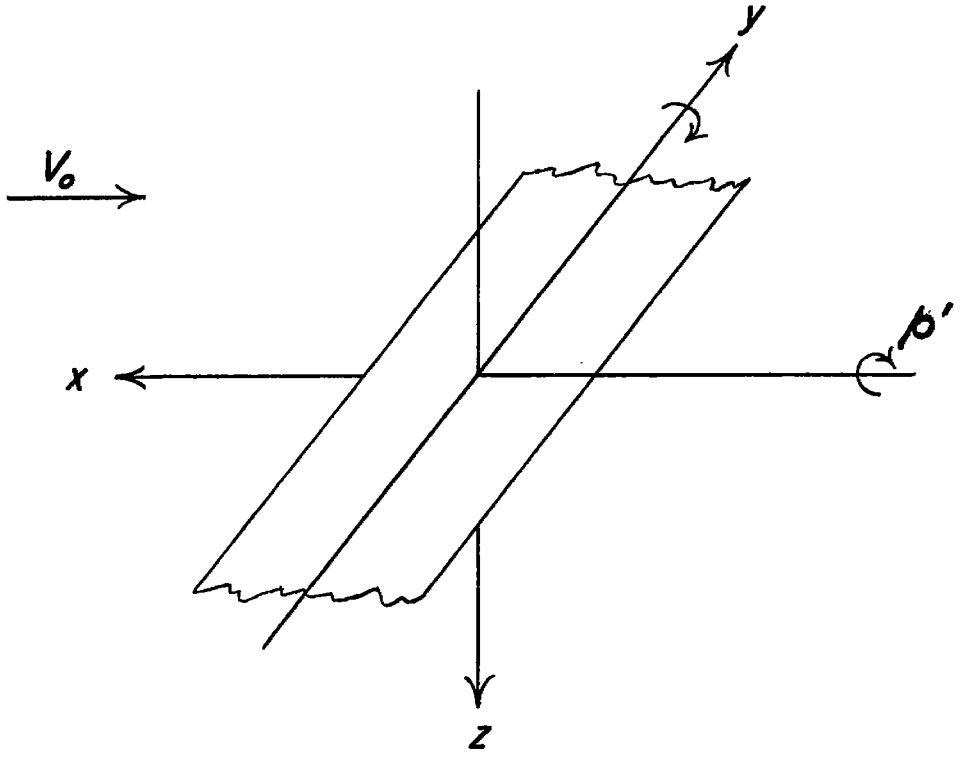

(b) Stability axes.

Figure 1.- Rectangular wing of infinite aspect ratio at a finite angle of attack.

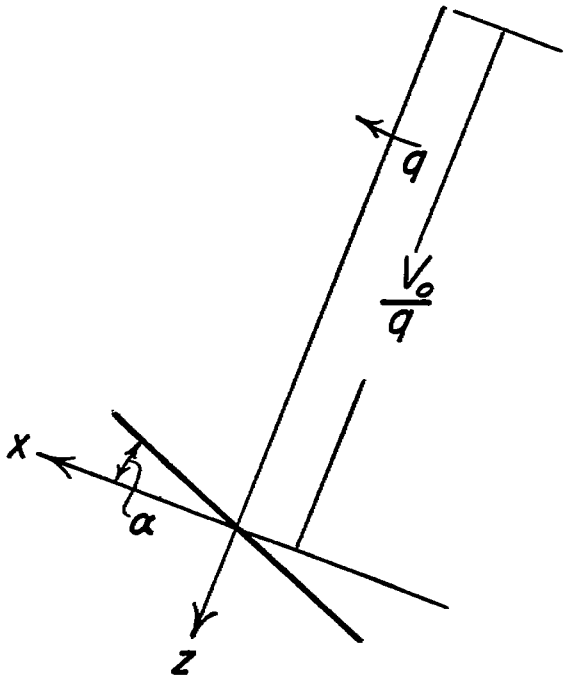

Figure 2.- A set of axes fixed to an airfoil which has a constant rate of pitch.

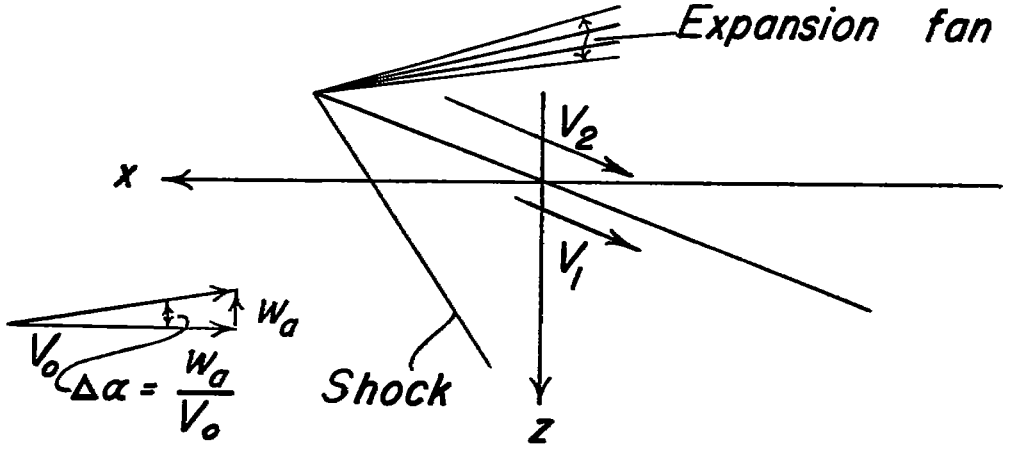

Figure 3.- Illustration of change in free-stream direction viewed from the stability axes for a given increment in angle of attack.

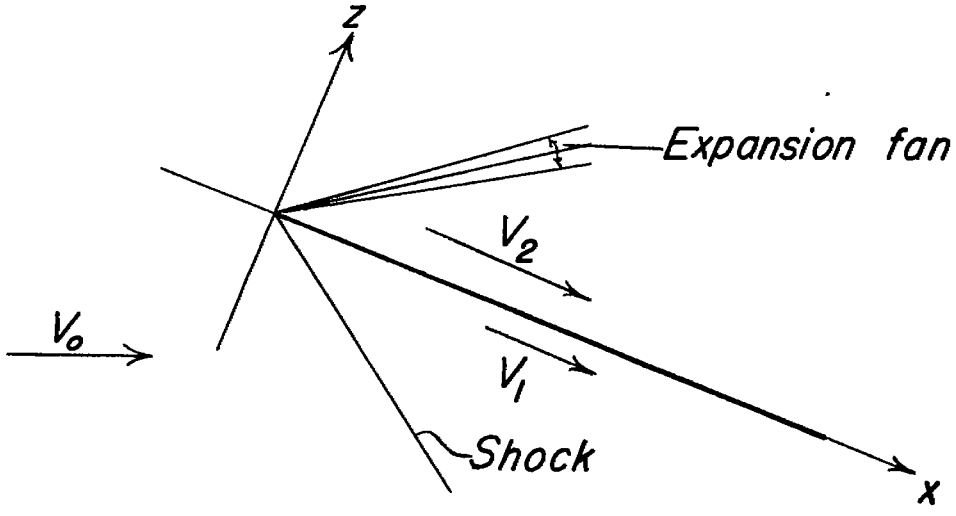

(a) Side view.

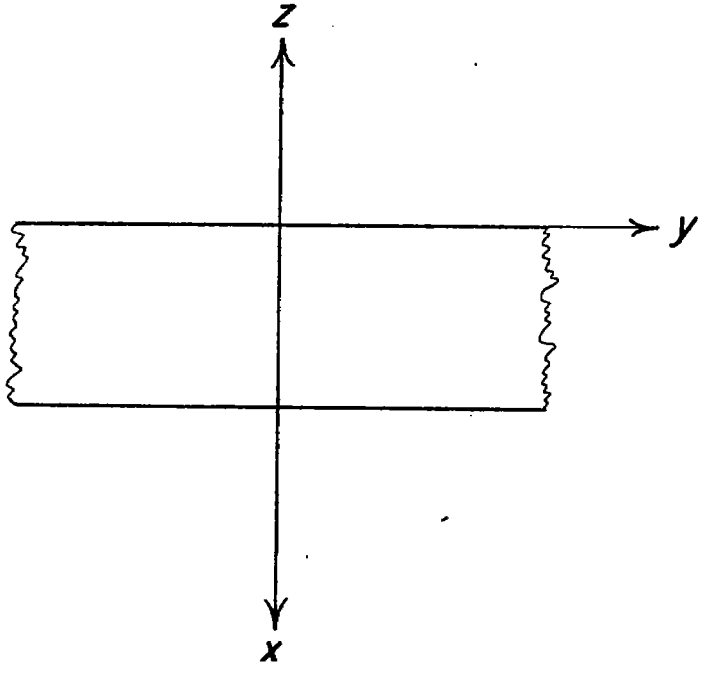

(b) Rear view from free-stream direction.

Figure 4.- Coordinate axes used in analysis of flow over upper surface.

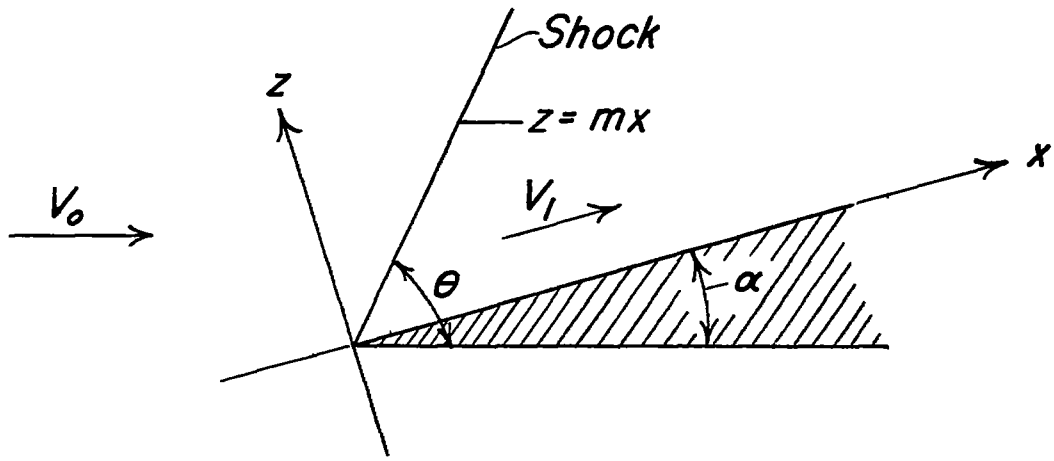

Figure 5.- Coordinate axes used in analysis of perturbed flow behind a two-dimensional shock.

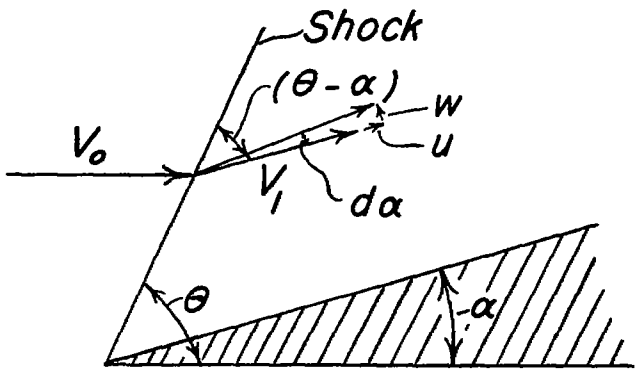

Figure 6.- Velocity components associated with perturbed flow behind a two-dimensional shock.

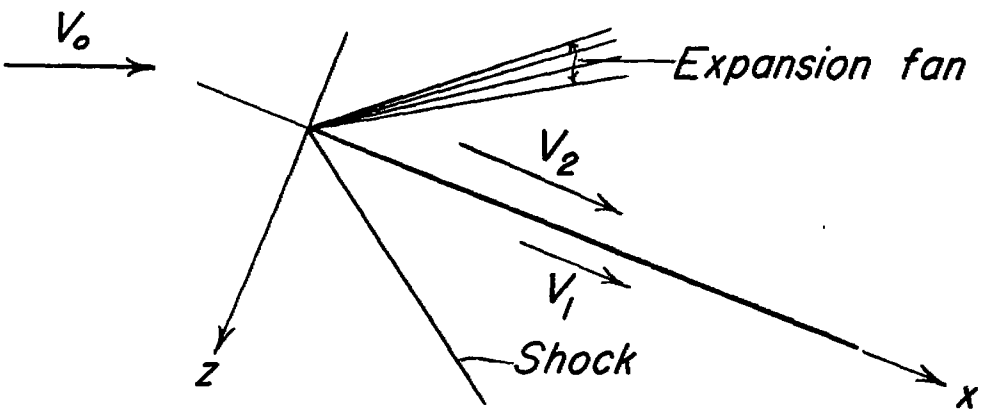

Figure 7.- Coordinates used in analyzing flow over lower surface of an airfoil.

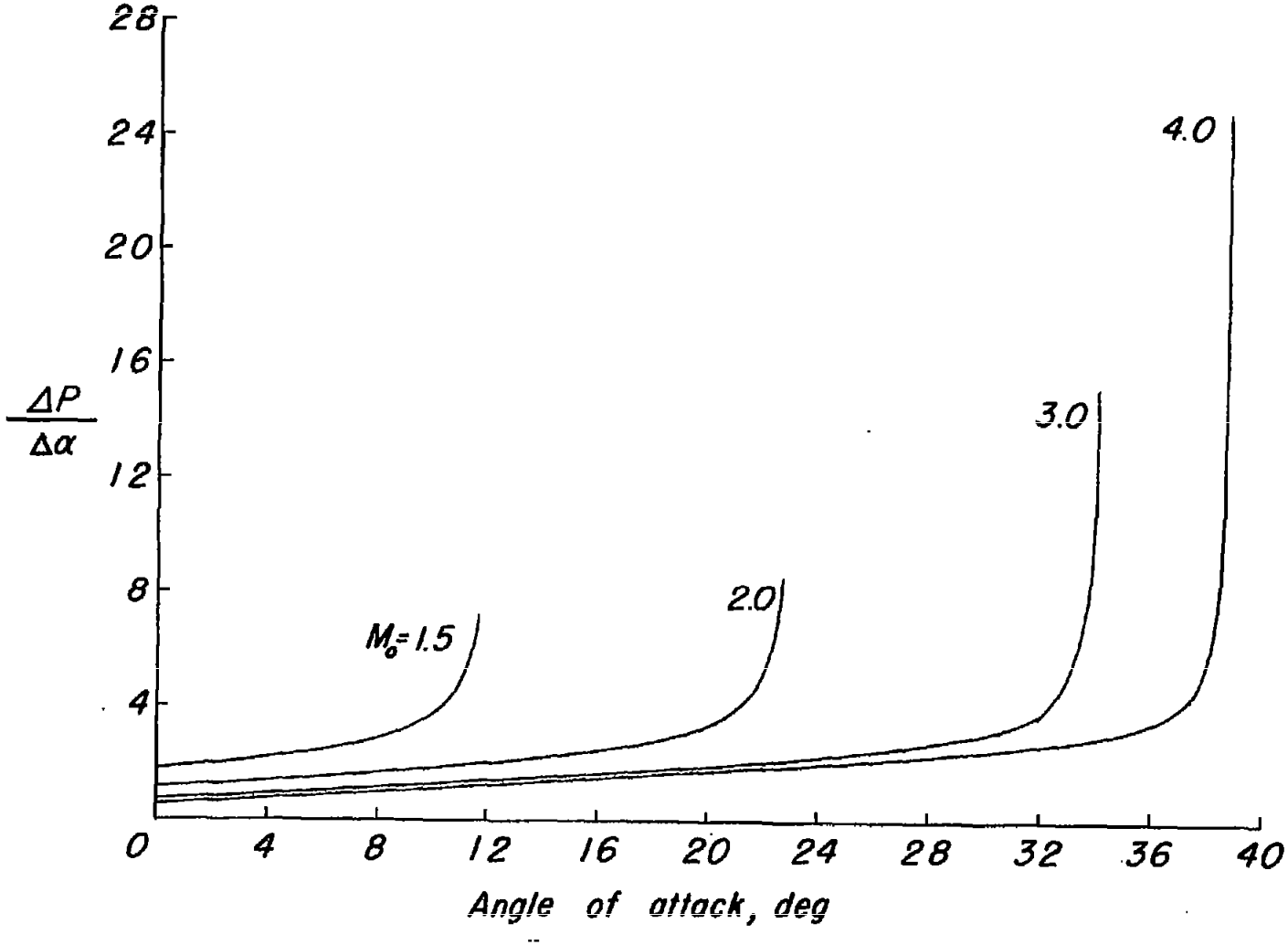

Figure 8.- Variation of $\Delta P/\Delta\alpha$ with angle of attack on lower surface of an airfoil for various Mach numbers.

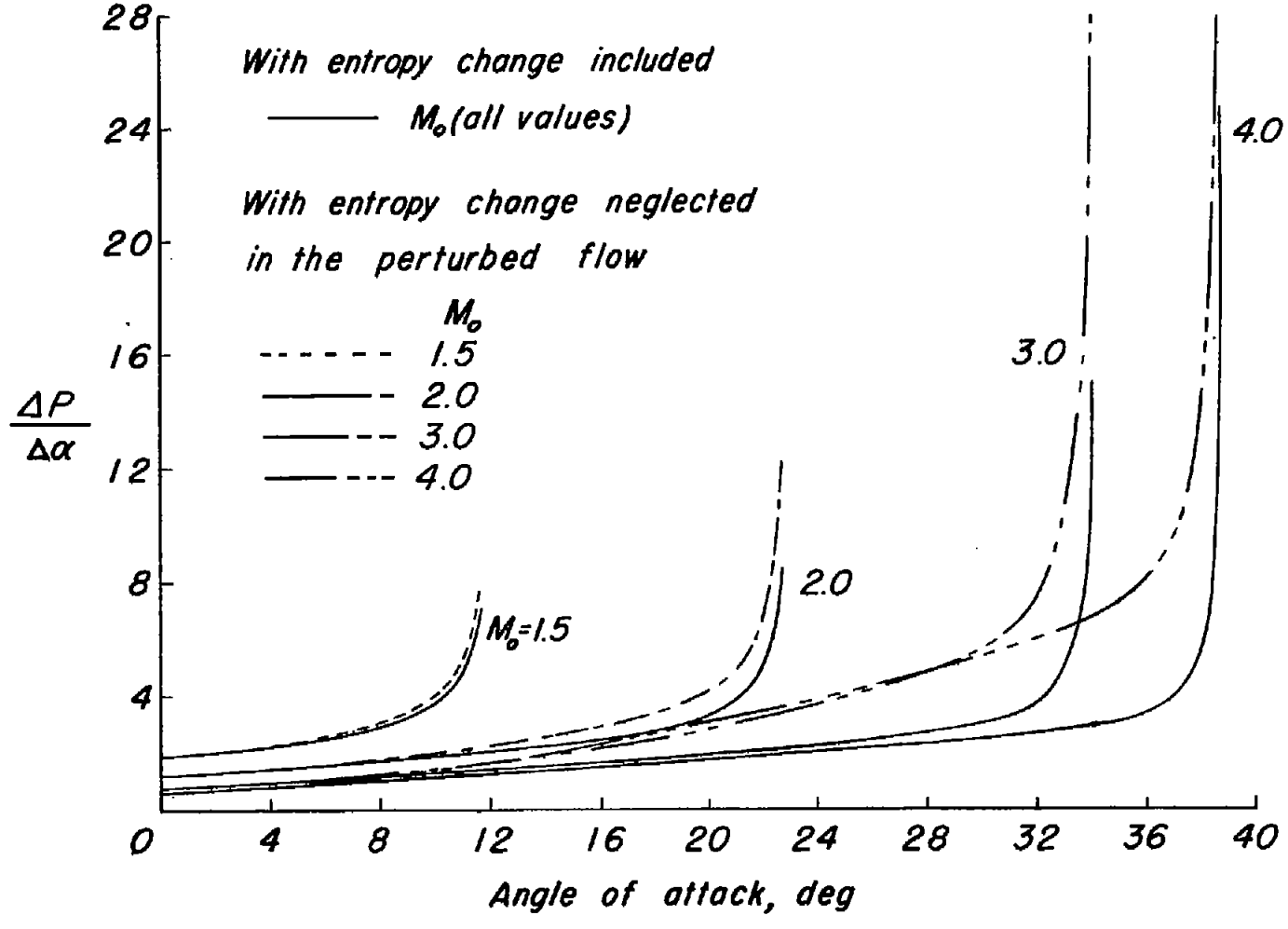

Figure 9.- Comparison of values of $\Delta P/\Delta\alpha$ on lower surface of an airfoil with and without change of entropy included in the perturbed flow.

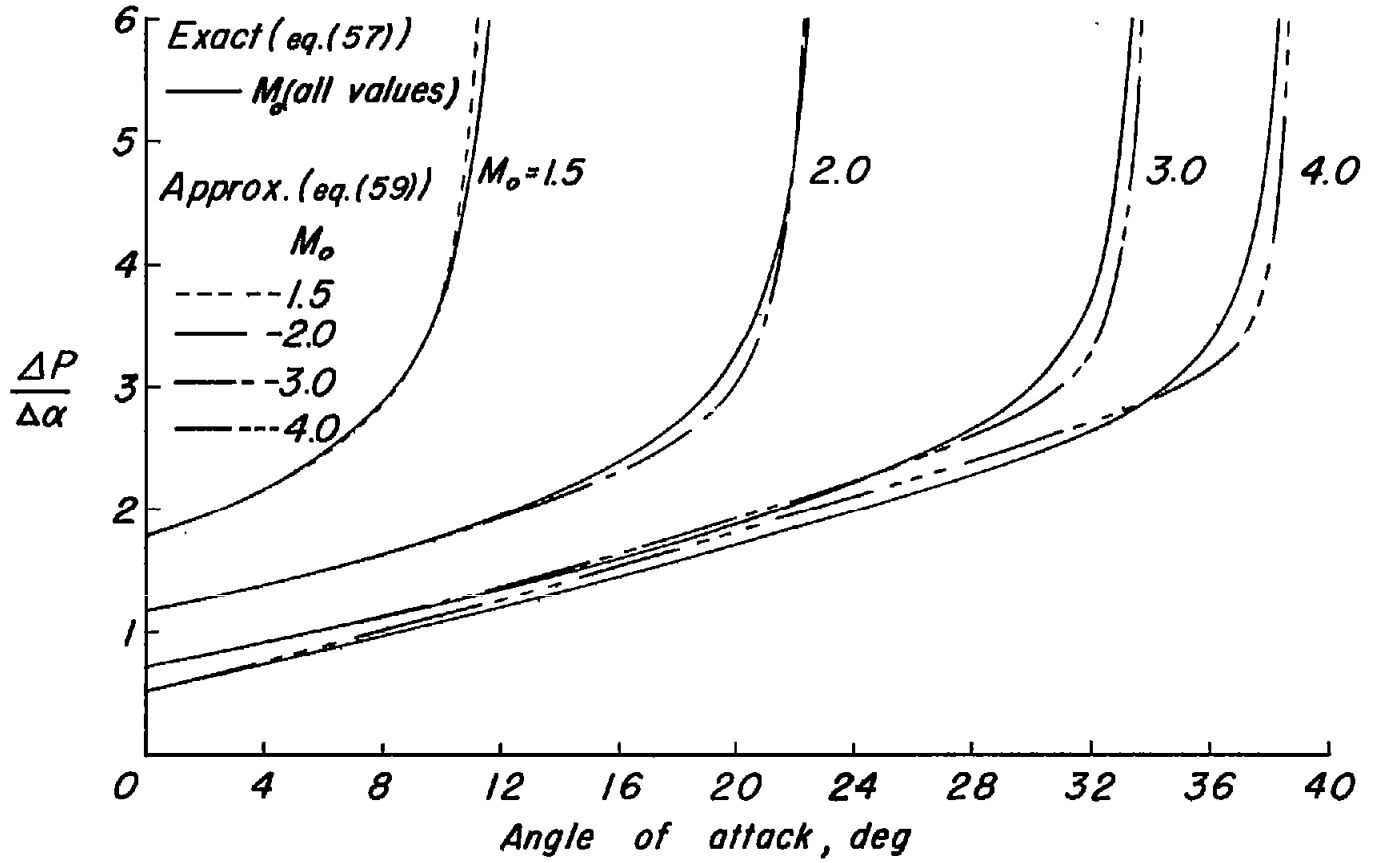

Figure 10.- Comparison between exact and approximate values of $\Delta P/\Delta\alpha$ on lower surface of an airfoil for various Mach numbers.

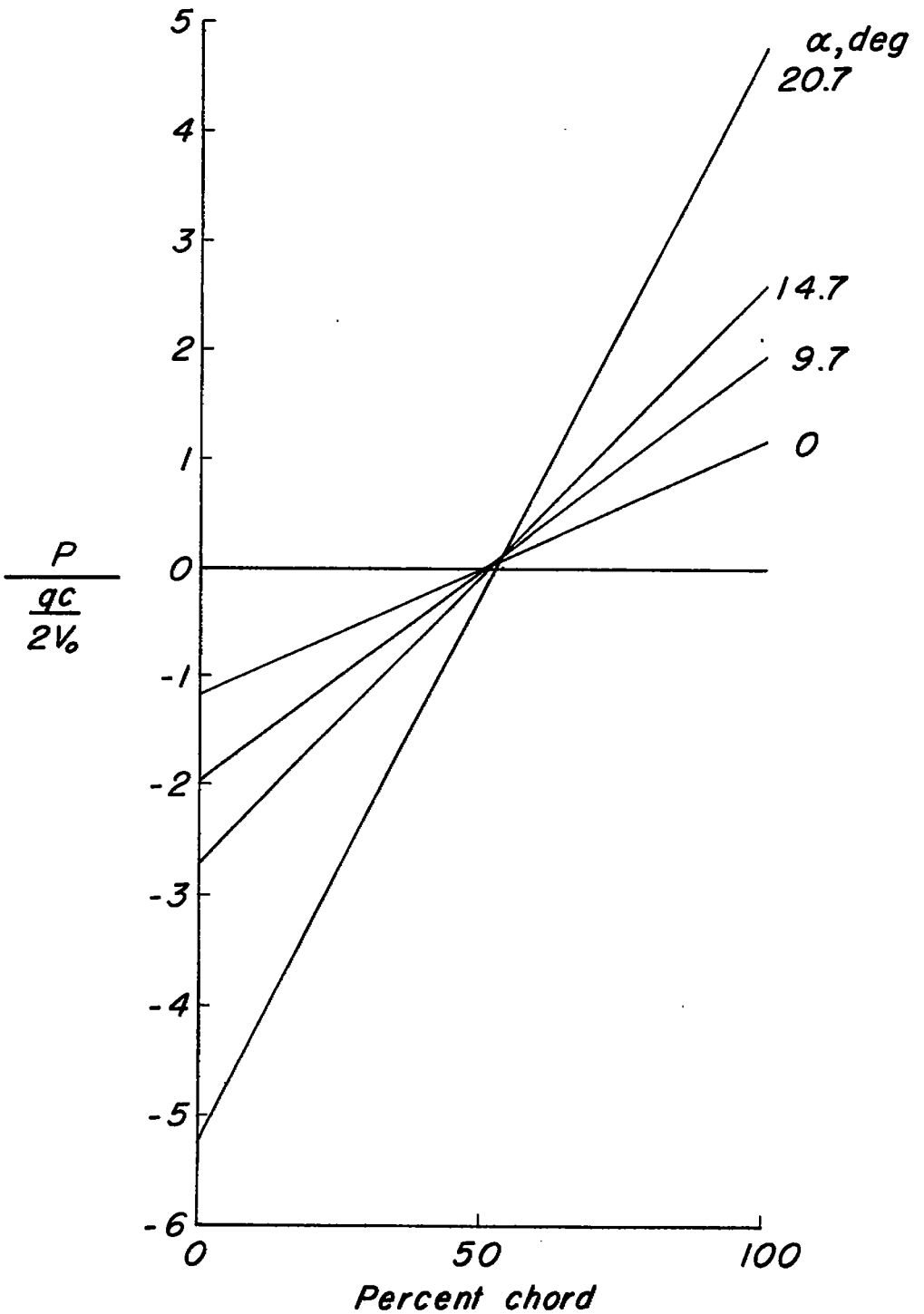

Figure 11.- Chordwise pressure distribution on lower surface of an airfoil pitching about its midchord point. M_o = 2.00.

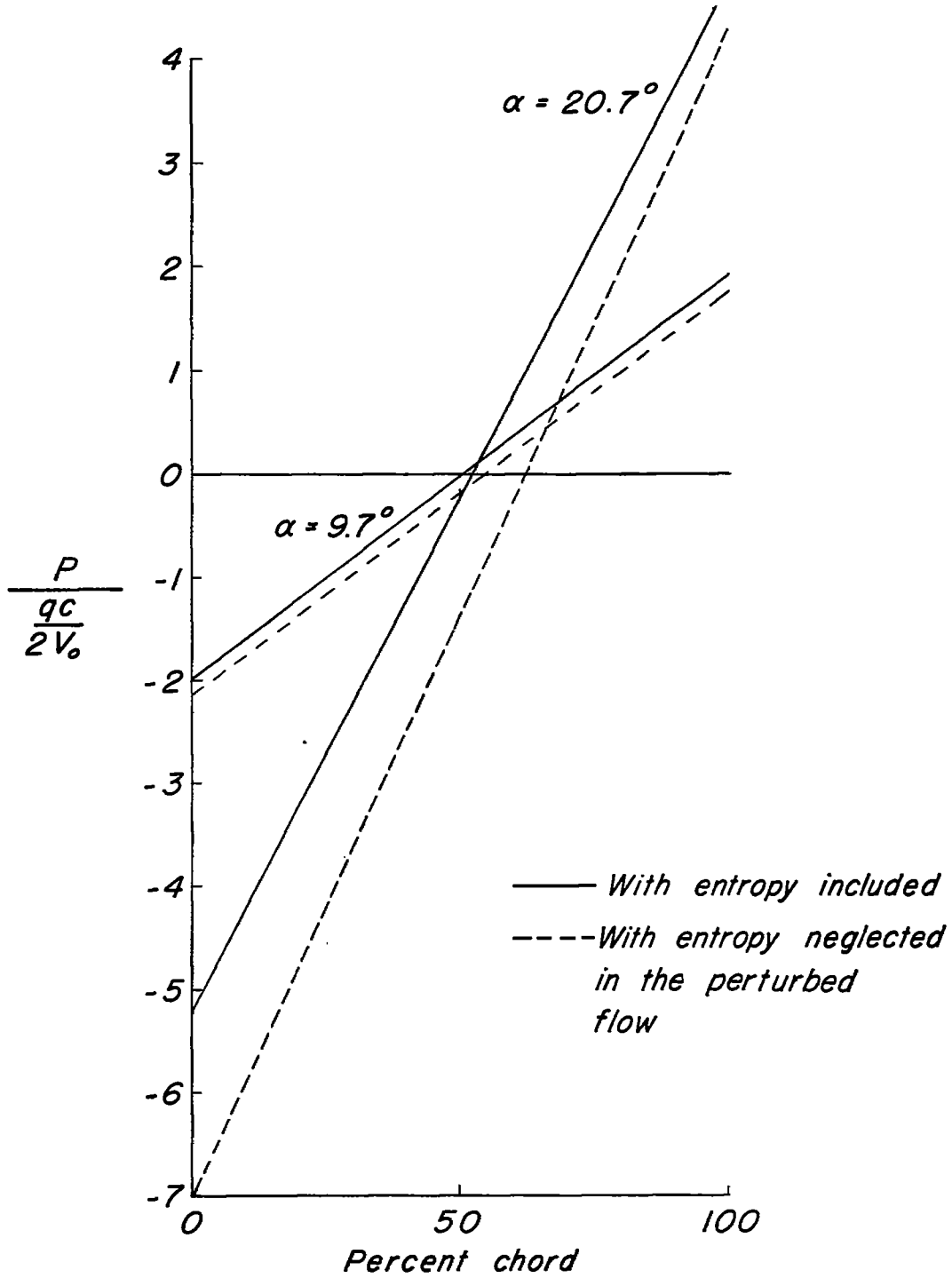

Figure 12.- Chordwise variation of pressure coefficient on lower surface of an airfoil pitching about its midchord point, with and without change of entropy included. $M_o = 2.00$; $\alpha_o = 9.7°$ and $20.7°$.

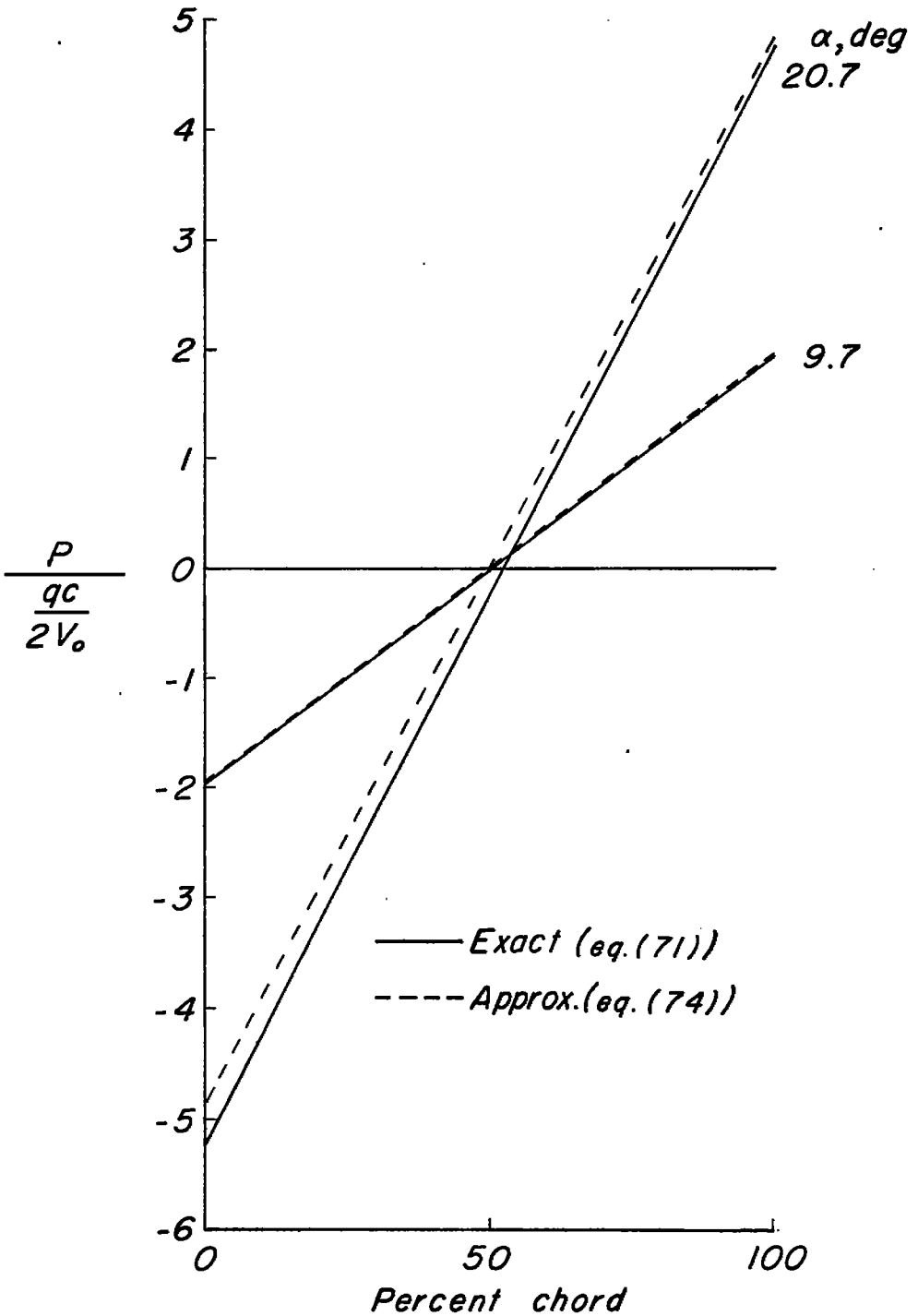

Figure 13.- Comparison between exact and approximate values of chordwise pressure on lower surface of an airfoil pitching about its midchord point. $M_0 = 2.00$; $\alpha_0 = 9.7^\circ$ and 20.7°.

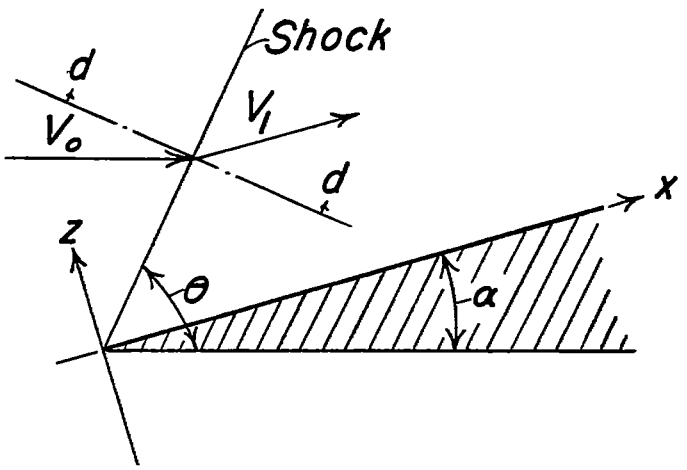

(a) Side view.

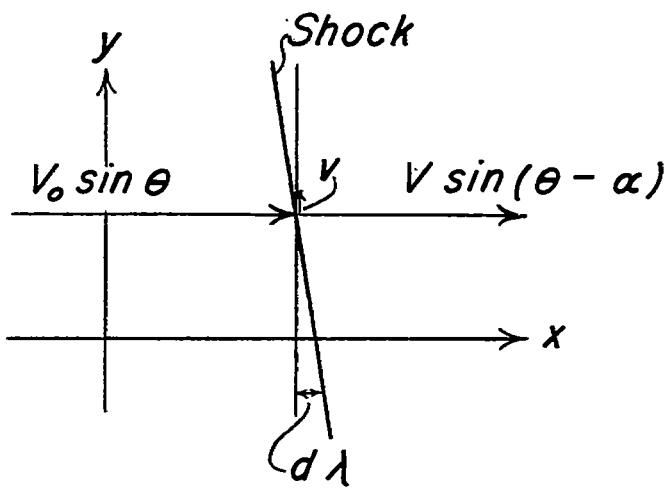

(b) View in plane d-d.

Figure 14.- Velocity components and associated data for two-dimensional shock with three-dimensional perturbed flow.

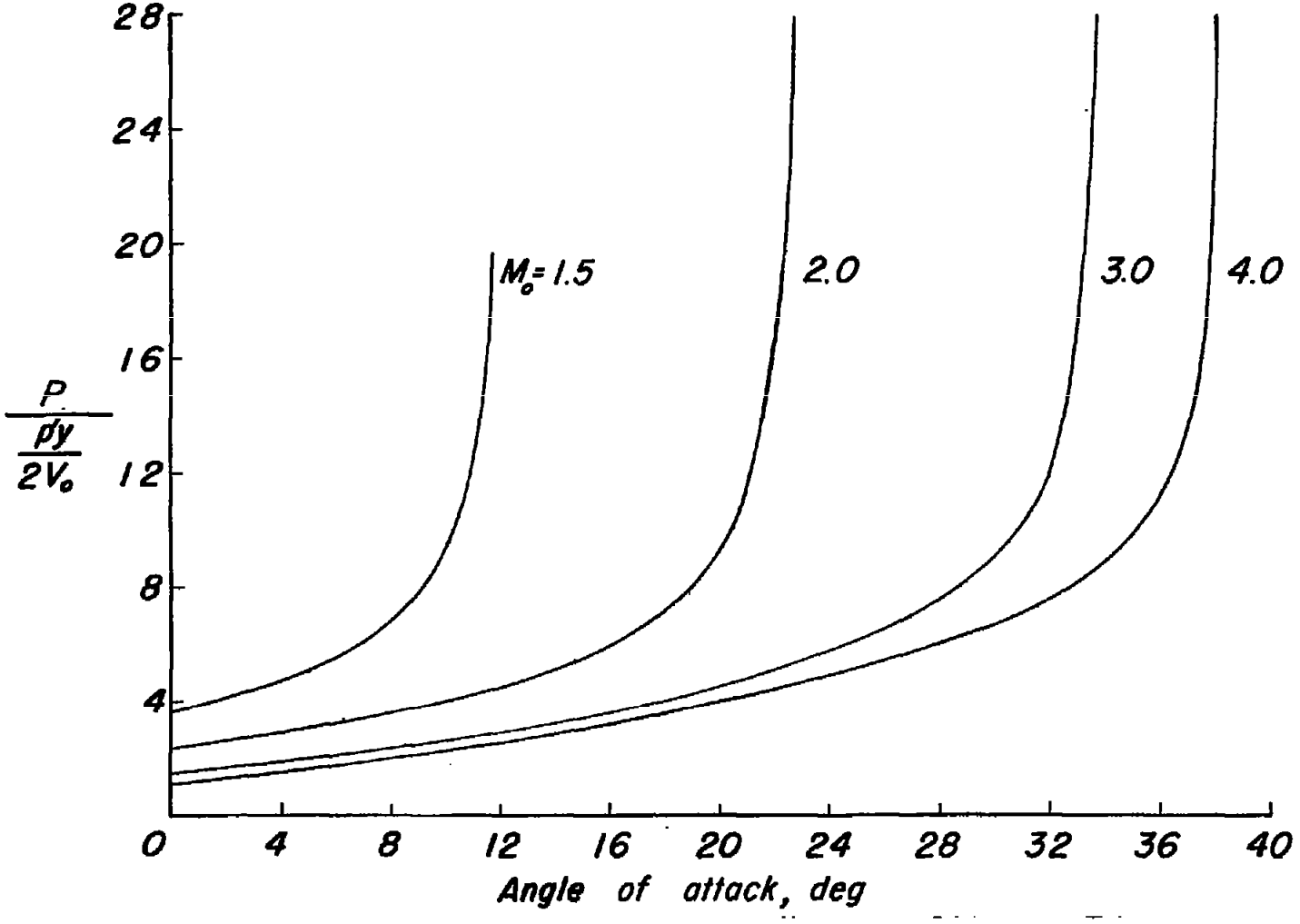

Figure 15.- Variation of pressure coefficient on lower surface of a rolling airfoil with angle of attack for various Mach numbers.

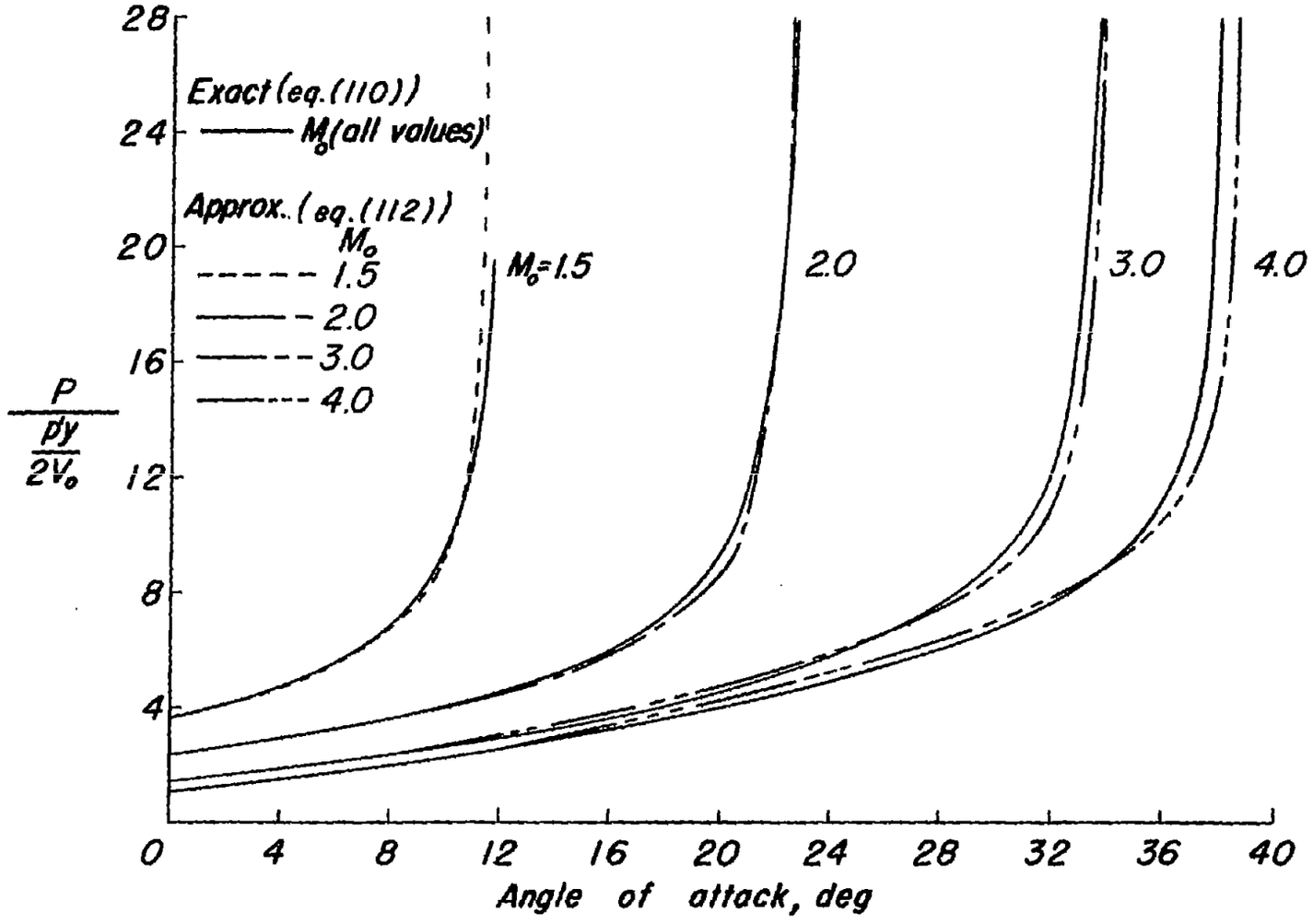

Figure 16.- Comparison between exact and approximate values of pressure coefficient on lower surface of a rolling airfoil for various Mach

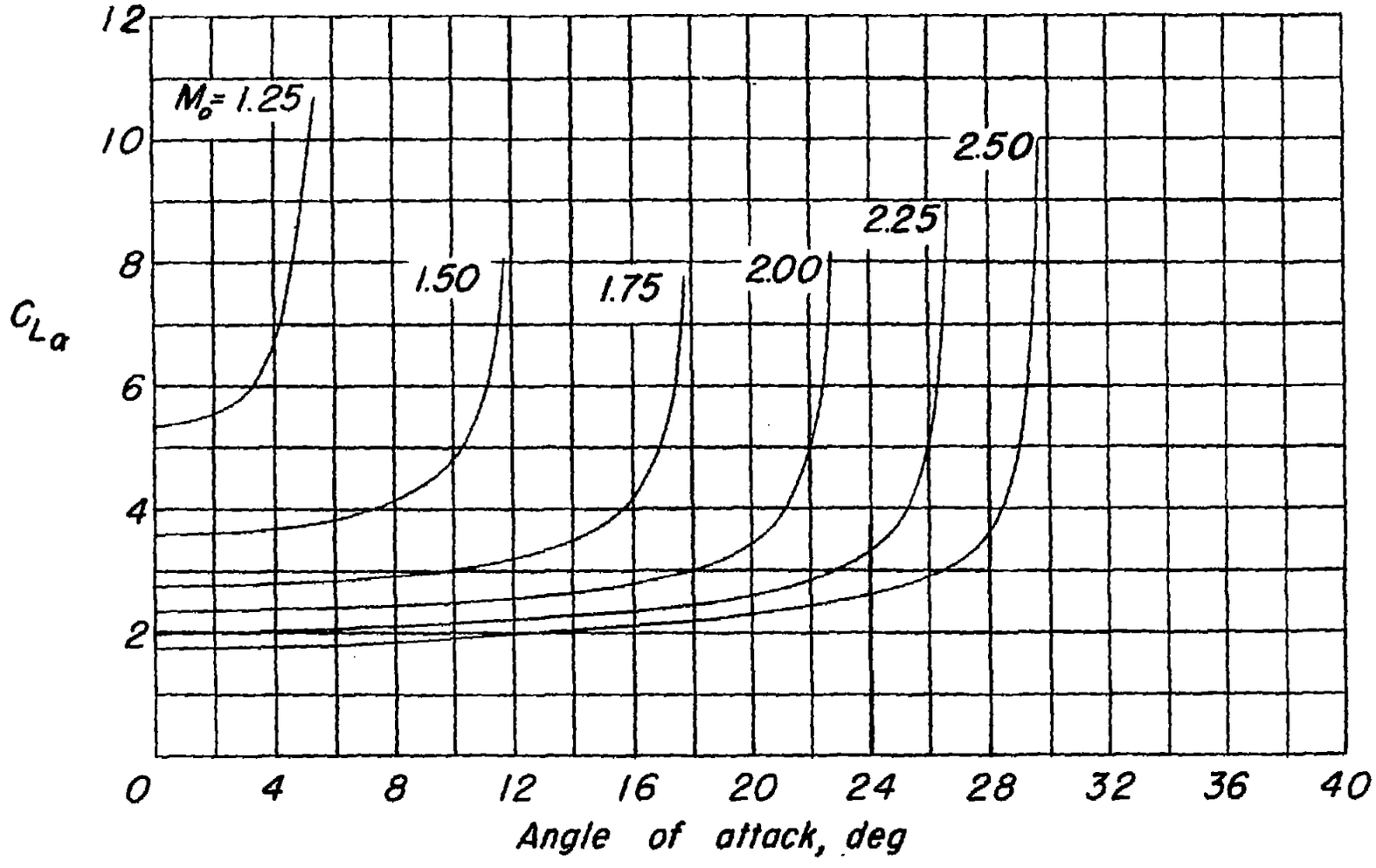

(a) M_o = 1.25 to 2.50.

Figure 17.- Variation of C_{L_α} with angle of attack for various Mach numbers.

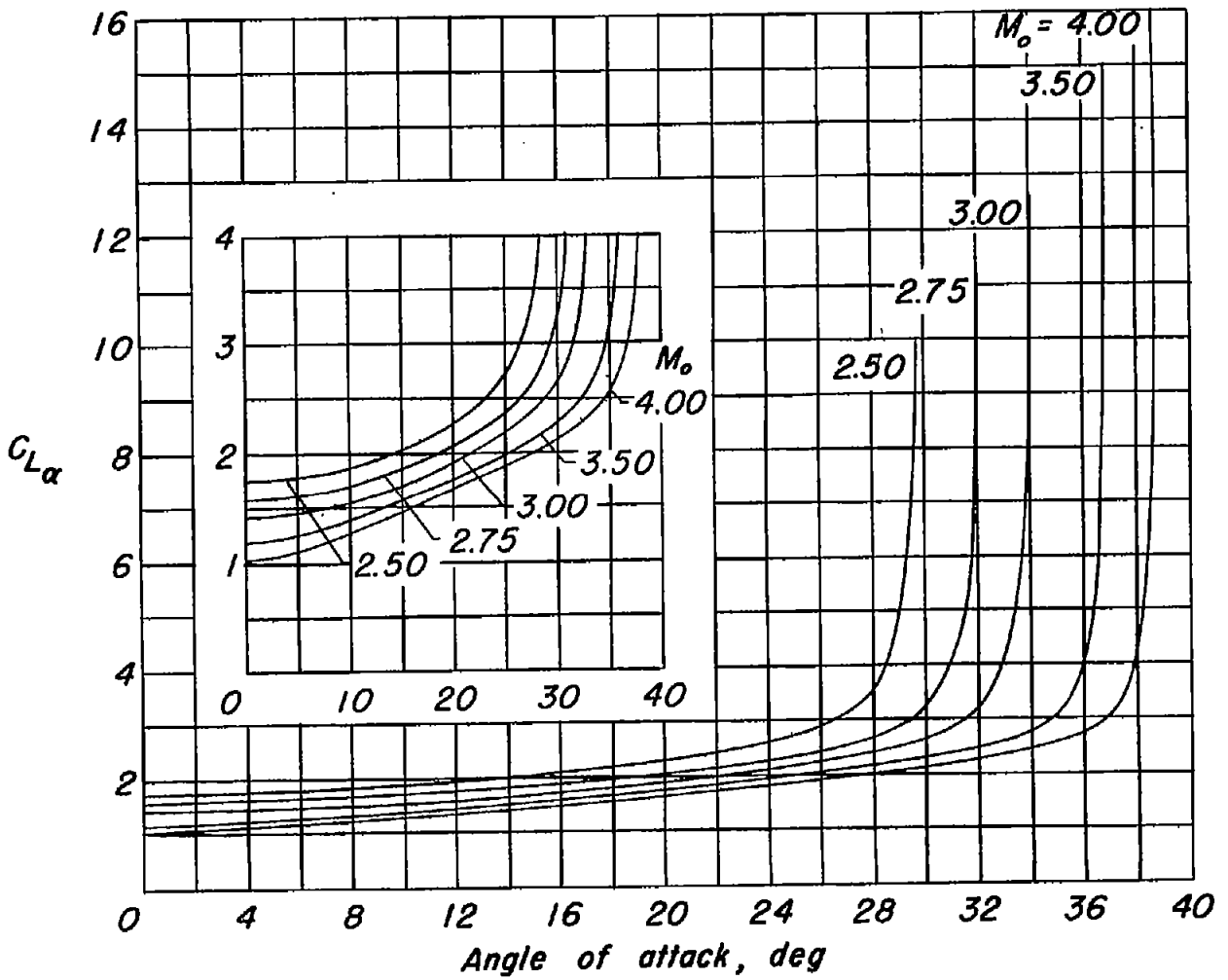

(b) M_o = 2.50 to 4.00.

Figure 17.- Concluded.

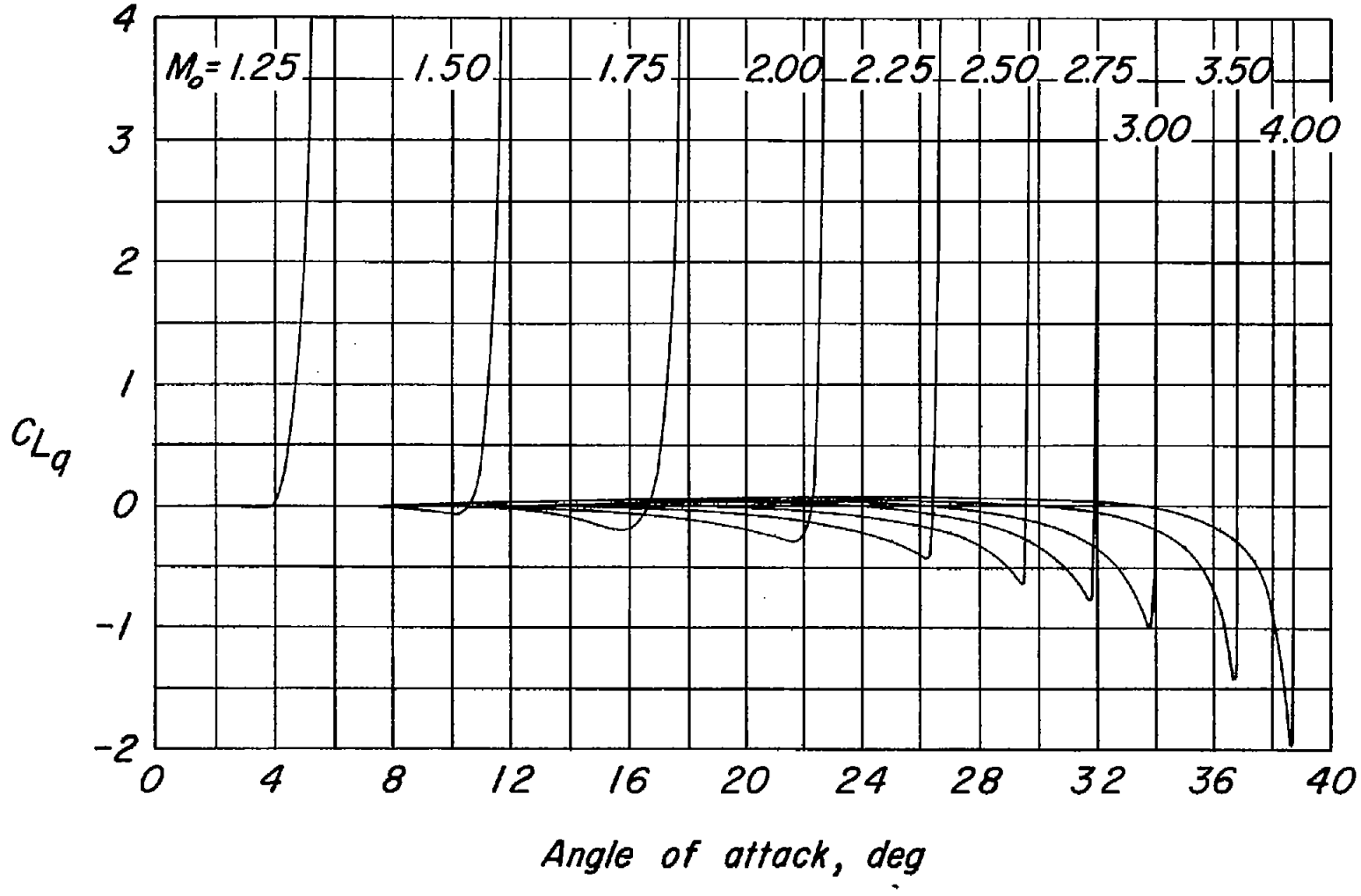

Figure 18.- Variation of C_{L_q} with angle of attack for various Mach numbers when axis of pitch is located at the midchord point.

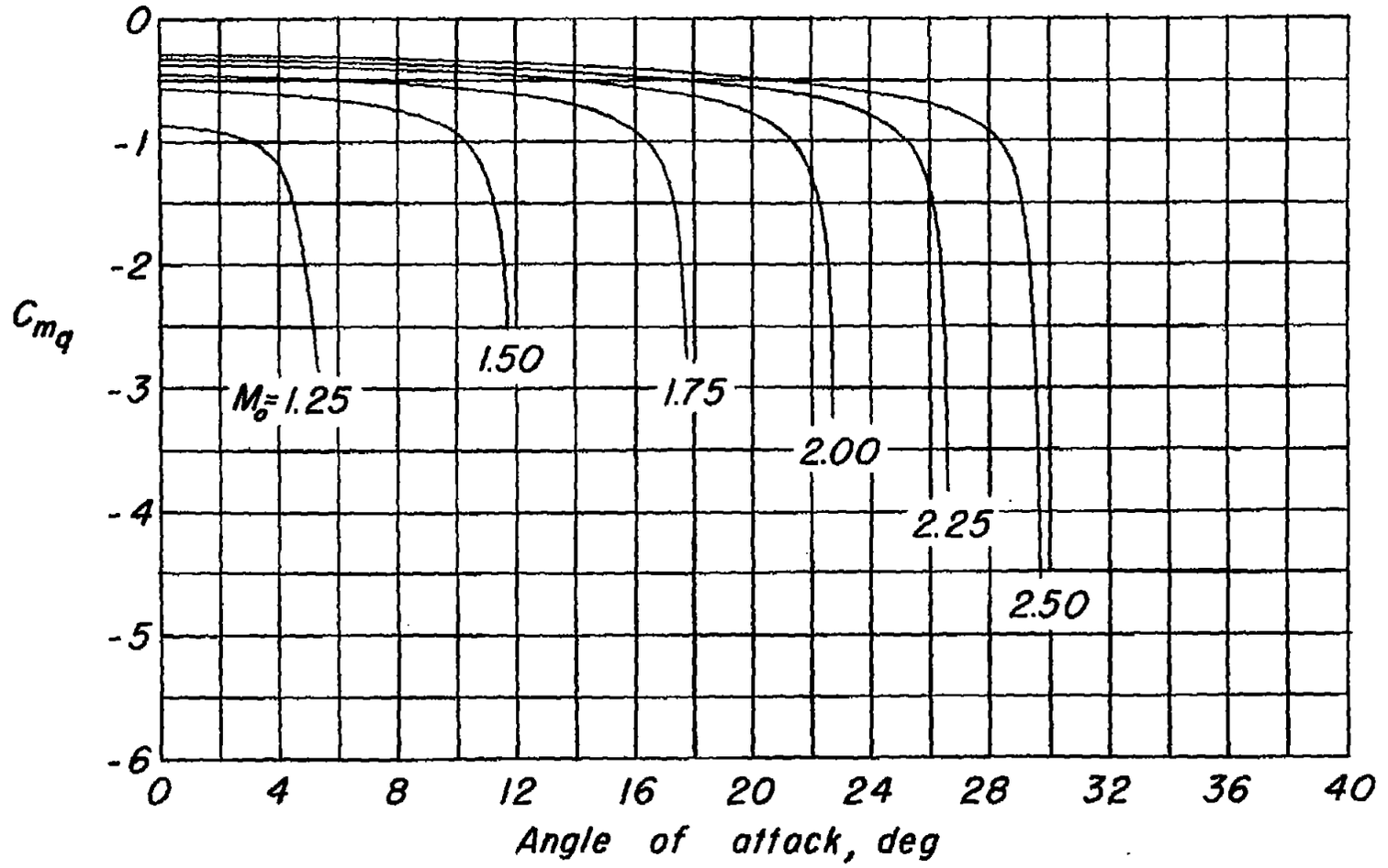

(a) M_o = 1.25 to 2.50.

Figure 19.- Variation of C_{m_q} with angle of attack for various Mach numbers when axis of pitch is located at the midchord point.

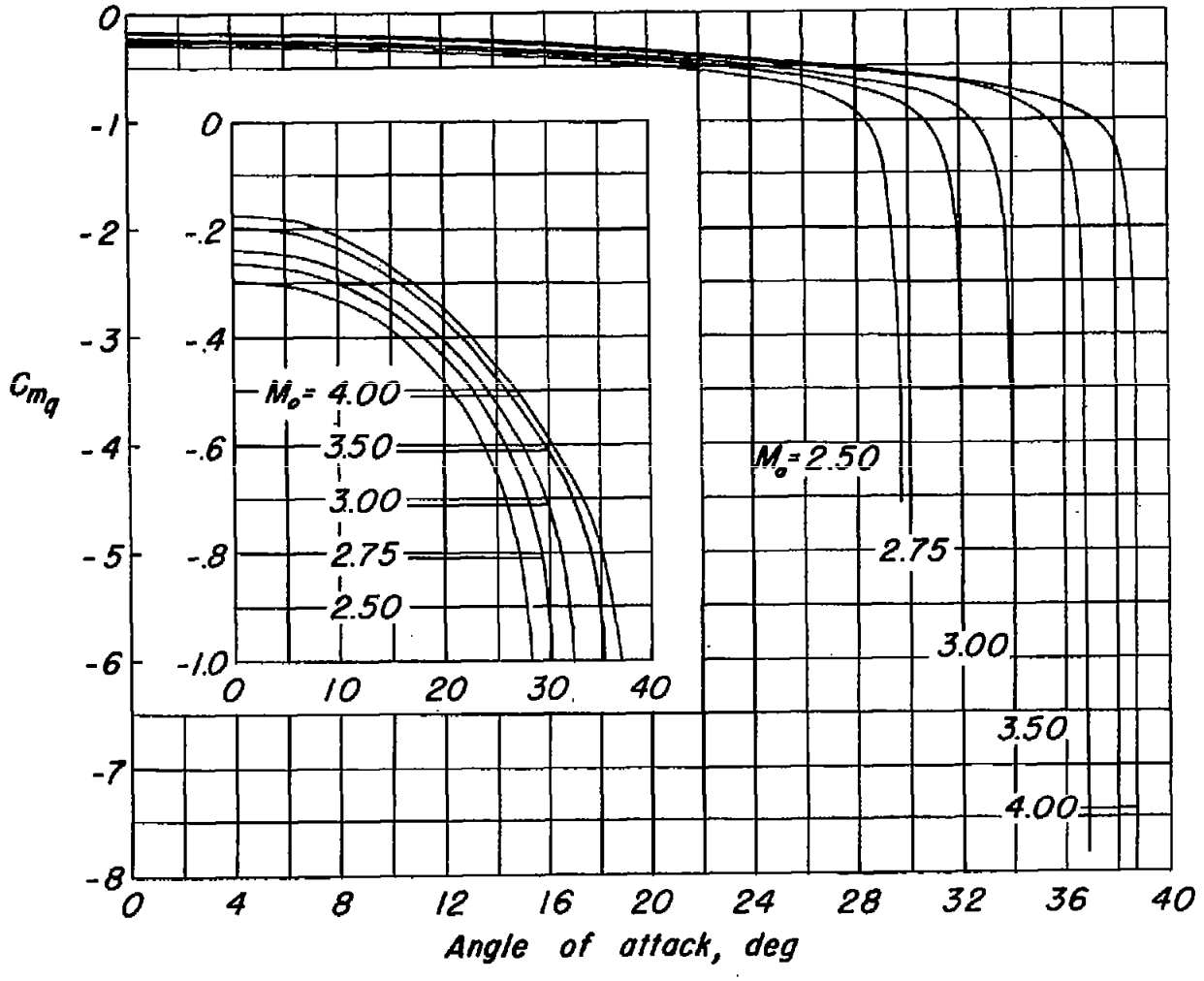

(b) M_O = 2.50 to 4.00.

Figure 19.- Concluded.

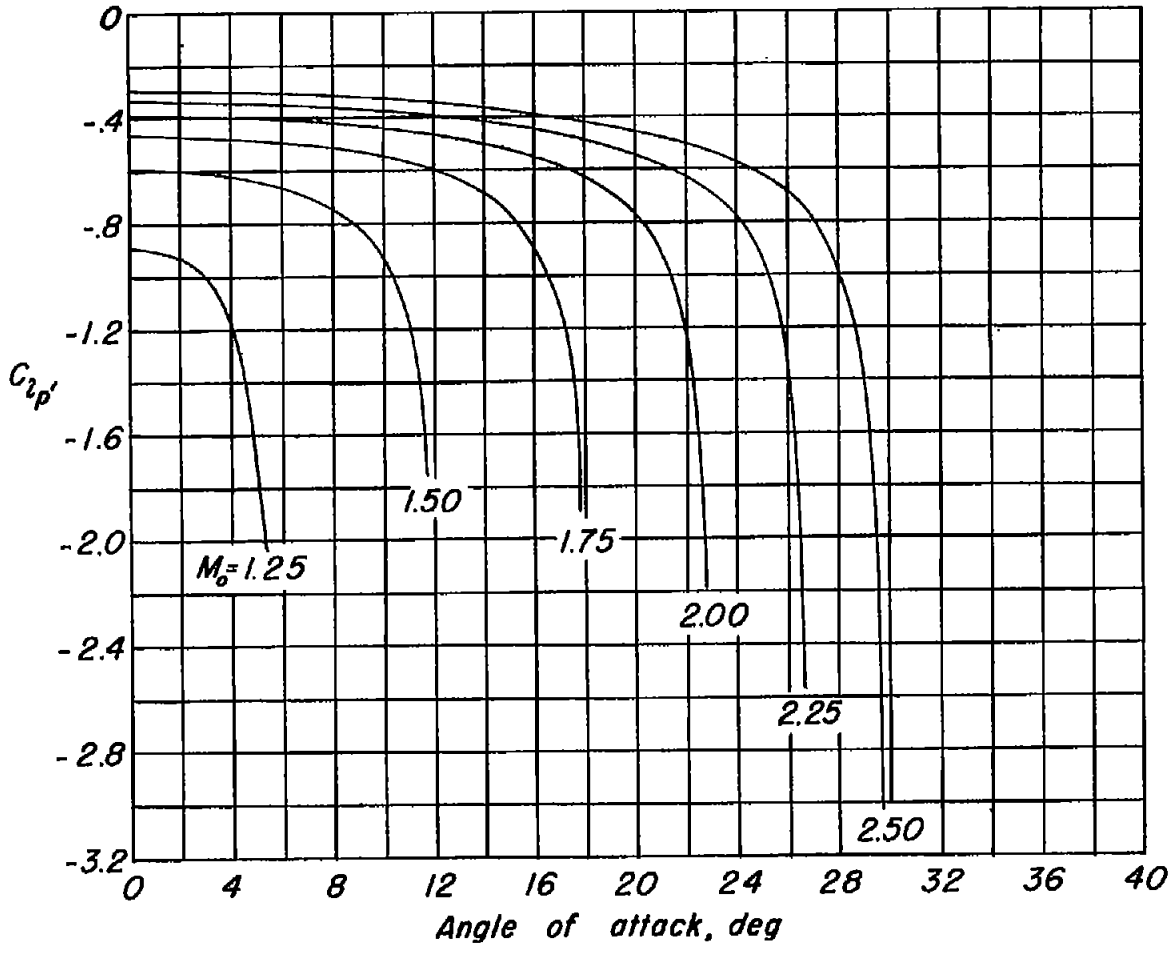

(a) M_o = 1.25 to 2.50.

Figure 20.- Variation of $C_{l_{p'}}$ with angle of attack for various Mach numbers.

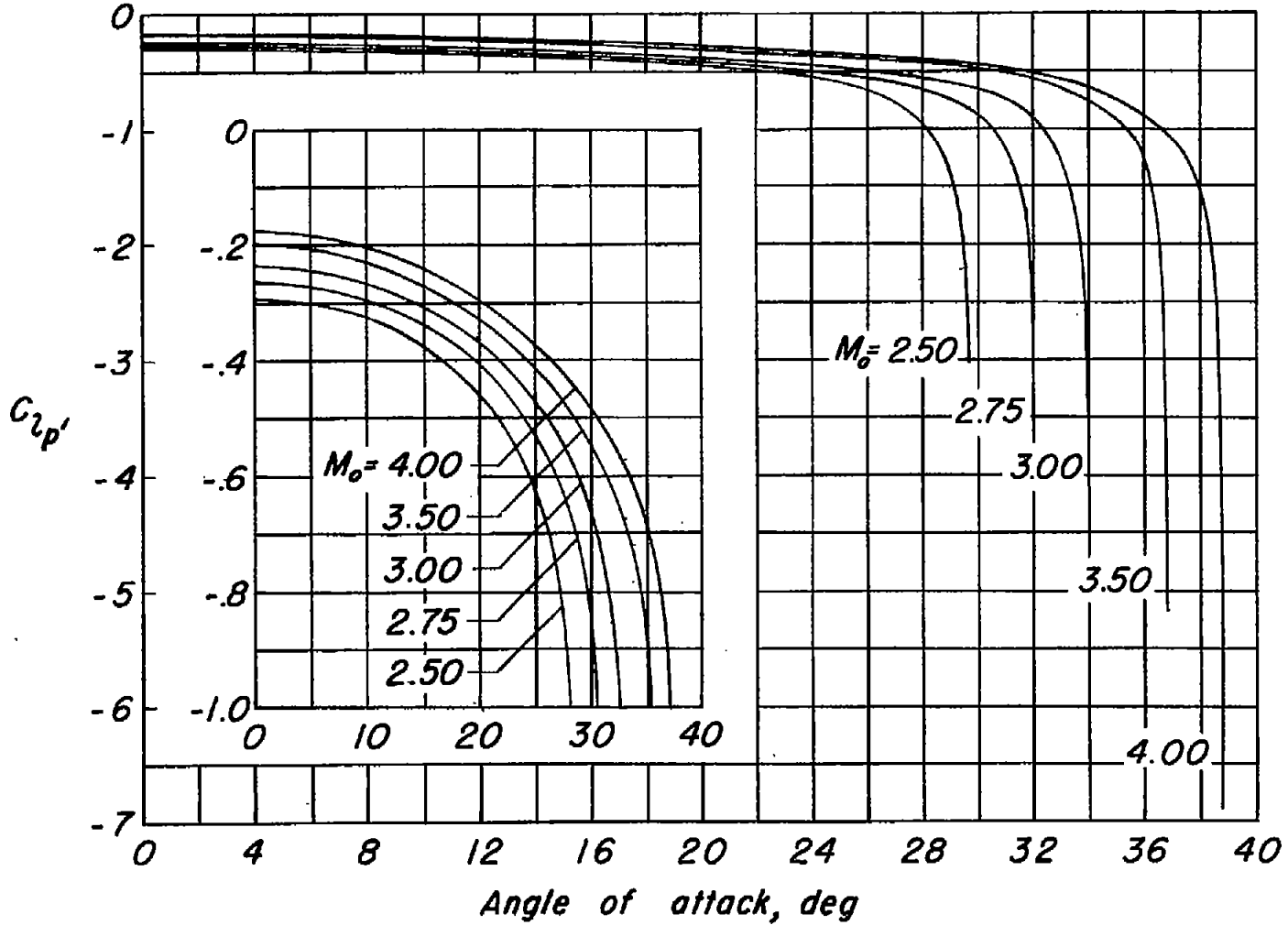

(b) M_o = 2.50 to 4.00.

Figure 20.- Concluded.

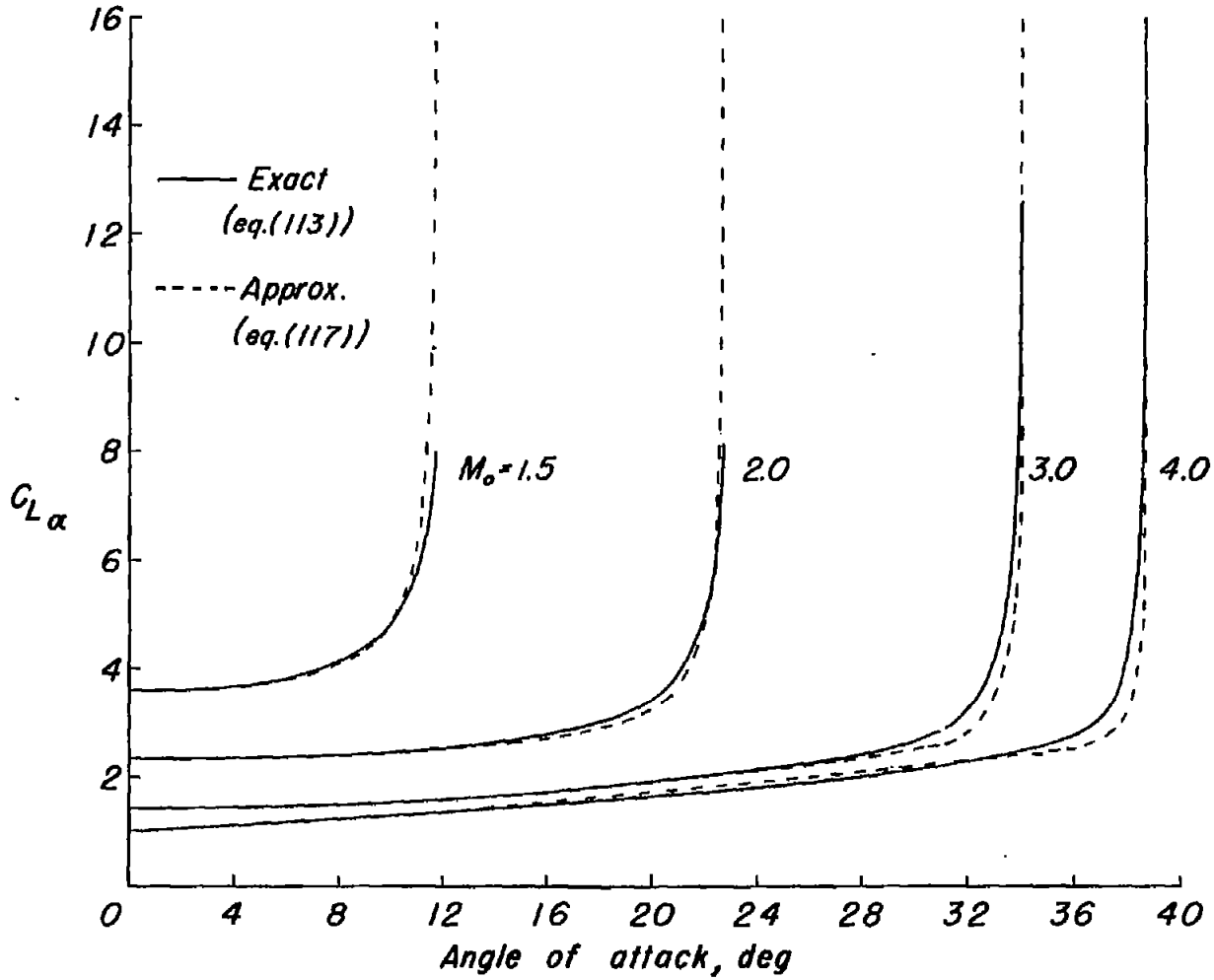

Figure 21.- Comparison between exact and approximate values of C_{L_α} for various Mach numbers.

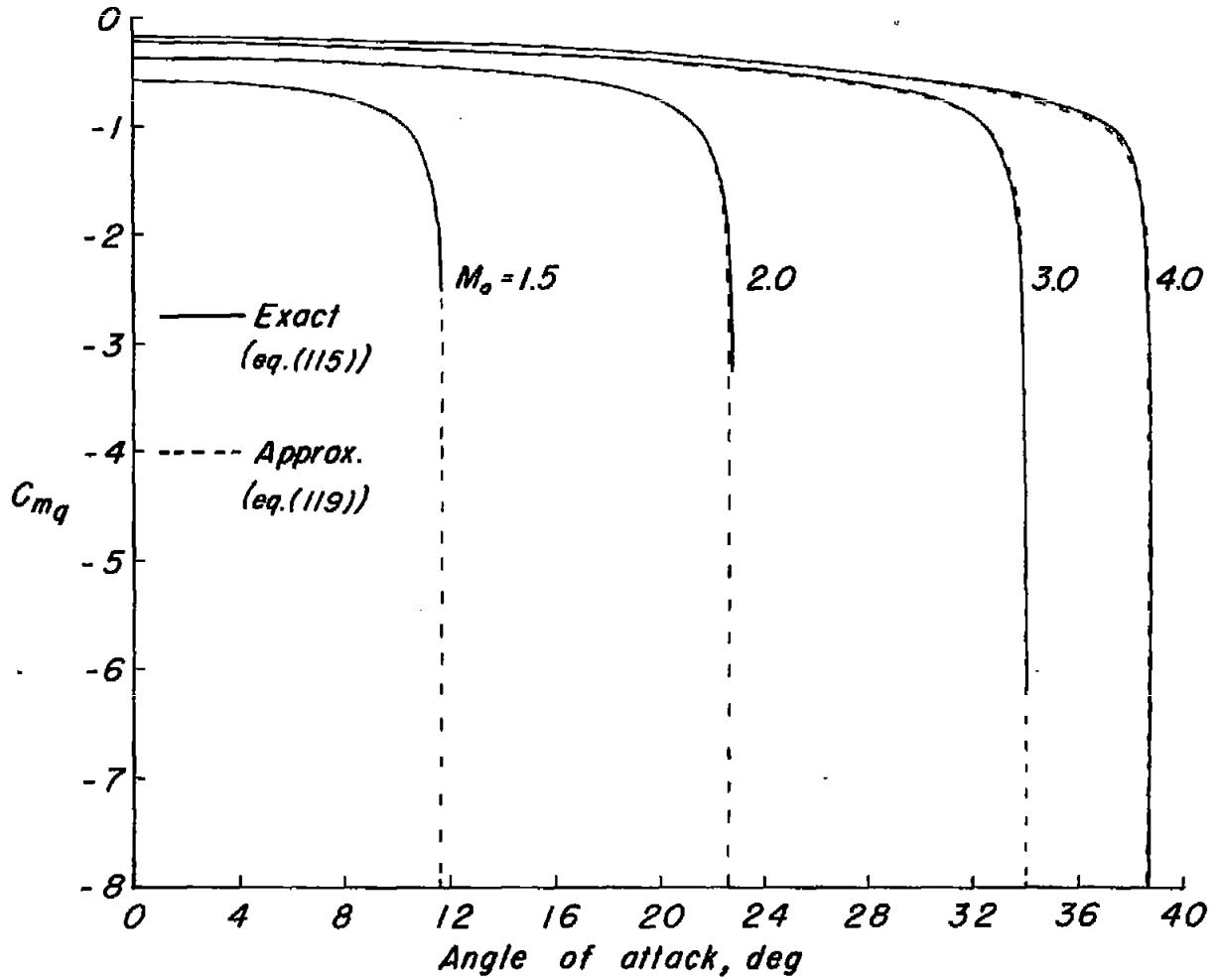

Figure 22.- Comparison between exact and approximate values of C_{m_q} for various Mach numbers when axis of pitch is located at midchord point.

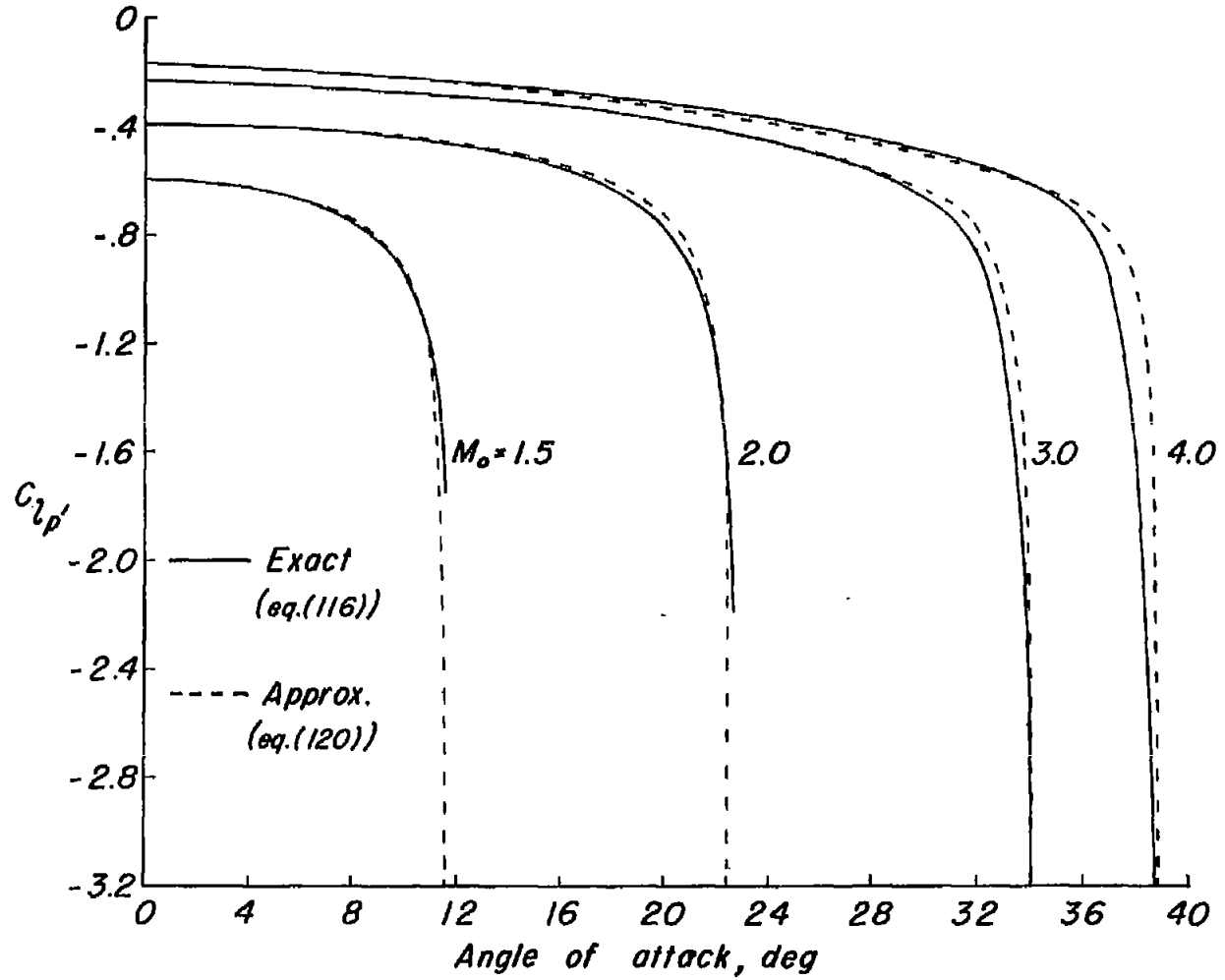

Figure 23.- Comparison between exact and approximate values of $C_{l_{p'}}$ for various Mach numbers.

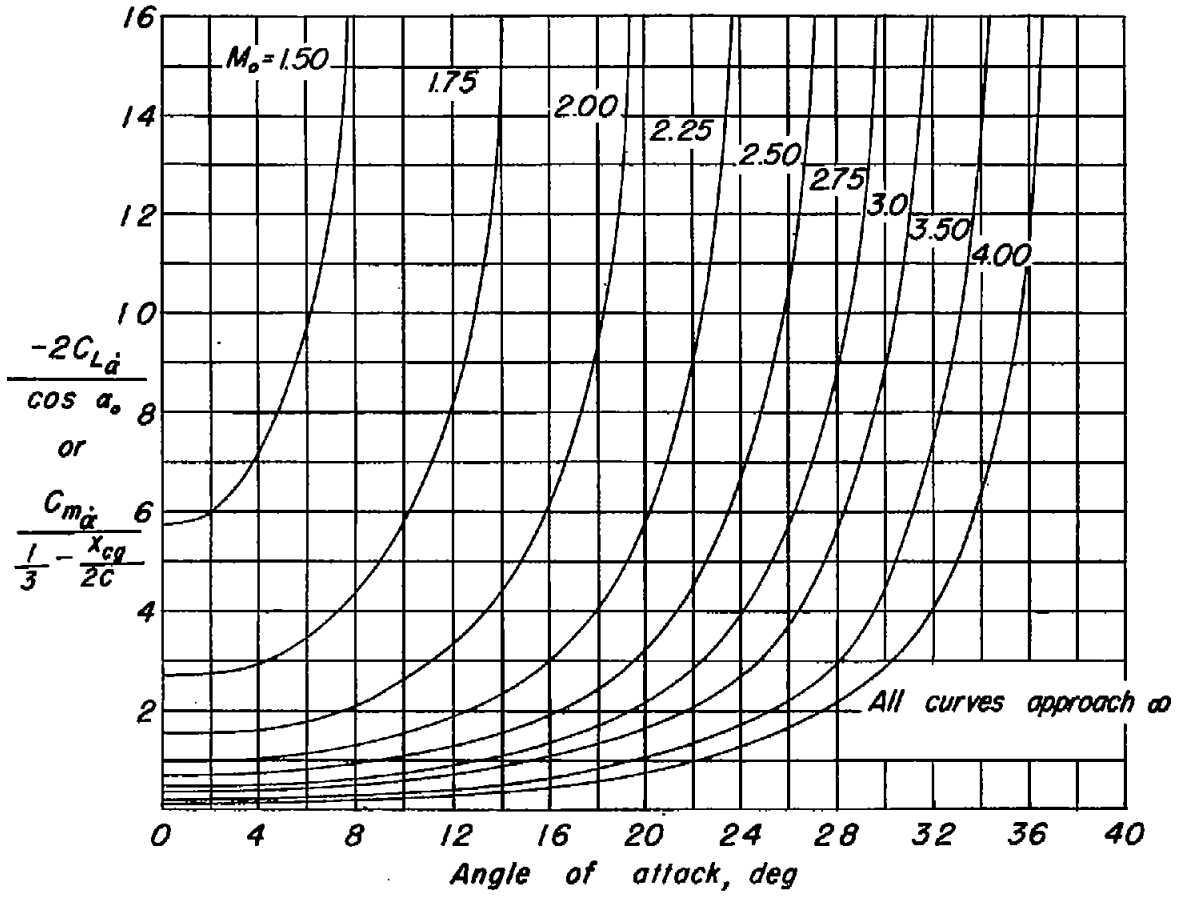

(a) M_o = 1.50 to 4.00.

Figure 24.- Variation of approximate values of $\frac{-2C_{L_{\dot{\alpha}}}}{\cos \alpha_o}$ or $\frac{C_{m_{\dot{\alpha}}}}{\frac{1}{3} - \frac{x_{cg}}{2c}}$ with angle of attack for various Mach numbers.

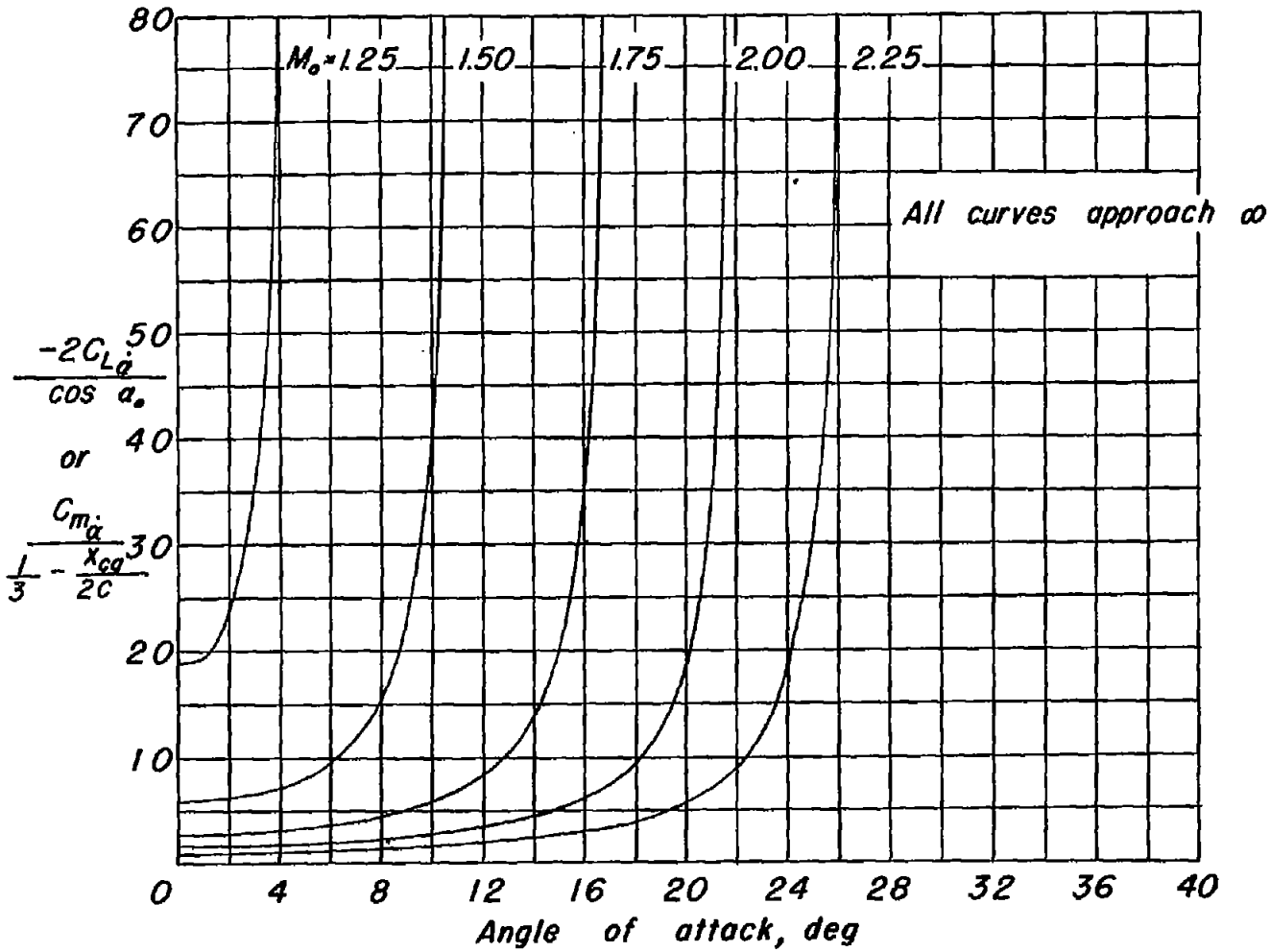

(b) M_o = 1.25 to 2.25.

Figure 24.- Continued.

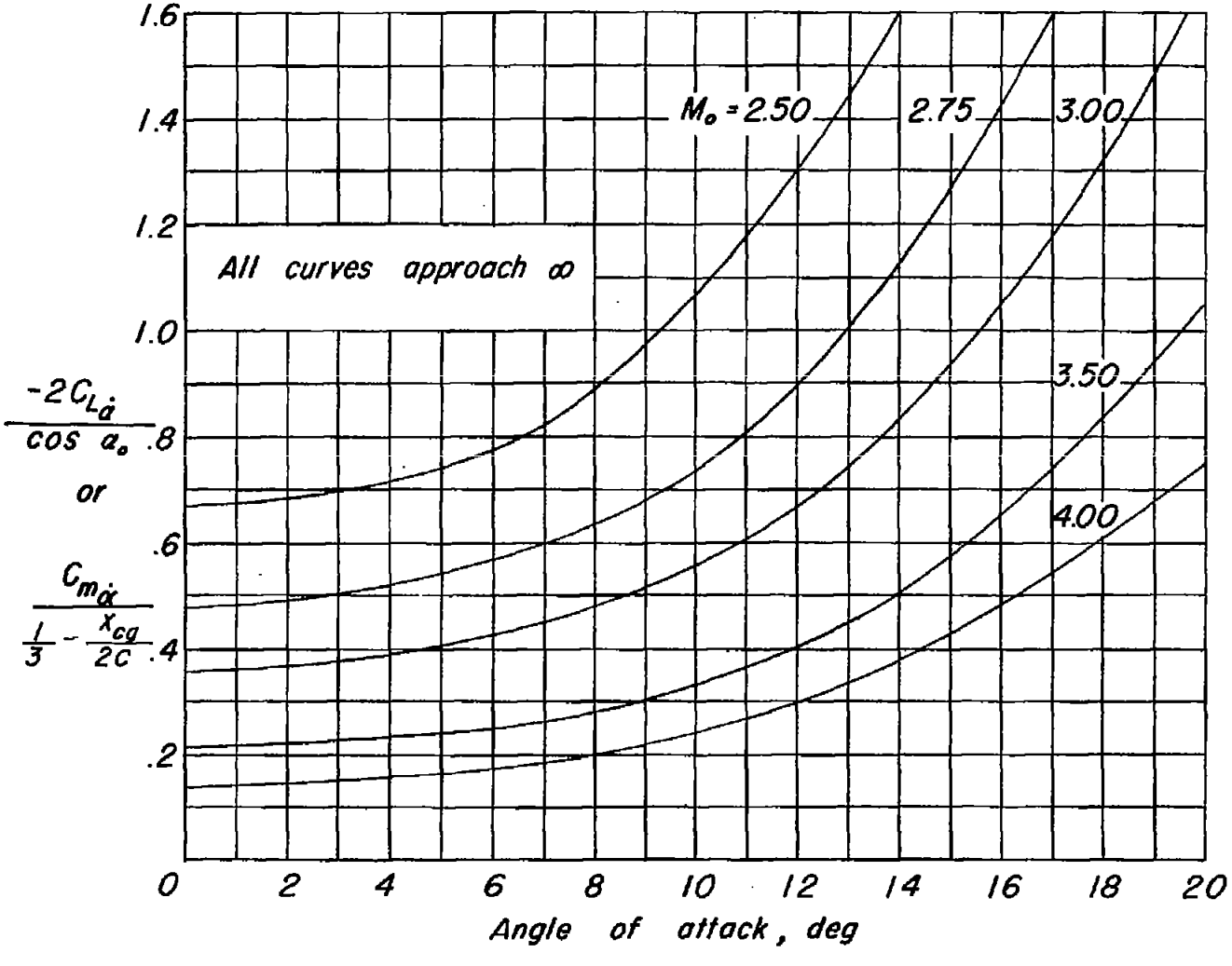

(c) M_o = 2.50 to 4.00.

Figure 24.- Concluded.

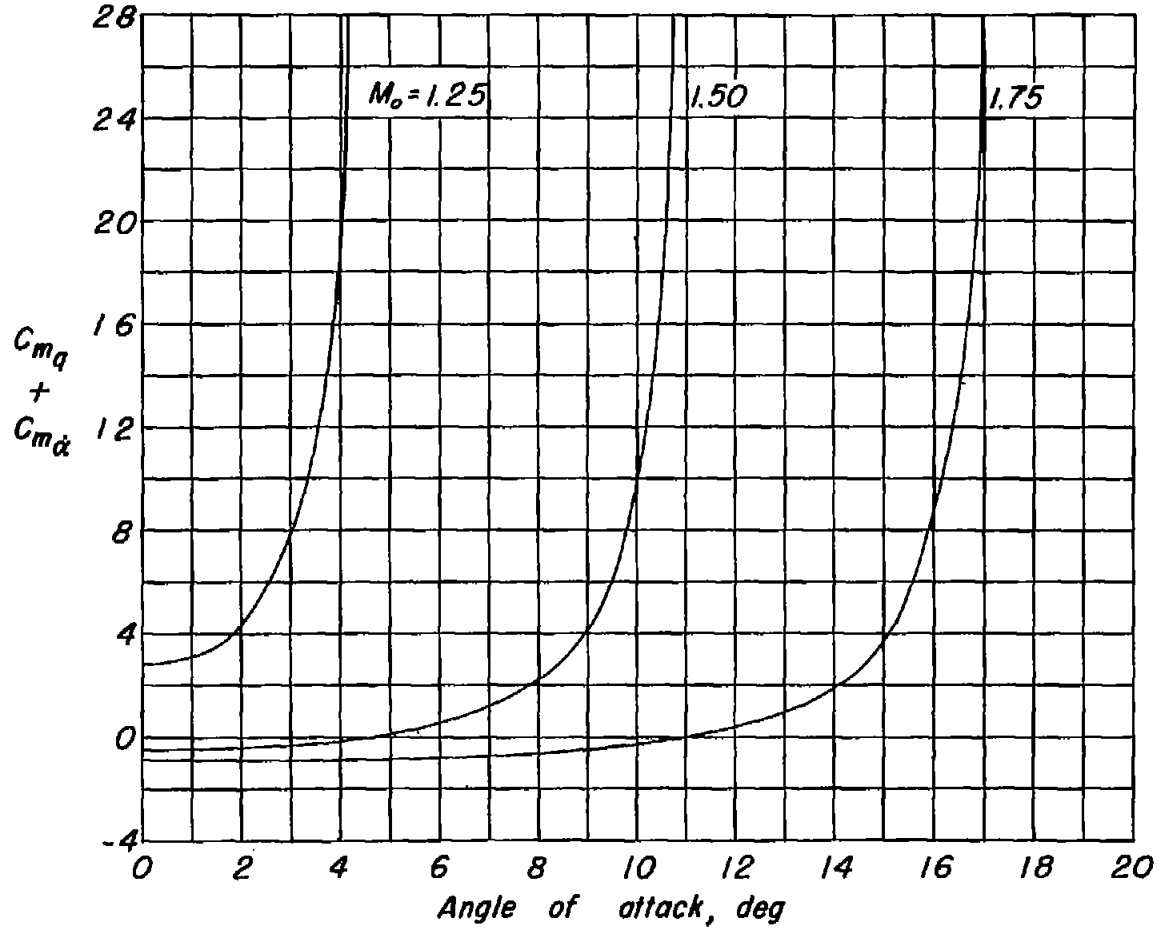

(a) $M_o = 1.25$ to 1.75.

Figure 25.- Variation of $C_{m_q} + C_{m_{\dot{\alpha}}}$ (calculated from approximate eqs. (119) and (124)) with angle of attack when center of gravity is located at leading edge.

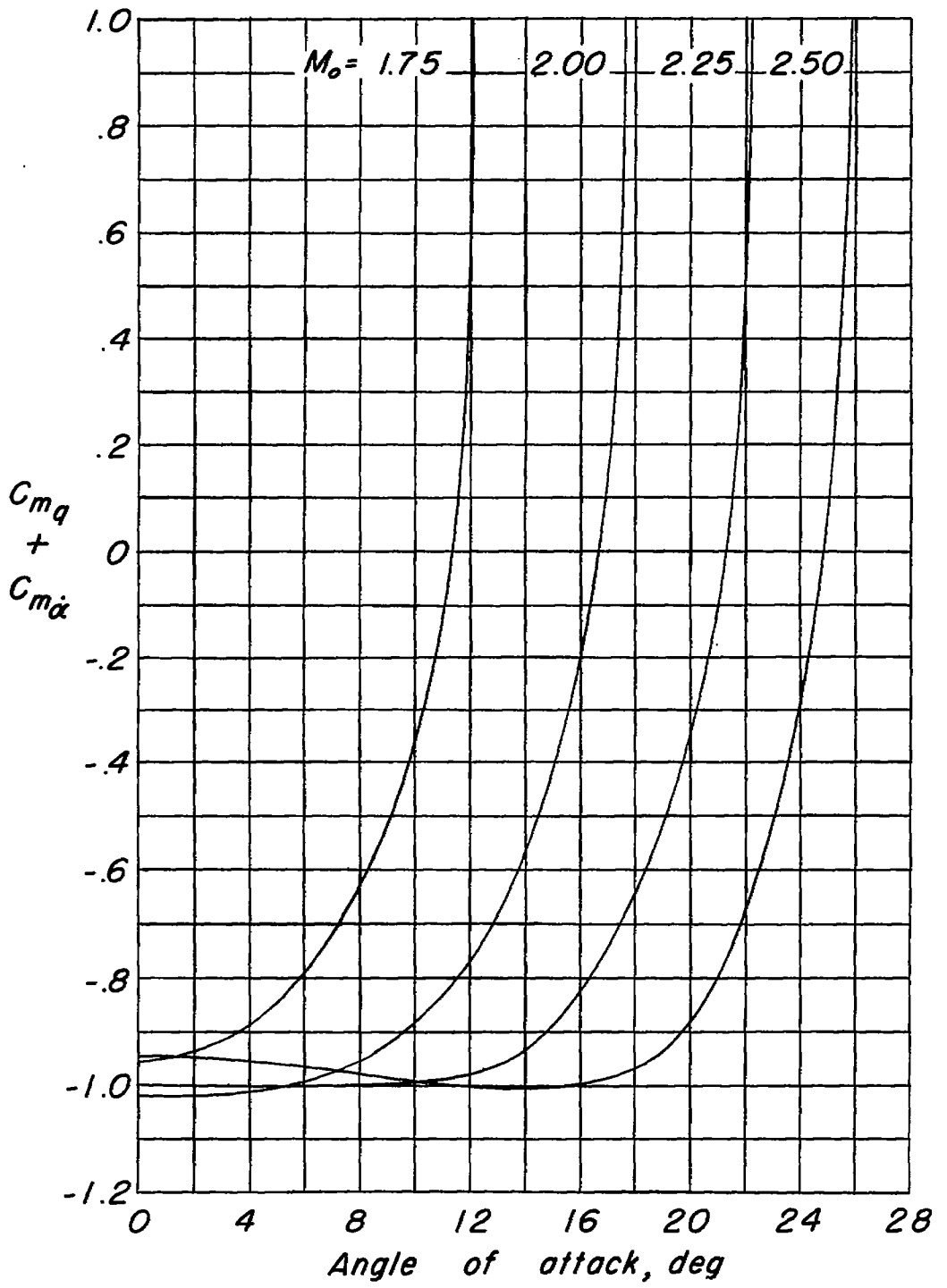

(b) M_o = 1.75 to 2.50.

Figure 25.- Continued.

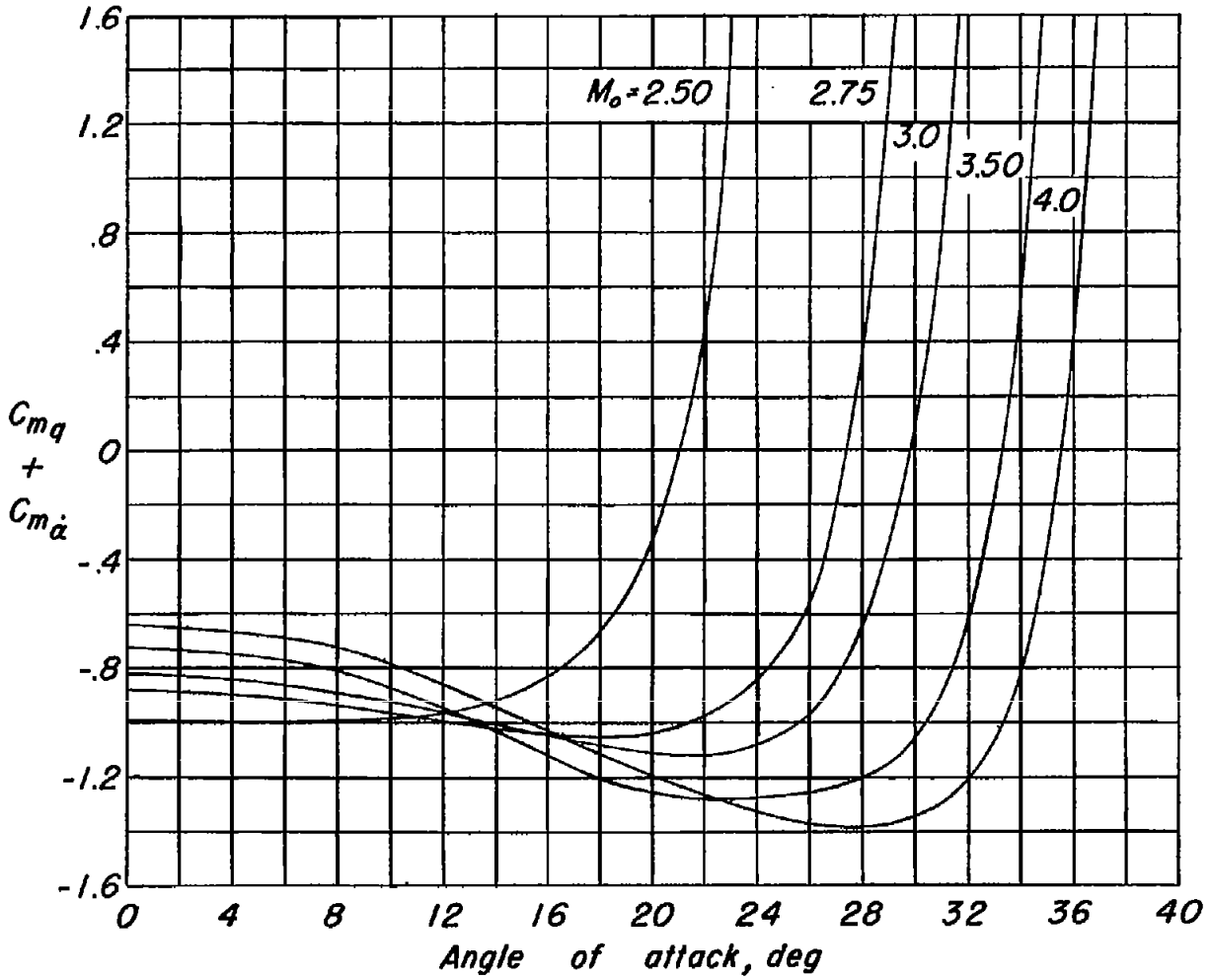

(c) M_o = 2.50 to 4.00.

Figure 25.- Concluded.

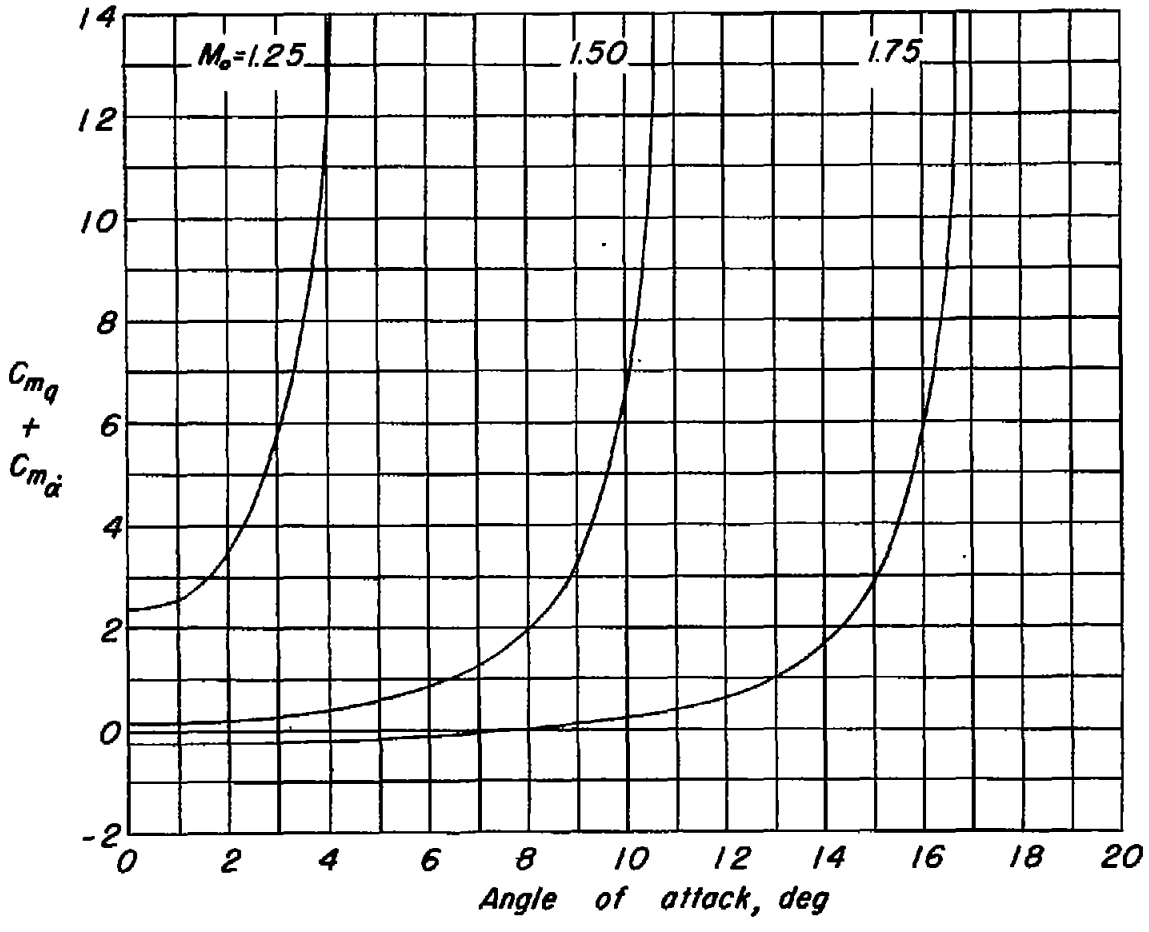

(a) M_o = 1.25 to 1.75.

Figure 26.- Variation of $C_{m_q} + C_{m_{\dot{\alpha}}}$ (calculated from approximate eqs. (119) and (124)) with angle of attack when center of gravity is located at quarter-chord point.

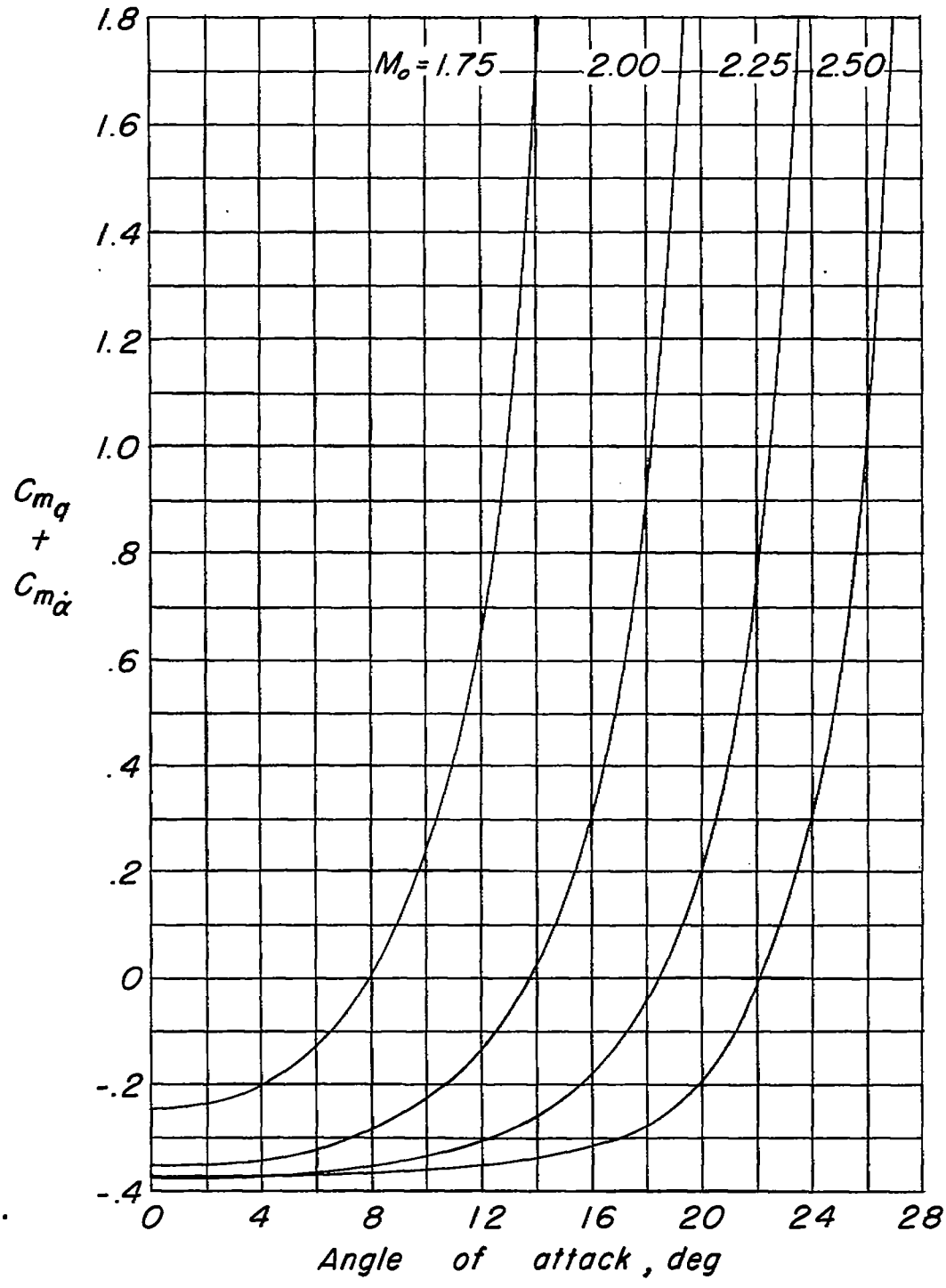

(b) M_o = 1.75 to 2.50.

Figure 26.- Continued.

(c) M_o = 2.50 to 4.00.

Figure 26.- Concluded.

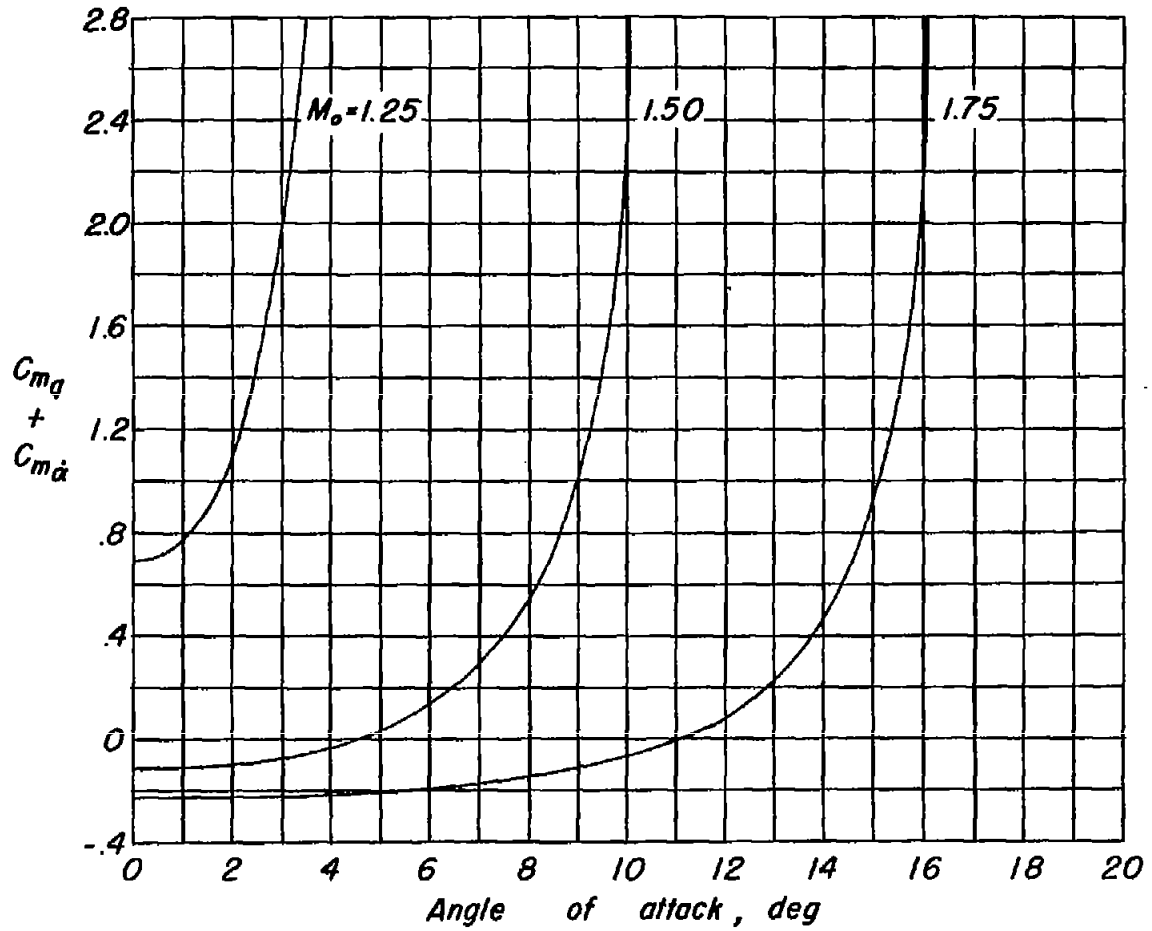

(a) M_o = 1.25 to 1.75.

Figure 27.- Variation of $C_{m_q} + C_{m_{\dot{\alpha}}}$ (calculated from approximate eqs. (119) and (124)) with angle of attack when center of gravity is located at mid-chord point.

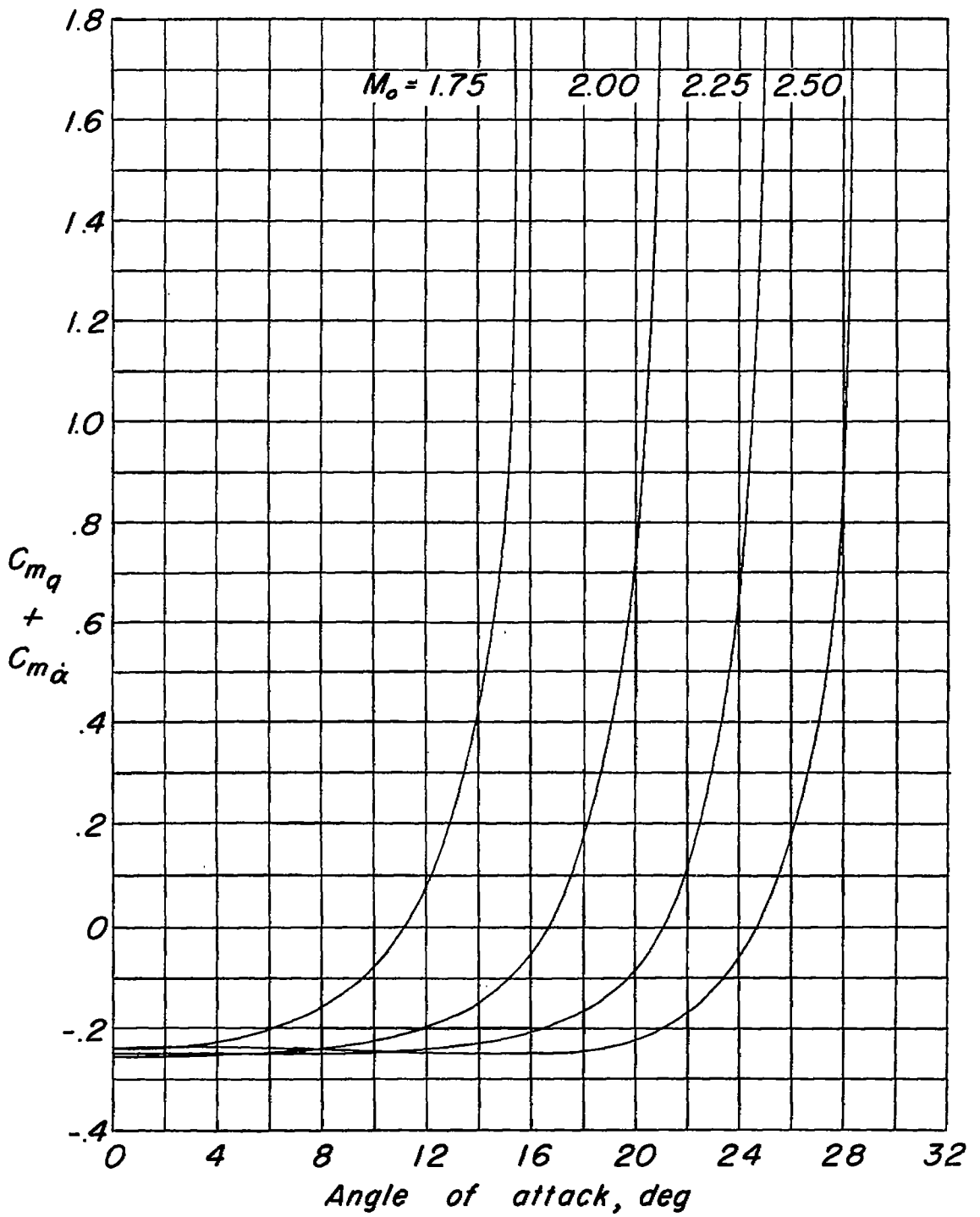

(b) M_o = 1.75 to 2.50.

Figure 27.- Continued.

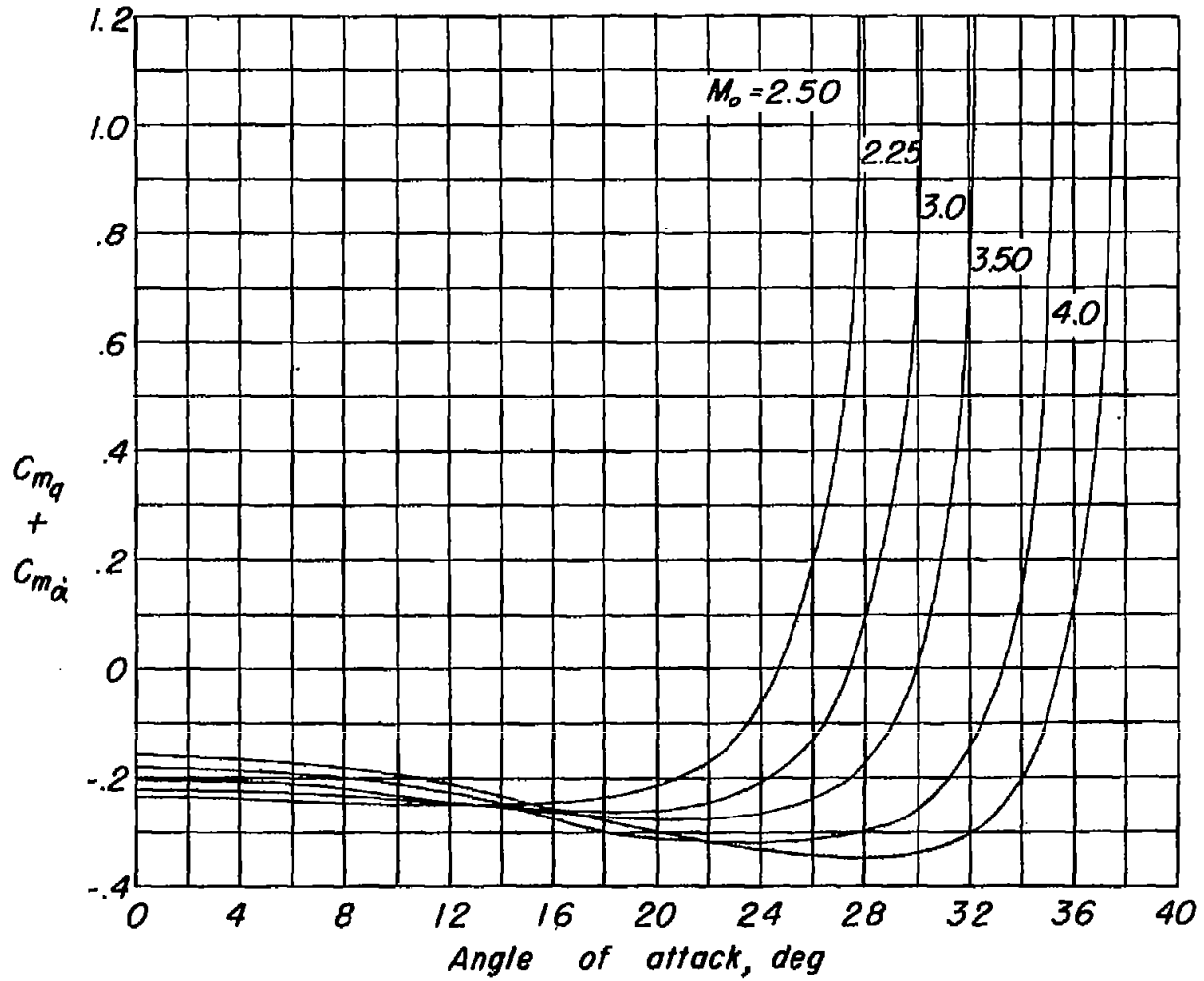

(c) M_o = 2.50 to 4.00.

Figure 27.- Concluded.

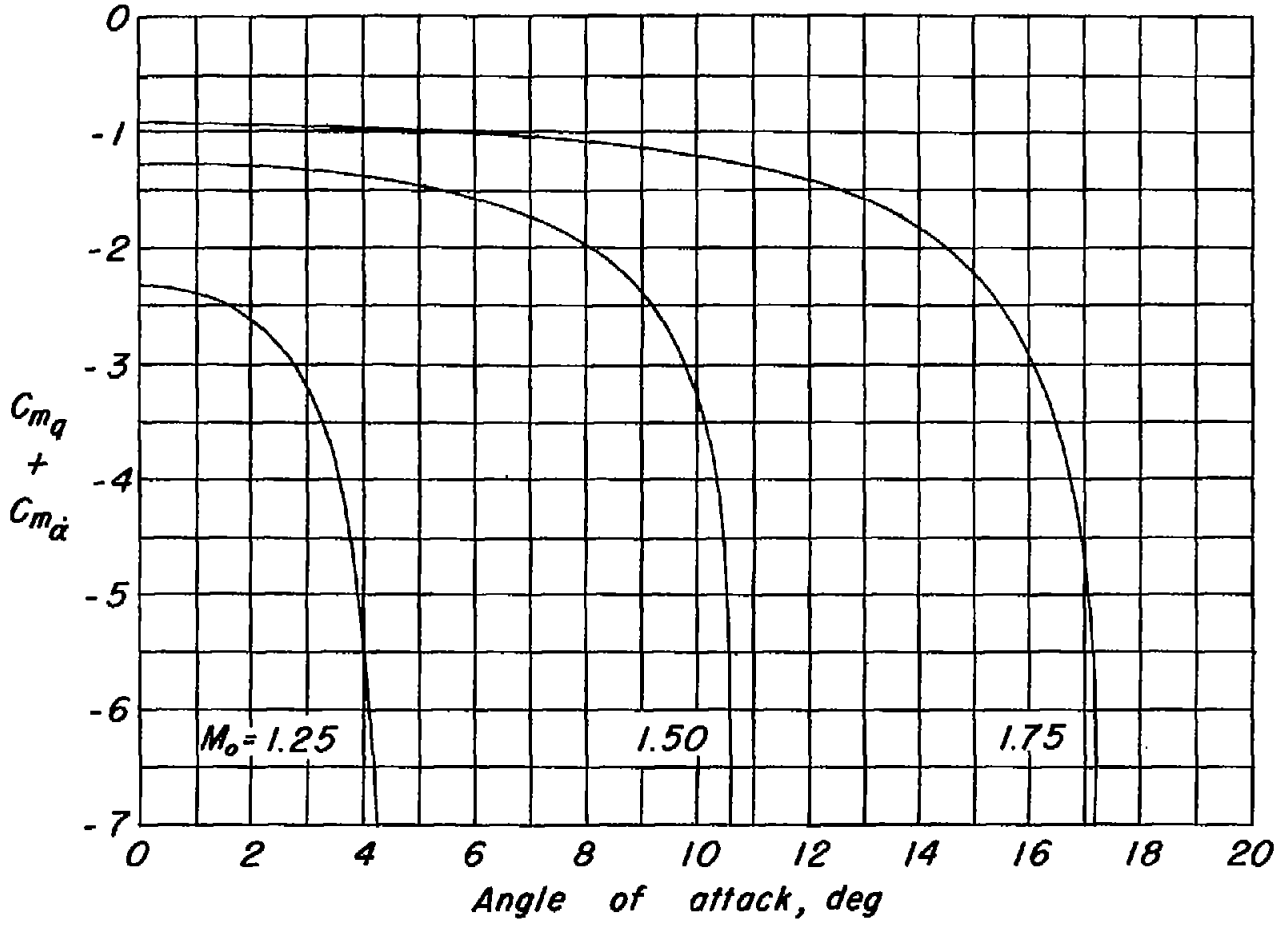

(a) M_o = 1.25 to 1.75.

Figure 28.- Variation of $C_{m_q} + C_{m_{\dot{\alpha}}}$ (calculated from approximate eqs. (119) and (124)) with angle of attack when center of gravity is located at three-quarter-chord point.

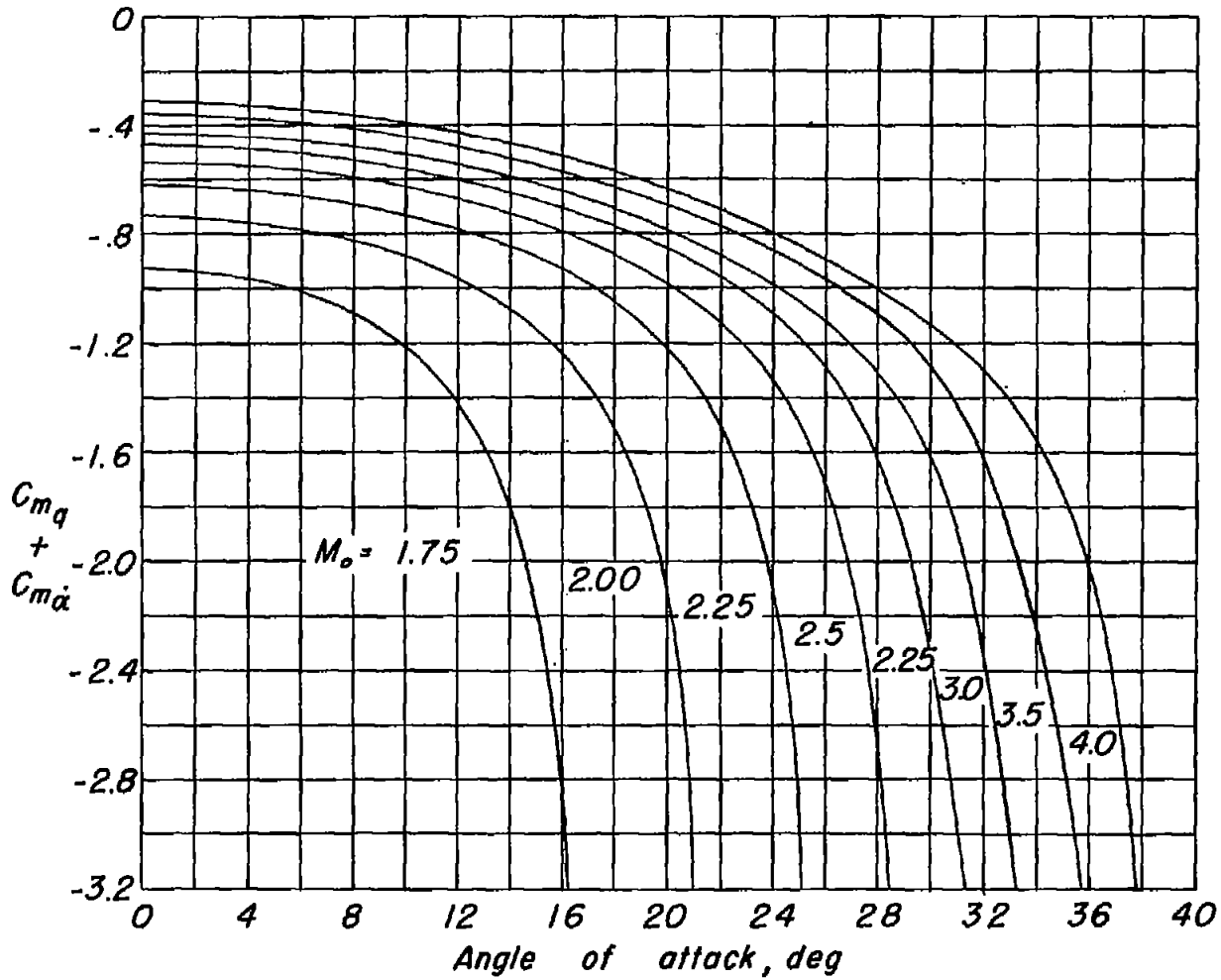

(b) M_o = 1.75 to 4.00.

Figure 28.- Concluded.

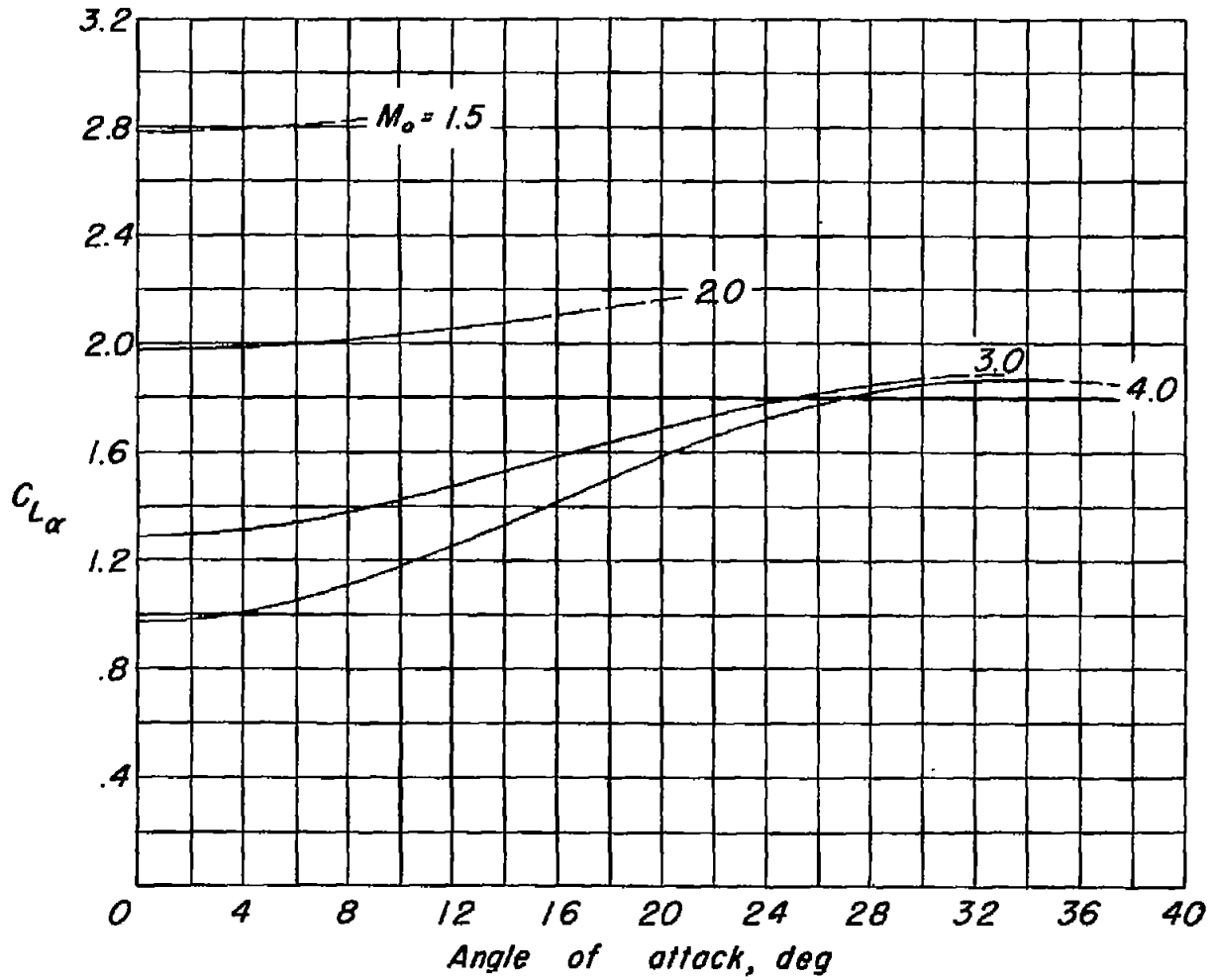

(a) Aspect ratio, 2.0.

Figure 29.- Variation of estimated C_{L_α} of rectangular wings with angle of attack for various Mach numbers. Aspect ratio, 2.0 and 4.0.

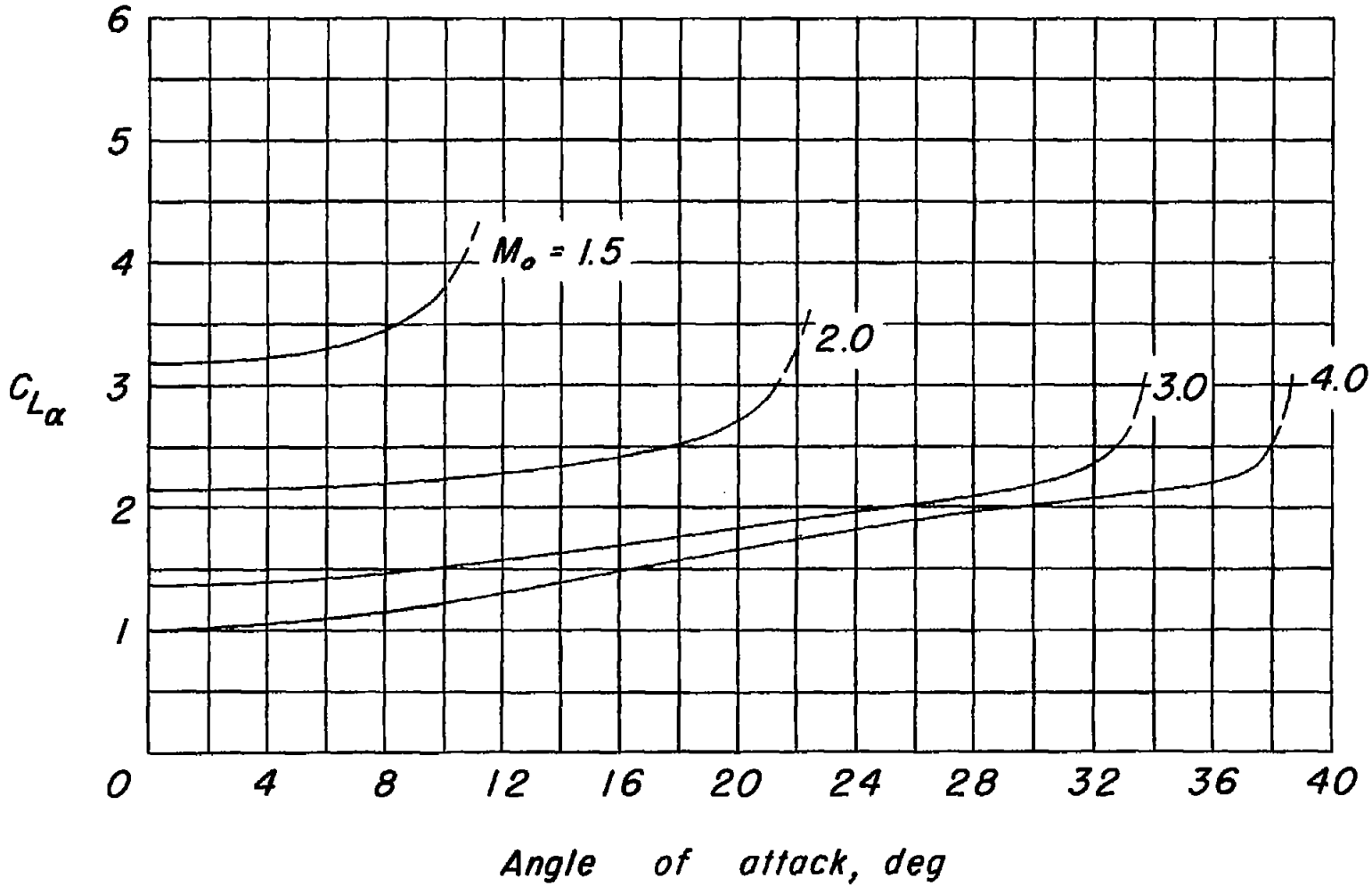

(b) Aspect ratio, 4.0.

Figure 29.- Concluded.

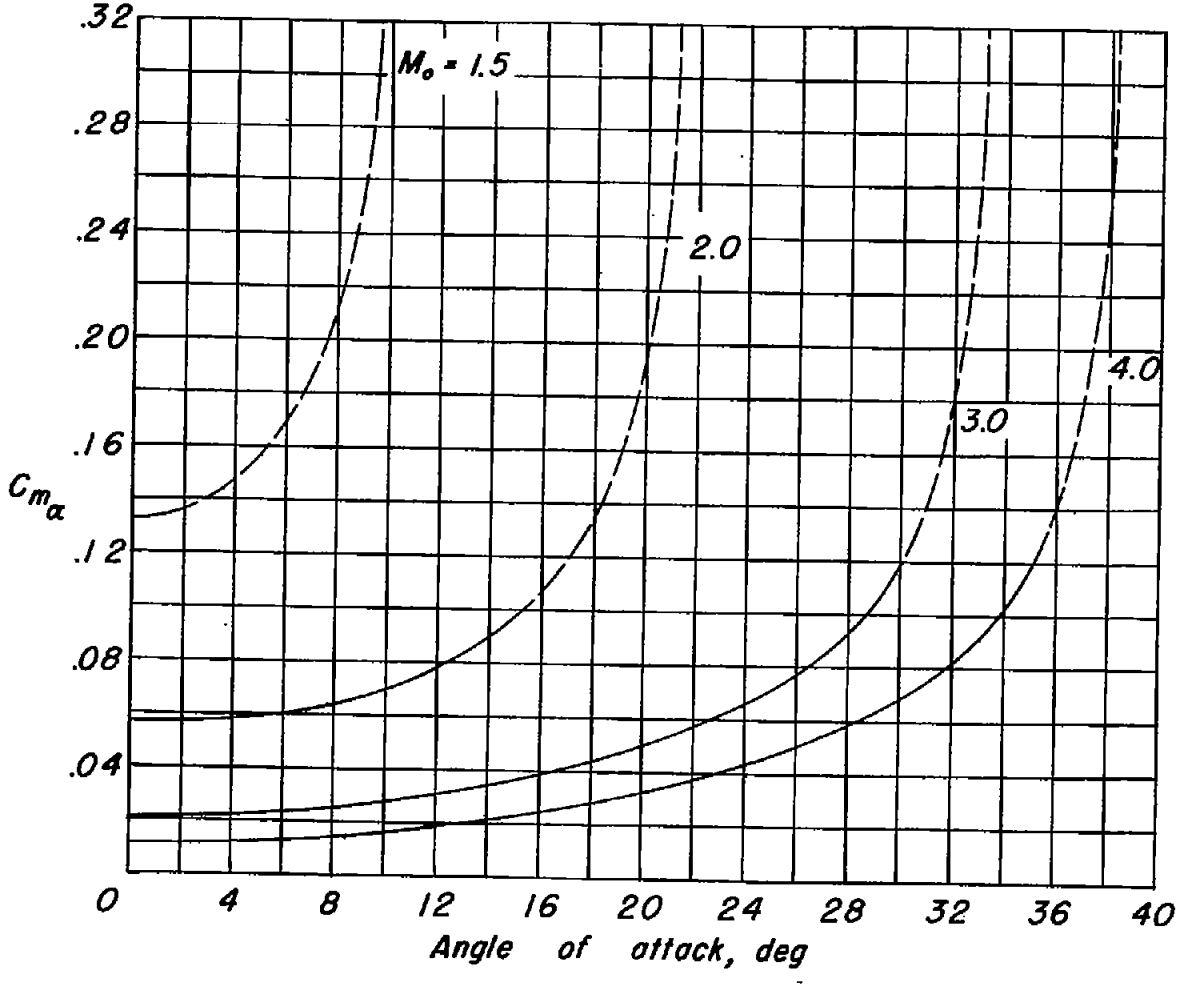

(a) Aspect ratio, 2.0.

Figure 30.- Variation of estimated C_{m_α} of rectangular wings with angle of attack for various Mach numbers. Aspect ratio, 2.0 and 4.0.

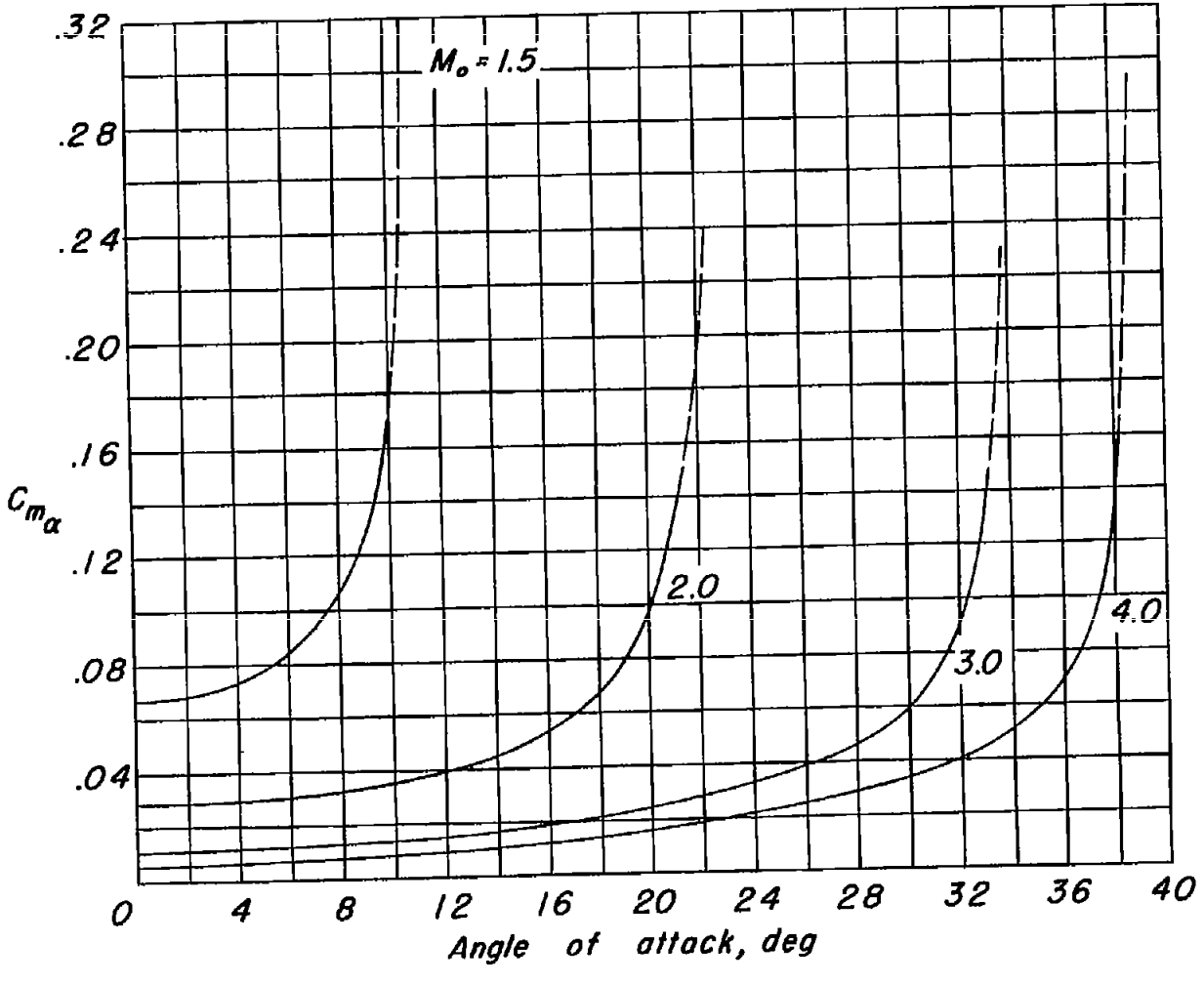

(b) Aspect ratio, 4.0.

Figure 30.- Concluded.

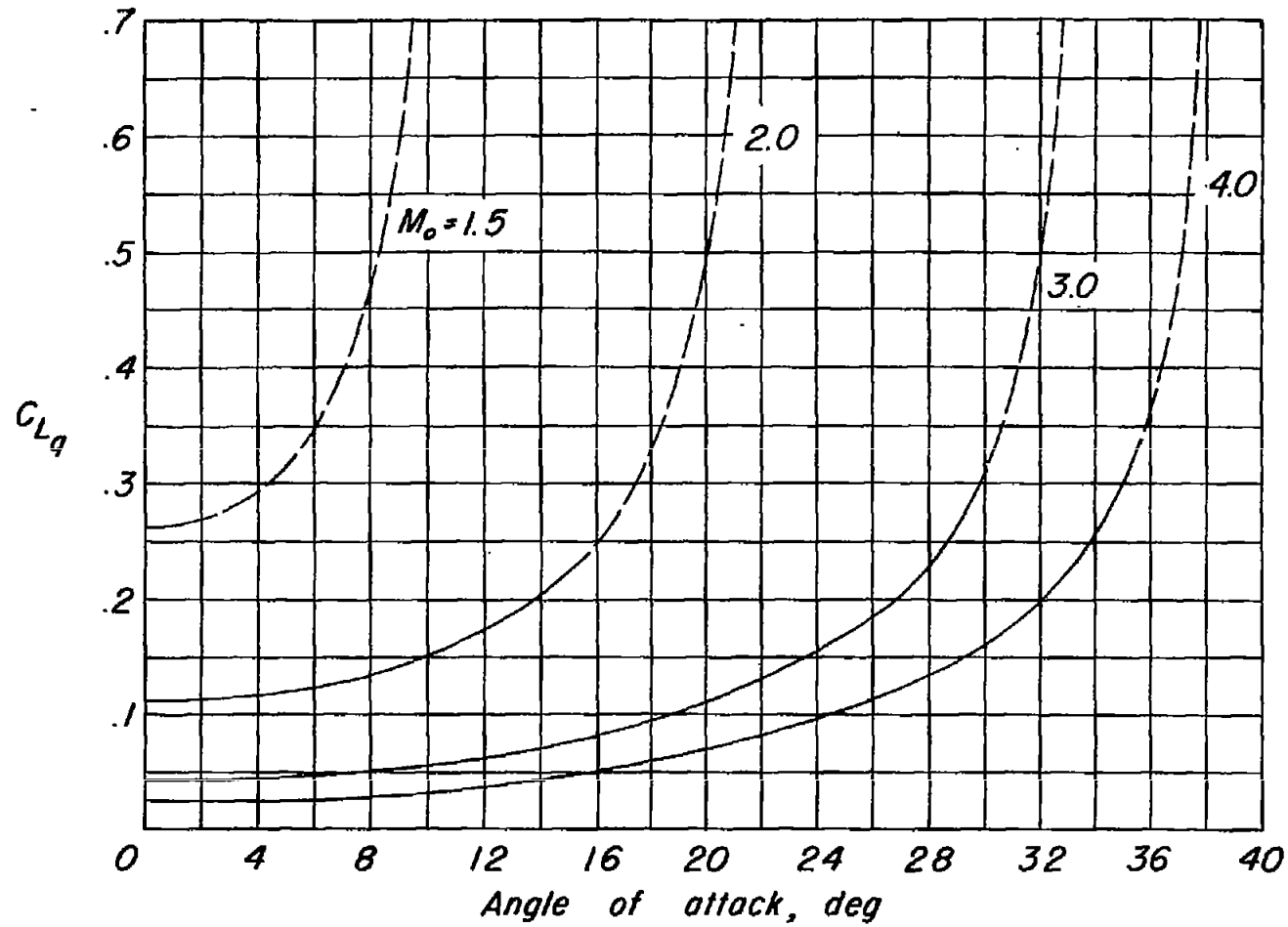

(a) Aspect ratio, 2.0.

Figure 31.- Variation of estimated C_{L_q} of rectangular wings with angle of attack for various Mach numbers. Aspect ratio, 2.0 and 4.0.

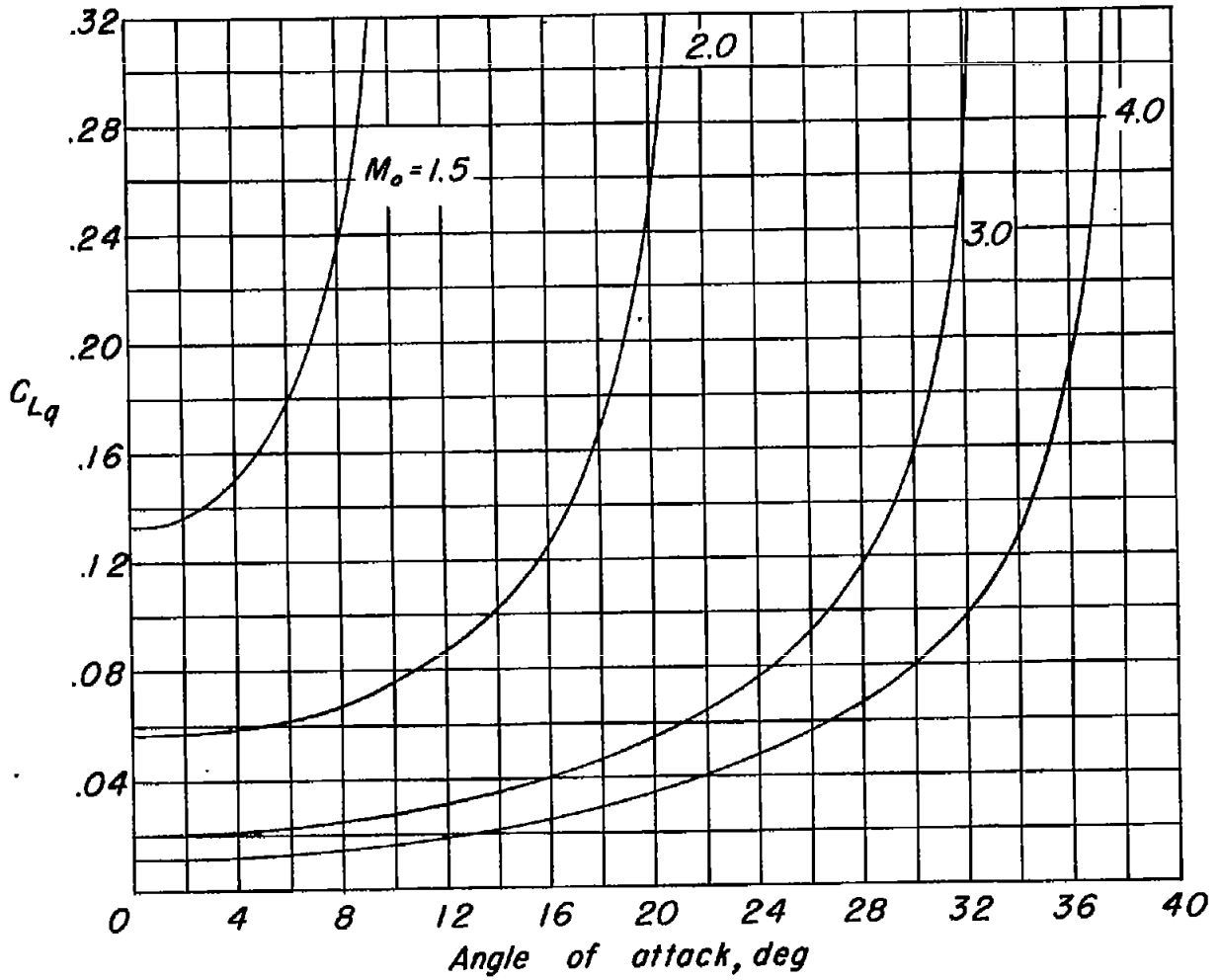

(b) Aspect ratio, 4.0.

Figure 31.- Concluded.

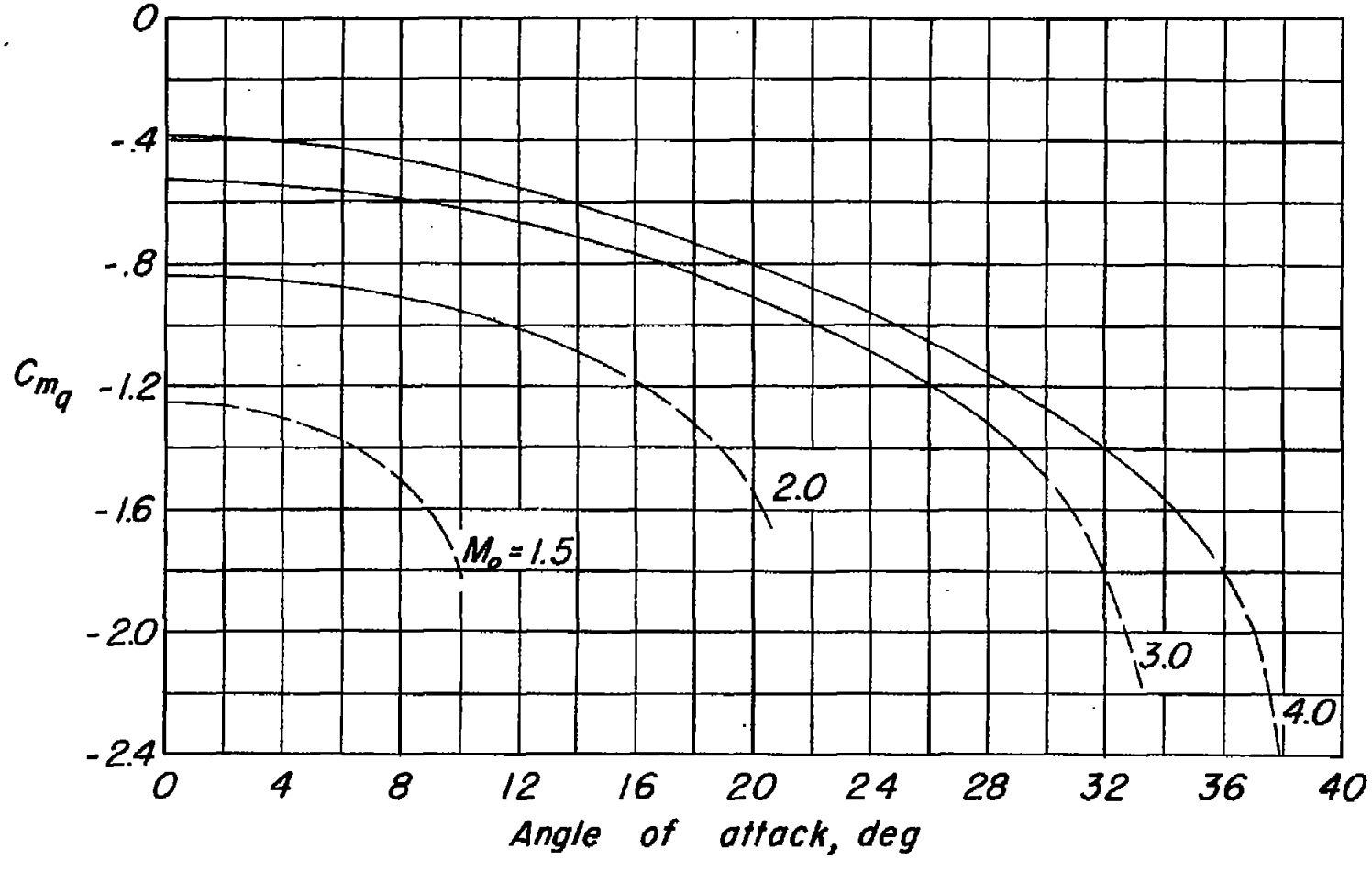

(a) Aspect ratio, 2.0.

Figure 32.- Variation of estimated C_{m_q} of rectangular wings with angle of attack for various Mach numbers. Aspect ratio, 2.0 and 4.0; center of gravity located at quarter-chord point.

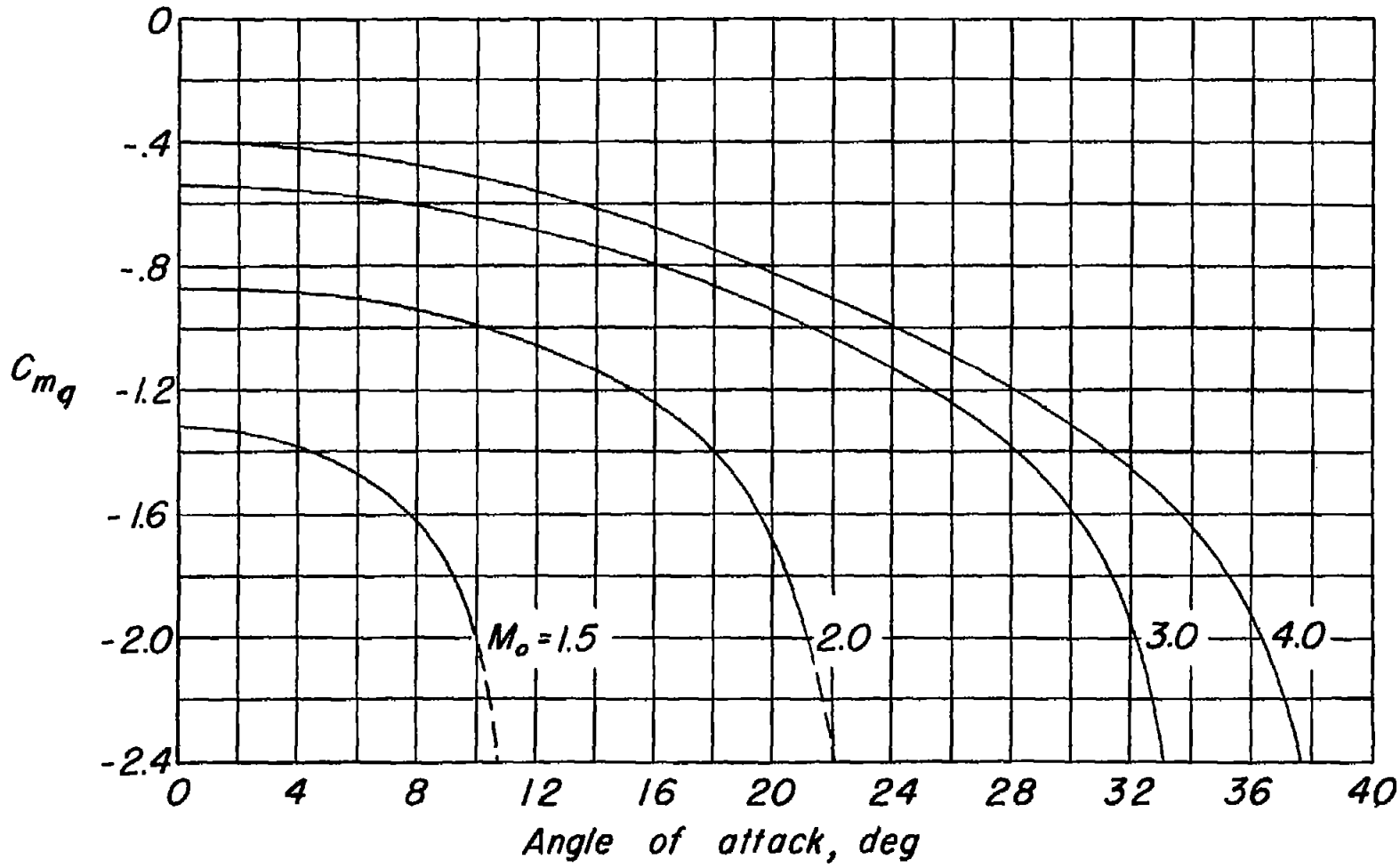

(b) Aspect ratio, 4.0.

Figure 32.- Concluded.

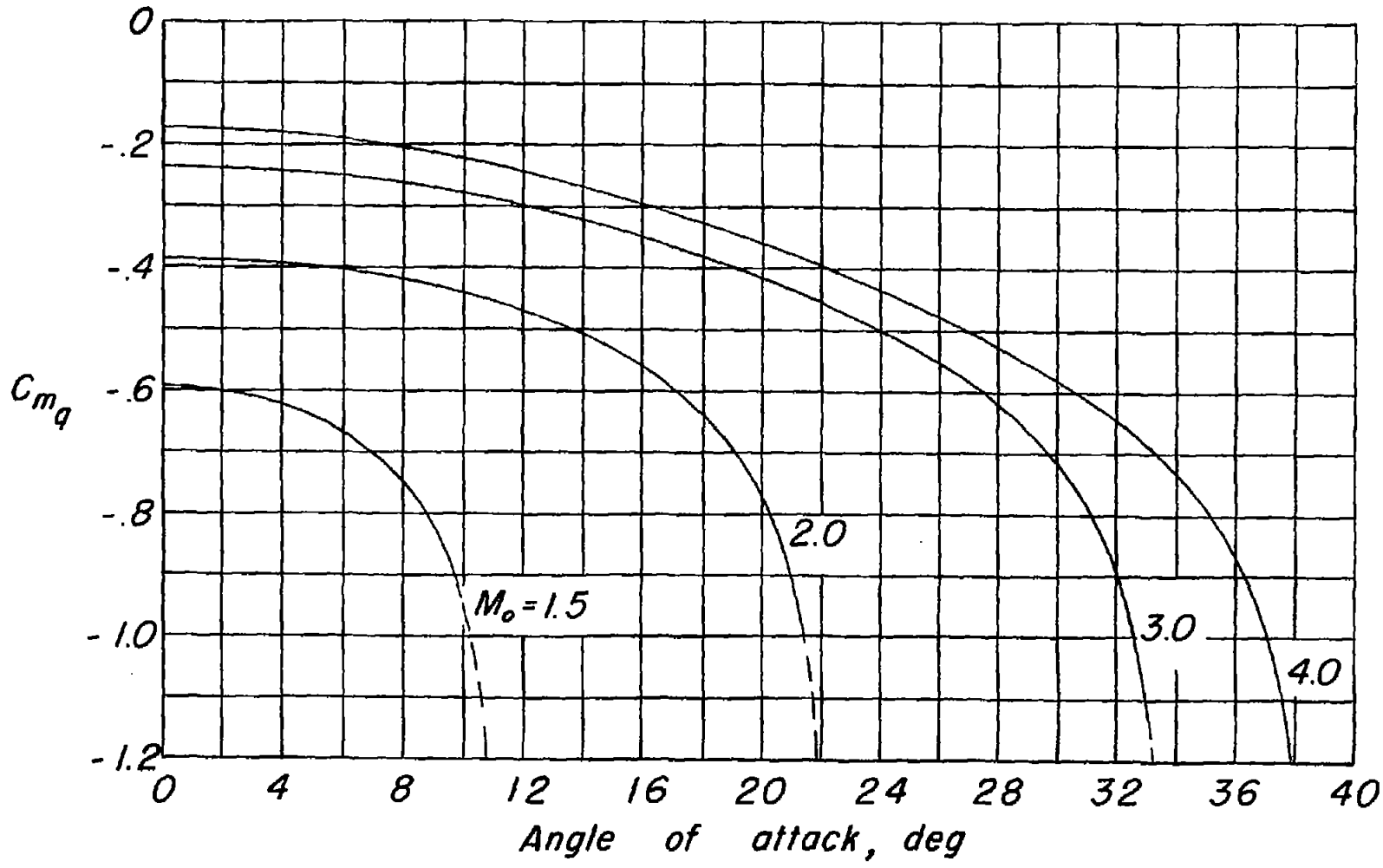

Figure 33.- Variation of estimated C_{m_q} of rectangular wings with angle of attack for various Mach numbers. Aspect ratio, 2.0 to ∞; center of gravity located at midchord point.

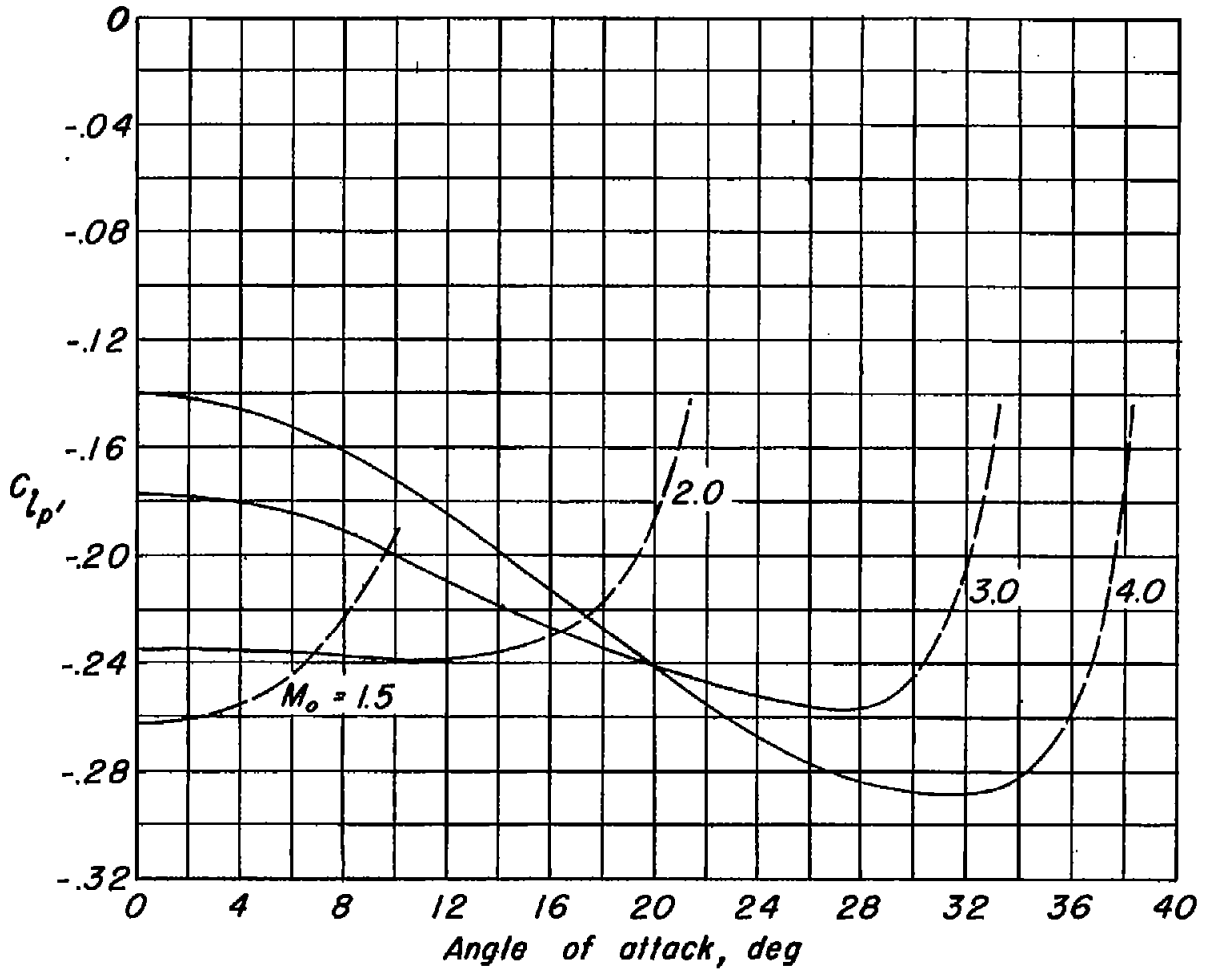

(a) Aspect ratio, 2.0.

Figure 34.- Variation of estimated $C_{l_{p'}}$ of rectangular wings with angle of attack for various Mach numbers. Aspect ratio, 2.0 and 4.0.

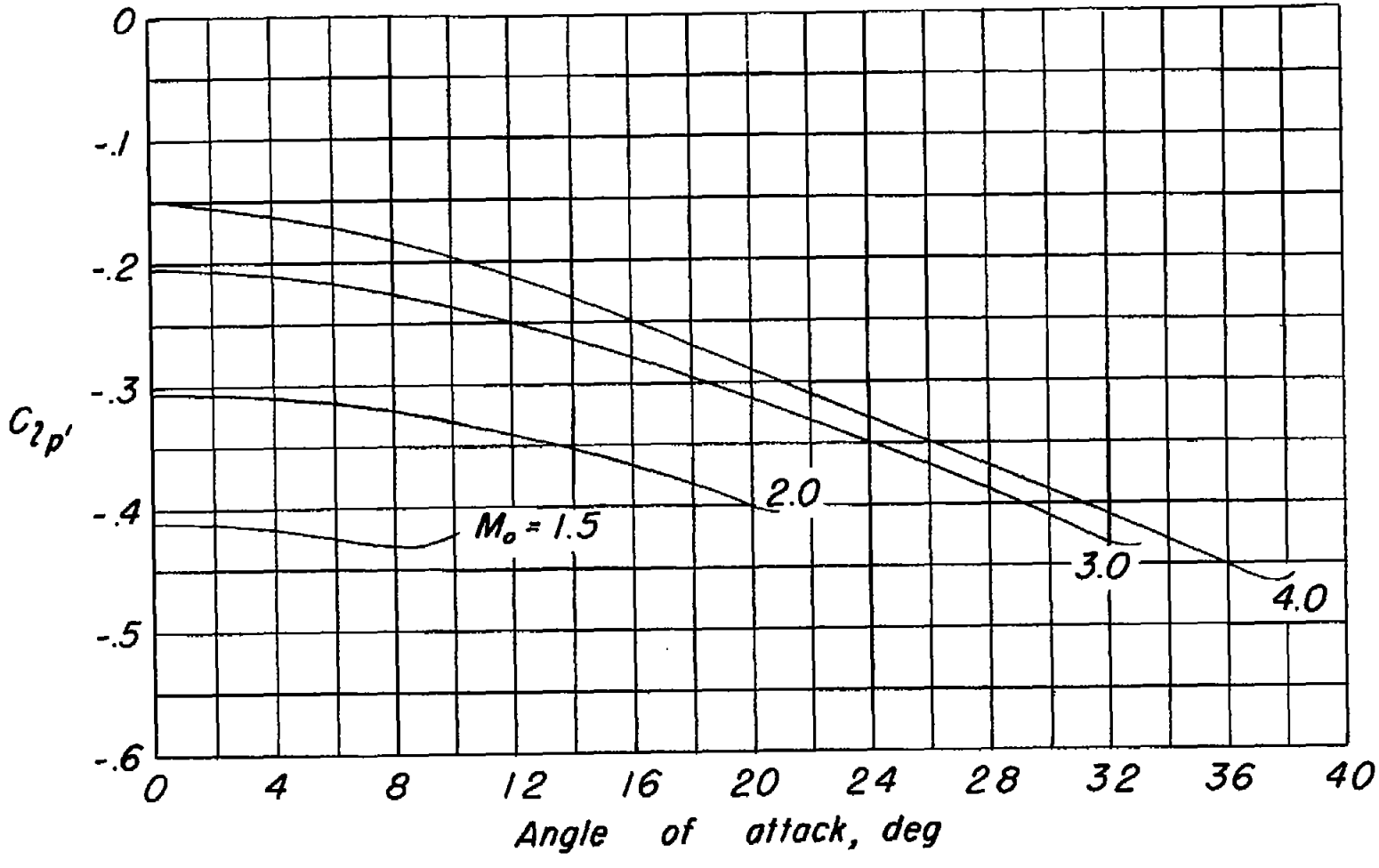

(b) Aspect ratio, 4.0.

Figure 34.- Concluded.

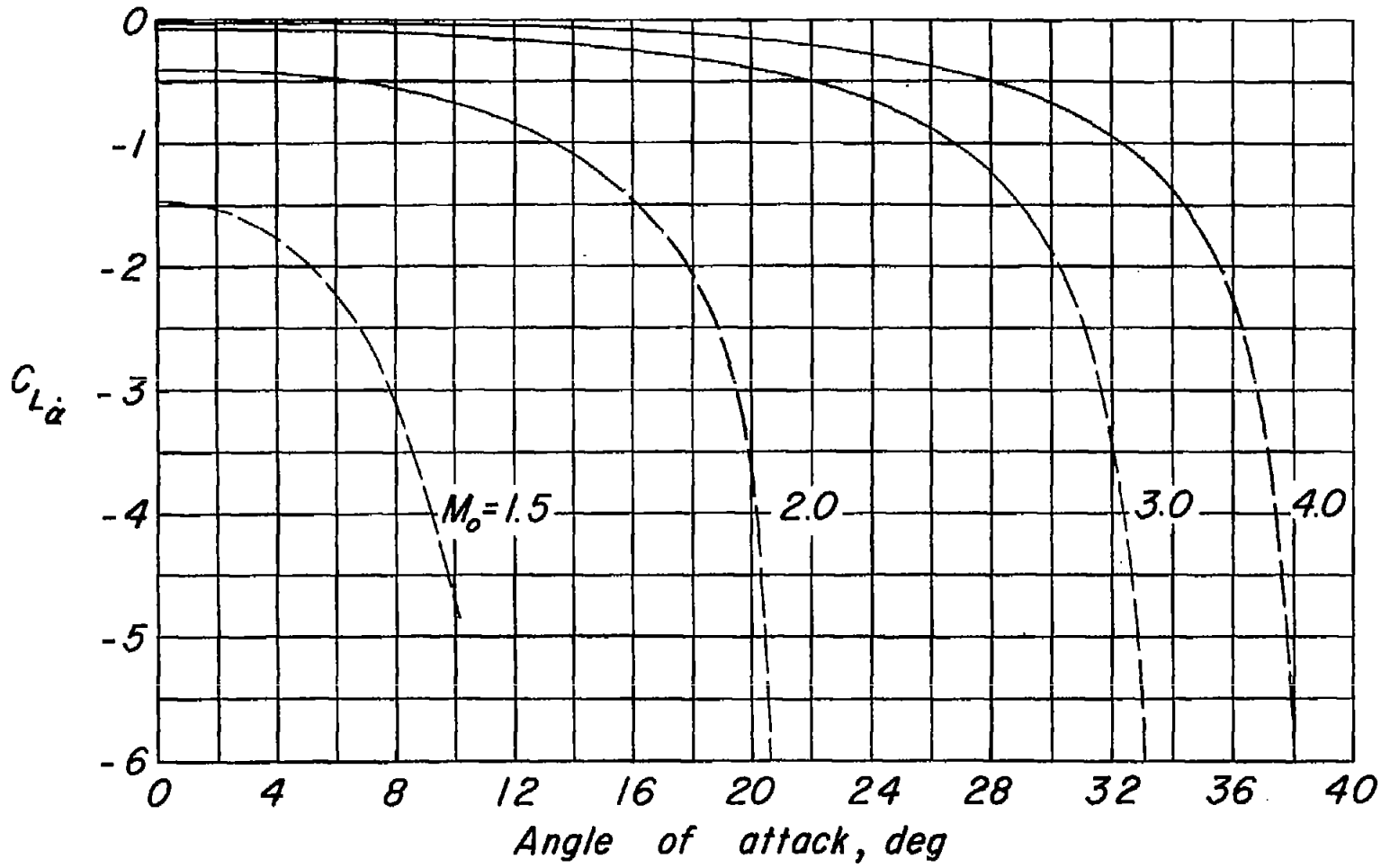

(a) Aspect ratio, 2.0.

Figure 35.- Variation of estimated $C_{L_{\dot{\alpha}}}$ of rectangular wings with angle of attack for various Mach numbers. Aspect ratio, 2.0 and 4.0.

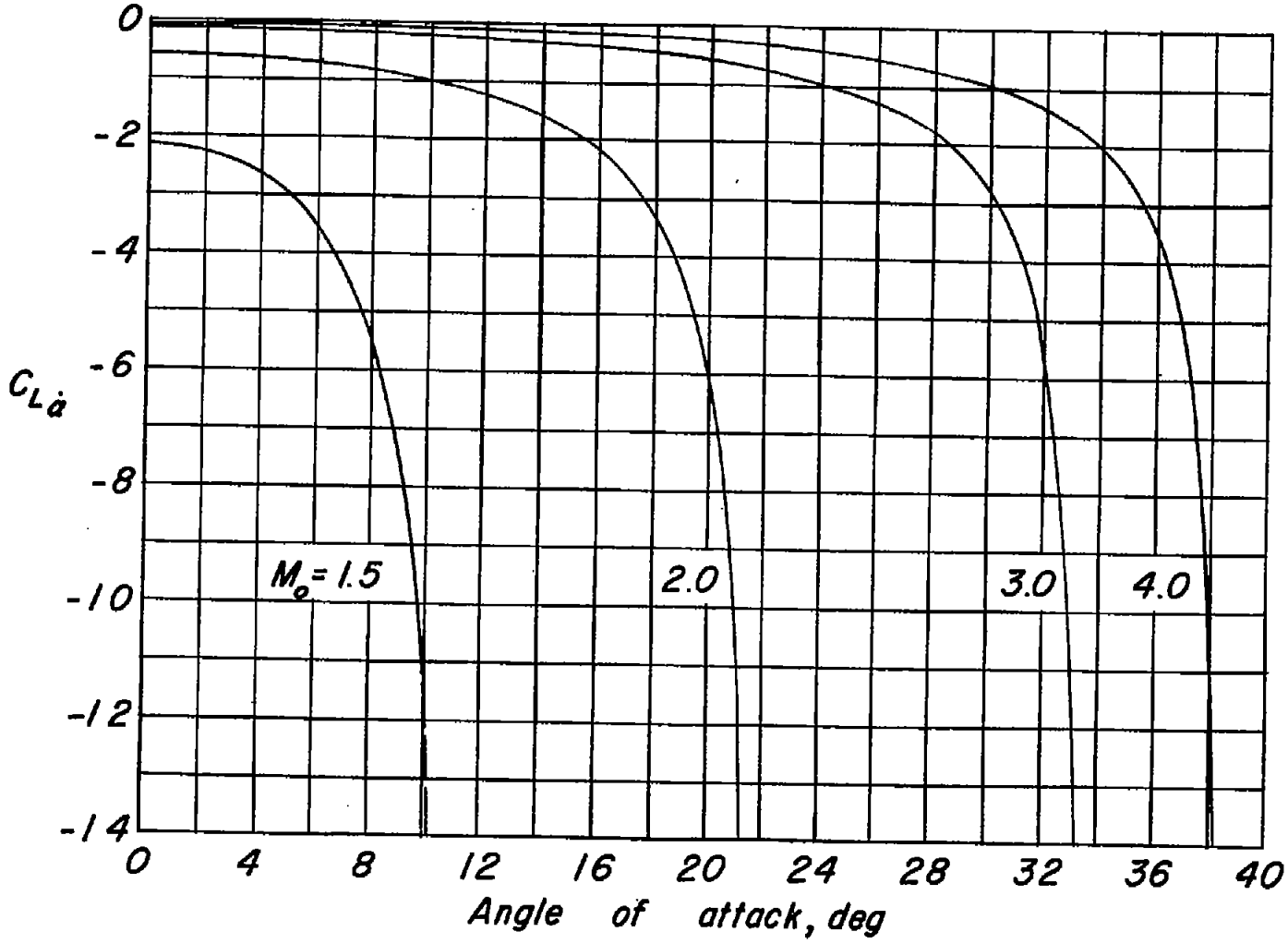

(b) Aspect ratio, 4.0.

Figure 35.- Concluded.

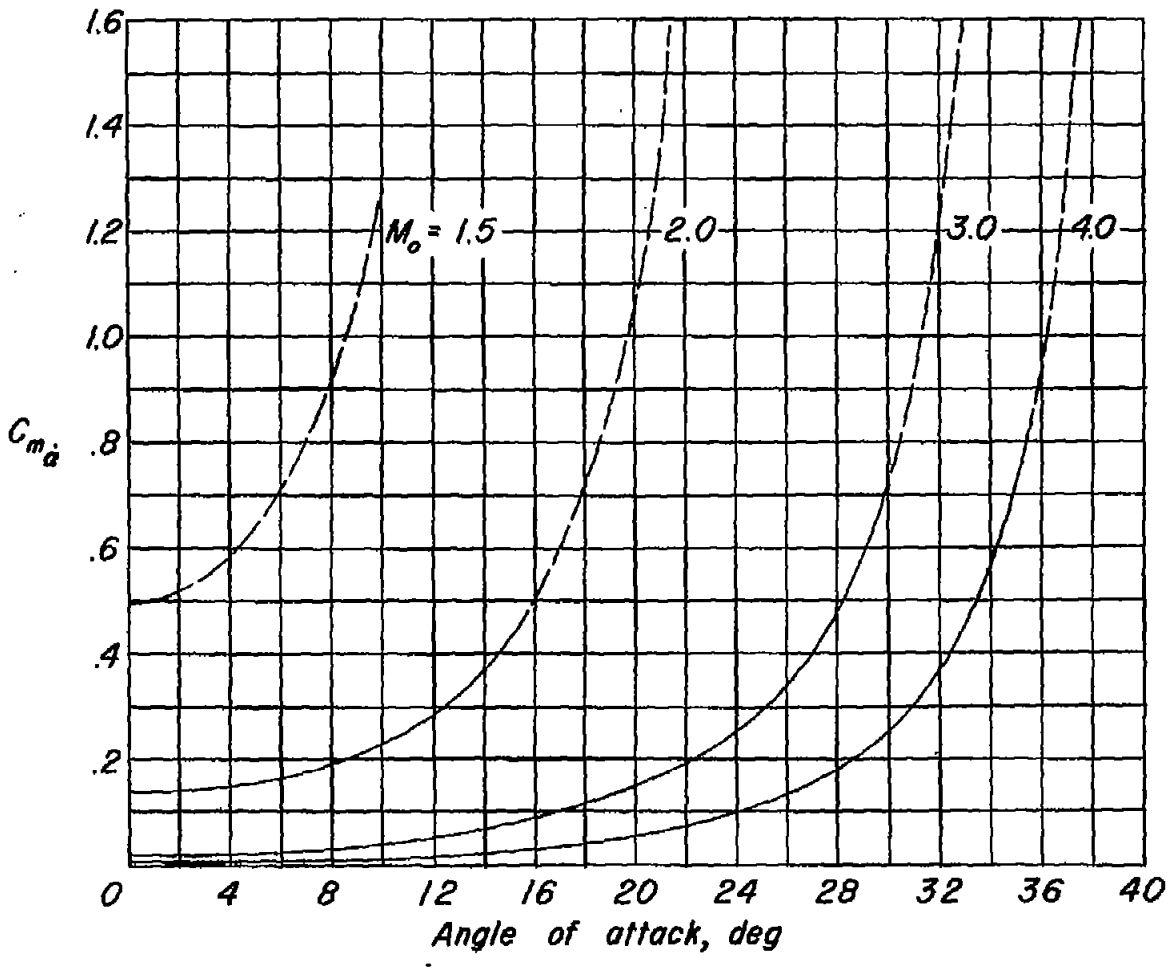

(a) Aspect ratio, 2.0.

Figure 36.- Variation of estimated $C_{m_{\dot{\alpha}}}$ of rectangular wings with angle of attack for various Mach numbers. Aspect ratio, 2.0 and 4.0; center of gravity located at quarter-chord point.

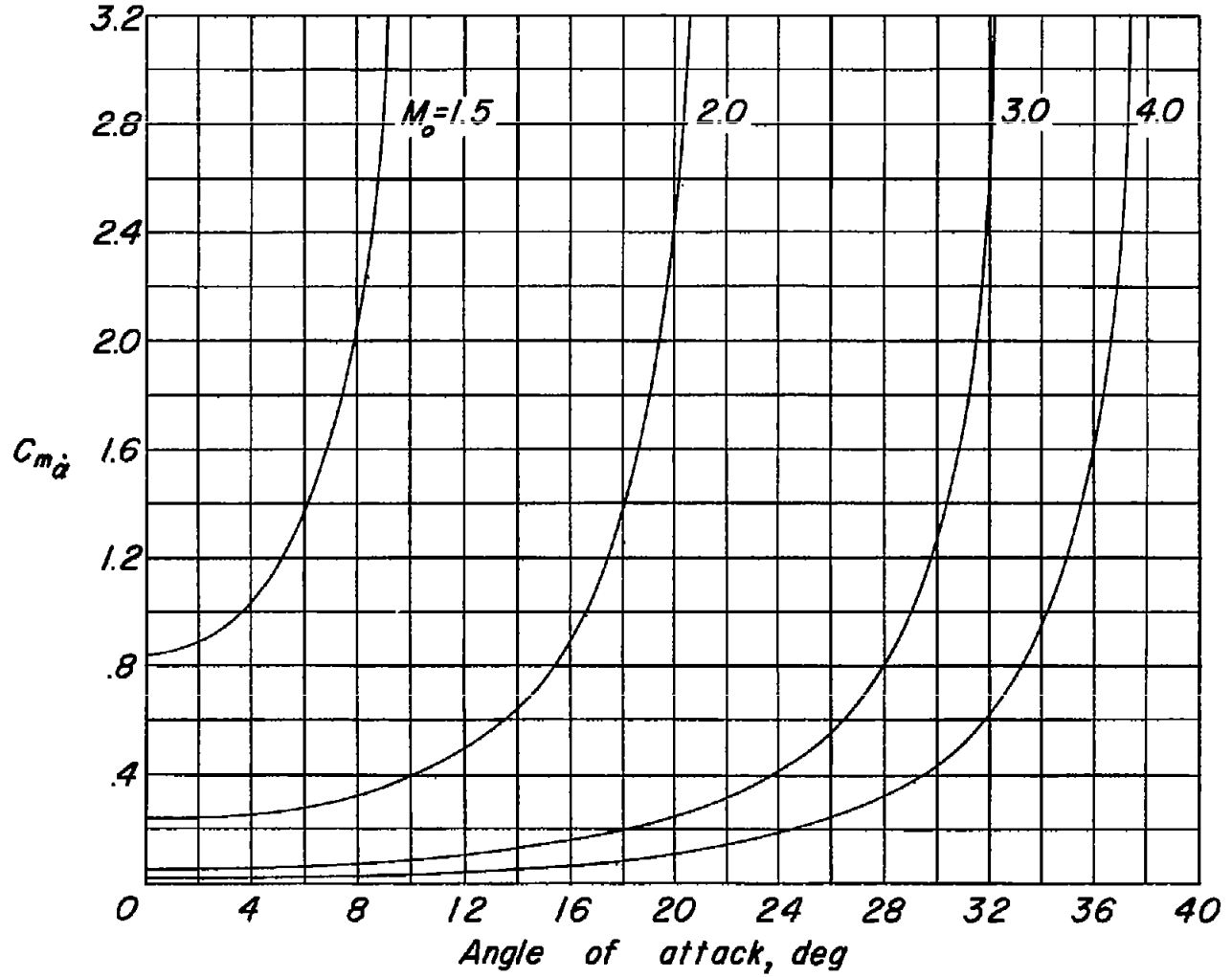

(b) Aspect ratio, 4.0.

Figure 36.- Concluded.

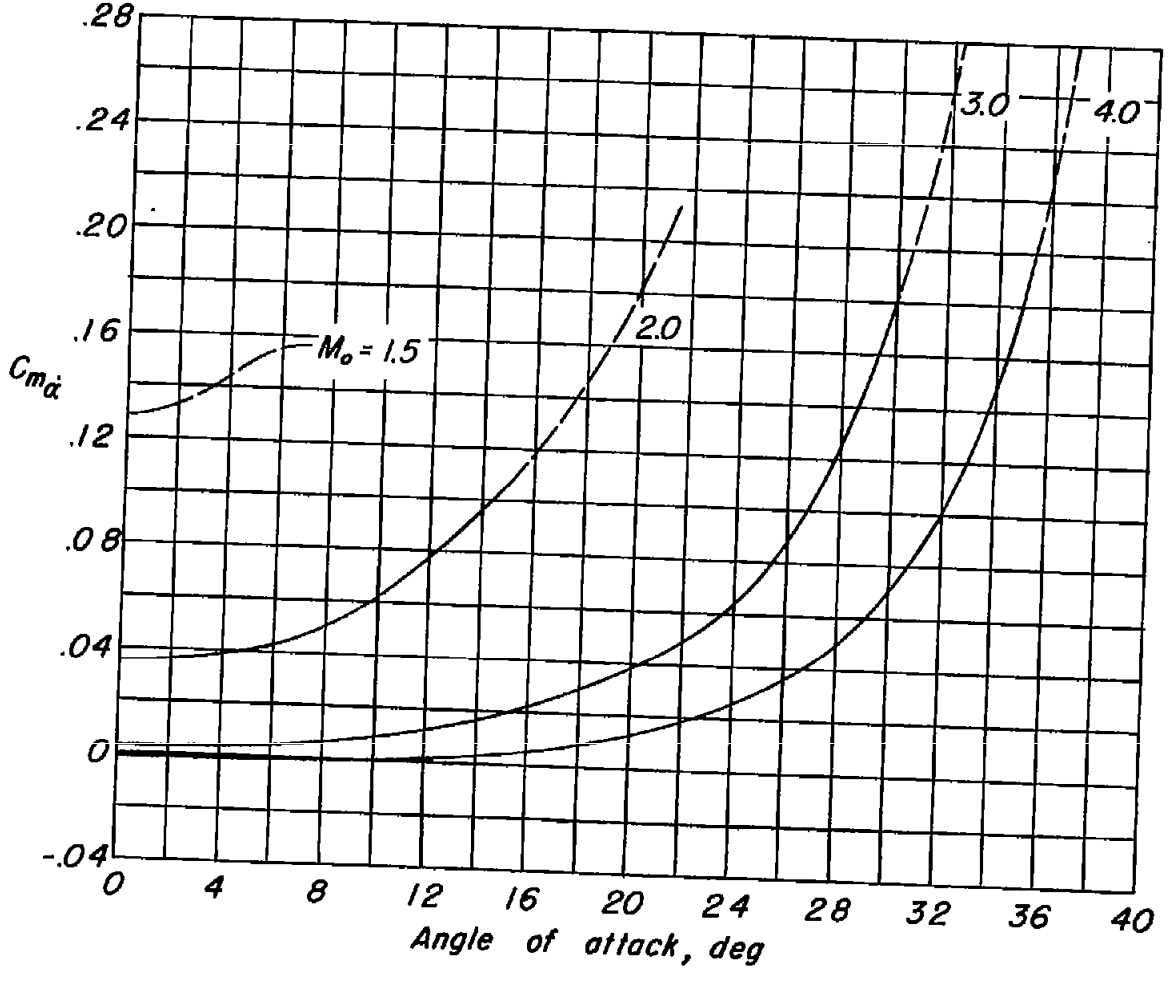

(a) Aspect ratio, 2.0.

Figure 37.- Variation of estimated $C_{m_{\dot{\alpha}}}$ of rectangular wings with angle of attack for various Mach numbers. Aspect ratio, 2.0 and 4.0; center of gravity located at midchord point.

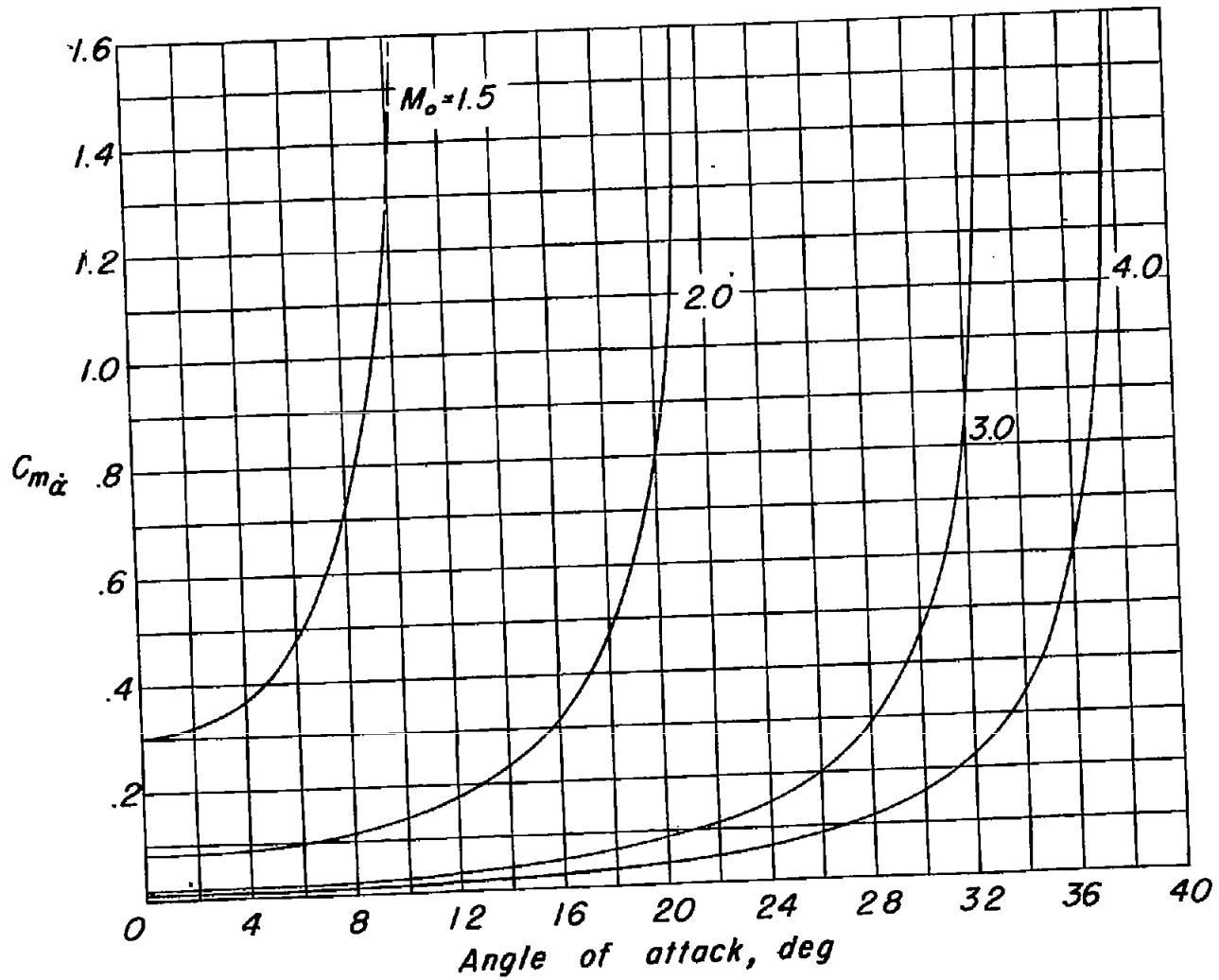

(b) Aspect ratio, 4.0.

Figure 37.- Concluded.

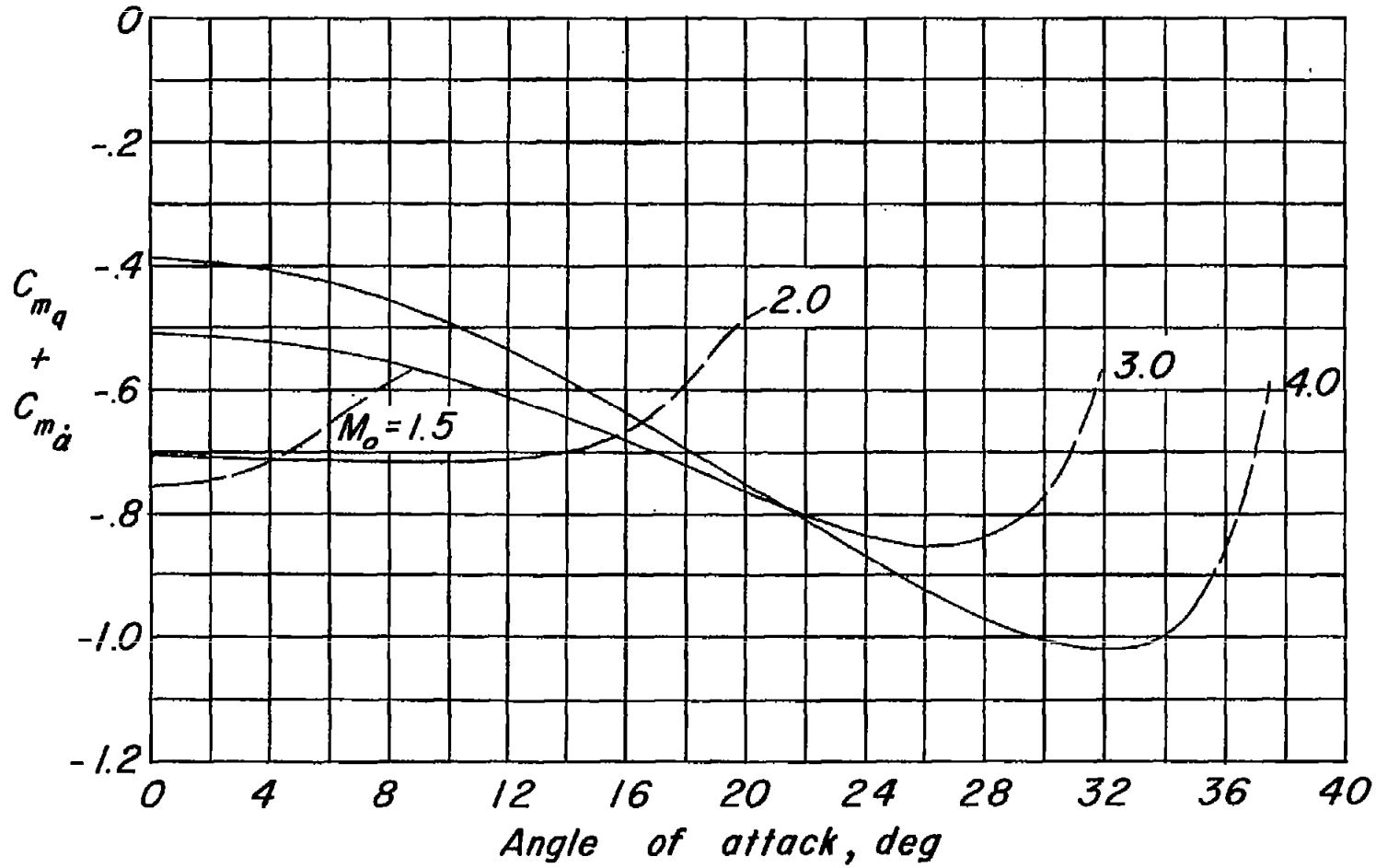

(a) Aspect ratio, 2.0.

Figure 38.- Variation of estimated $C_{m_q} + C_{m_{\dot{\alpha}}}$ of rectangular wings for various Mach numbers. Aspect ratio, 2.0 and 4.0; center of gravity located at quarter-chord point.

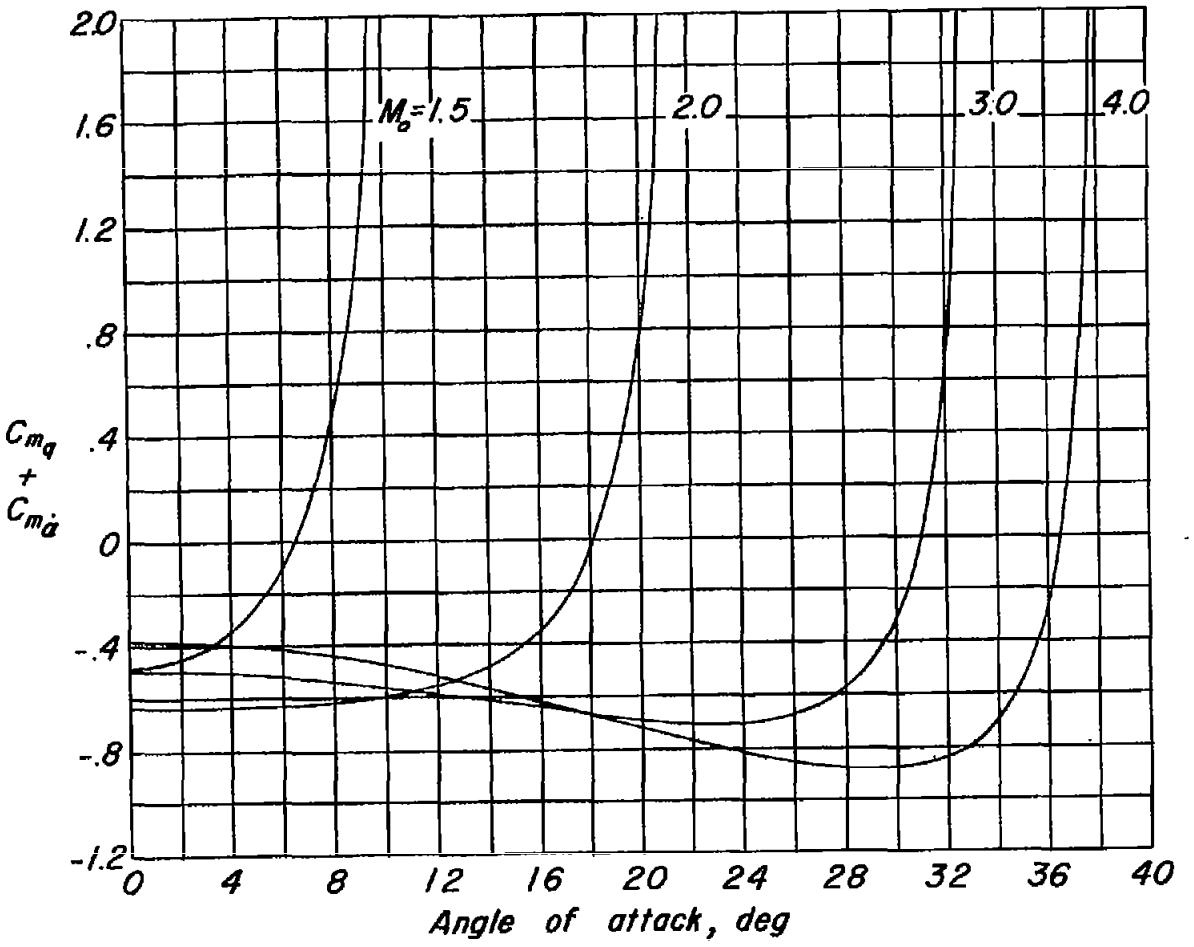

(b) Aspect ratio, 4.0.

Figure 38.- Concluded.

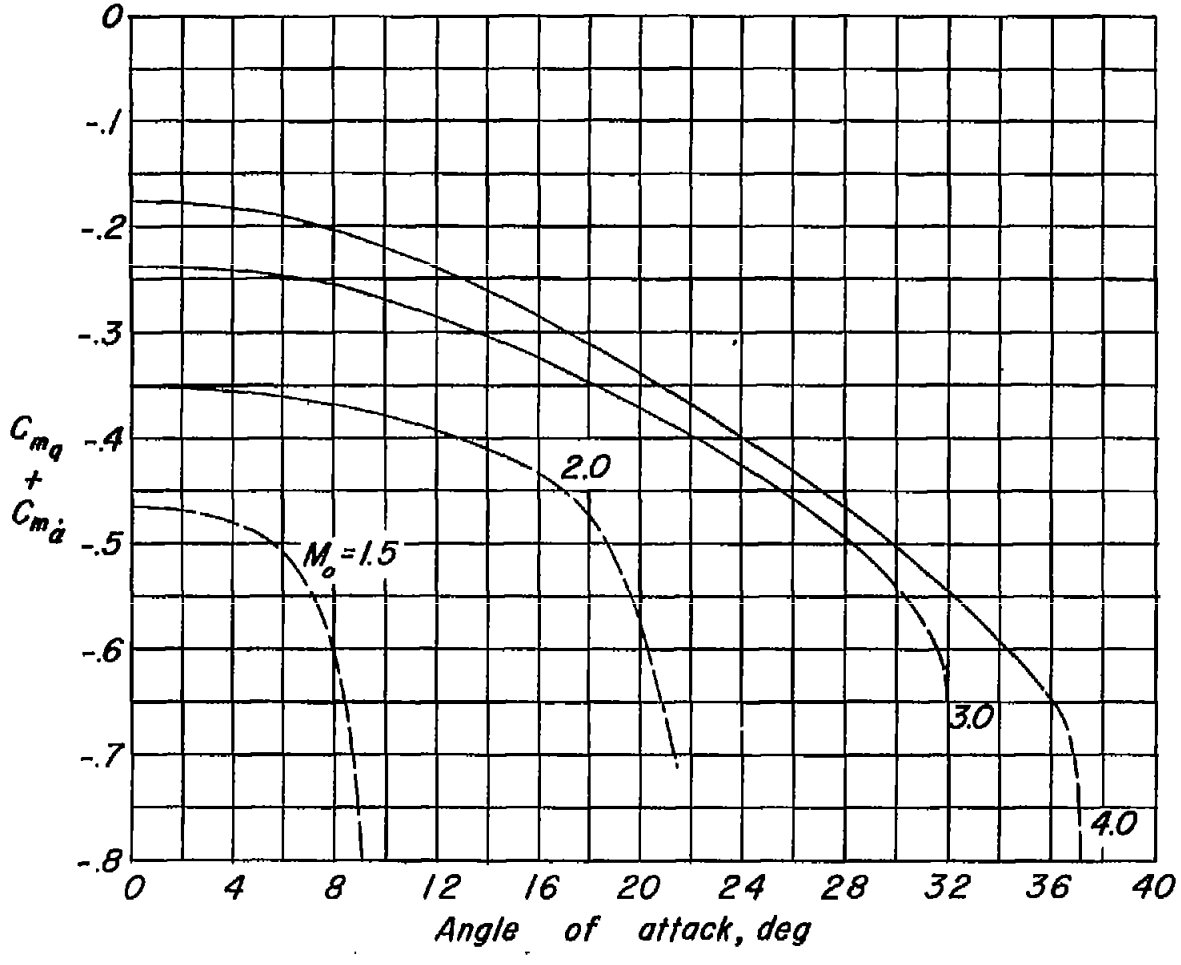

(a) Aspect ratio, 2.0.

Figure 39.- Variation of estimated $C_{m_q} + C_{m_{\dot{\alpha}}}$ of rectangular wings for various Mach numbers. Aspect ratio, 2.0 and 4.0; center of gravity located at midchord point.

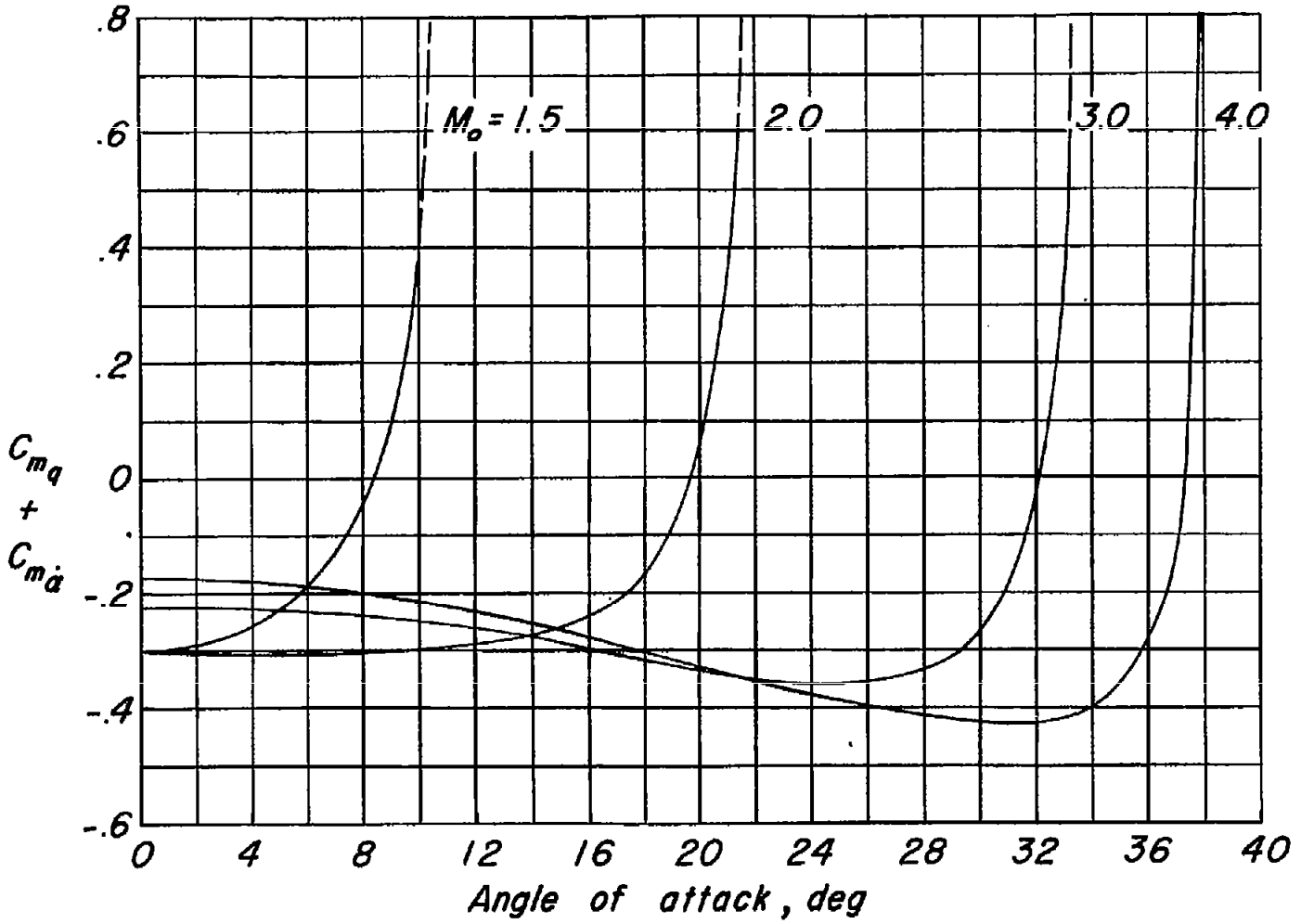

(b) Aspect ratio, 4.0.

Figure 39.- Concluded.